F 1503/3
FF
8 000000 561183

BULETINUL INSTITUTULUI POLITEHNIC DIN IAŞI

DITAT DE
NIVERSITATEA TEHNICĂ „Gh.ASACHI", IAŞI

Tomul XLIII (XLVII)
Fasc. 3–4

Secția III

ELECTROTEHNICĂ
ENERGETICĂ
ELECTRONICĂ

1997

BULETINUL INSTITUTULUI POLITEHNIC DIN IAŞI

Tomul XLIII (XLVII)
Fasc. 3–4

Secţia III

ELECTROTEHNICĂ. ENERGETICĂ. ELECTRONICĂ

1997

EDITORIAL STAFF

Prof. Dr. Eng. **MIHAI GAFIŢANU** (President)
Prof. Dr. Eng. **VICTOR BULACOVSCHI** (Vice-President)
Prof. Dr. Eng. **LIVIU GROLL** (Vice-President)
Prof. Dr. Eng. **GHEORGHE ZET** (Secretary)
Prof. Dr. Doc. Eng. **ALFRED BRAIER** (Editor)
Prof. Dr. Eng. **HUGO ROSMAN** (Editor)
Prof. Dr. Eng. **MIHAIL VÒICU** (Head of the Exchange Service)
Prof. Dr. Eng. **DIMITRIE ALEXA**
Prof. Dr. Eng. **ION BALASANIAN**
Prof. Dr. **AUREL BEJANCU**
Prof. Dr. Eng. **MIRCEA COZMÎNCĂ**
Prof. Dr. Eng. **SPIRIDON CREŢU**
Prof. Dr. Eng. **ION GIURMA**
Prof. Dr. Eng. **AURELIA GRIGORIU**
Prof. Dr. Eng. **CONSTANTIN PREDA**
Prof. Dr. Eng. **PAULICĂ RĂILEANU**

The **Bulletin of the Polytechnic Institute of Jassy** is edited by
the **Technical University "Gh.Asachi"** (the former Polytechnic Institute), Jassy.

TEXredaction:
B. Grigoriu, A. Rotaru
Technical University of Jassy

BULETINUL INSTITUTULUI POLITEHNIC DIN IAŞI
BULLETIN OF THE POLYTECHNIC INSTITUTE OF JASSY
Tomul XLIII (XLVII), Fasc. 3–4 1997

Secţia III

ELECTROTEHNICĂ. ENERGETICĂ. ELECTRONICĂ

SUMAR

Pag.

HUGO ROSMAN, Asupra conceptului de cuadripol general (franc., rez. rom.) 7

RADU URSULEAN, Calculul senzitivităţii diferenţiale: o metodă alternativă pentru cazul regimului tranzitoriu (engl., rez. rom.) 15

DORIN BELAUS, Asupra posibilităţii de realizare a egalităţii impedanţelor echivalente la poarta de intrare a unui cuadripol general liniar, neautonom, la funcţionarea la gol şi în scurtcircuit (franc., rez. rom.) 19

VALERIU MUNTEANU şi DANIELA TĂRNICERIU, Echivalenţa dintre diferite structuri IIR ale sistemelor liniar-variante în timp (engl., rez. rom.) 27

DAMIAN IMBREA, N. COJAN şi CLARISSA GÂTLAN, Identificarea defectelor nedetectabile în circuite combinaţionale utilizând analiza stemurilor multiple (engl., rez. rom.) 35

DANIELA TĂRNICERIU şi VALERIU MUNTEANU, Bancuri QMF modificate realizate cu filtre eliptice de ordin par (engl., rez. rom.) 41

CLAUDIA BONCIU şi CRISTIAN BONCIU, Aspecte privind explorarea 2D şi 3D cu ultrasunete (franc., rez. rom.) 49

LAURENŢIU DIMITRIU şi LILIANA VORNICU, Frecvenţmetru cu microprocesor. Aspecte software. Funcţionarea cu măsurarea perioadei (engl., rez. rom.) 57

CRISTINA SCHREINER şi ROMEO CIOBANU, Fenomene de descărcări parţiale în câmp electric nesinusoidal, specifice izolaţiilor compozite ale unor maşini electrice speciale (engl., rez. rom.) 63

LIVIA COCIU, Un model analitic al procesului de extrudere a foliilor din polietilenă (engl., rez. rom.) 71

I. SUCHAR, Asupra reversibilităţii micromotoarelor magnetoelectrice cu comutaţie statică (engl., rez. rom.) 79

COSTEL-EMIL TEODORU, Studiul optimizării funcţionării modulatorului într-o instalaţie de încercare a izolaţiei cablurilor de înaltă tensiune (franc., rez. rom.) 85

Pag.

CRISTIAN DOMNIŞORU, Caracteristica magnetică parţială în proiectarea maşinii de curent continuu (engl., rez. rom.) 93

PETRUŢ DUMA, CLARISSA GÂTLAN şi LUMINIŢA SCRIPCARIU, Comutator digital spaţial de un bit utilizat în centralele telefonice electronice de capacitate mică (engl., rez. rom.) 103

EUGEN BÂRLĂDEANU şi AL. POEATĂ, Contribuţii la optimizarea dezvoltării reţelelor electrice de distribuţie în condiţiile informaţiilor incerte (engl., rez. rom.) ... 109

DANIELA RĂDĂŞANU, M. GAVRILAŞ şi GH. GEORGESCU, Un procedeu de utilizare a reţelelor neuronale artificiale pentru evaluarea pierderilor de putere activă în reţelele electrice (engl., rez. rom.) 115

JAN IGNAT şi M. PROFIRE, Unele caracteristici ale regimului stabilizat de defect bifazat cu punere la pământ în reţele de distribuţie cu neutrul legat la pământ (engl., rez. rom.) 123

CĂTĂLIN-D. GĂLĂŢANU şi JAN IGNAT, Determinarea domeniilor de variaţie ale unor parametri proprii regimului de defect bifazat cu punere la pământ (engl., rez. rom.) 129

RECENZII 135

BULETINUL INSTITUTULUI POLITEHNIC DIN IAŞI
BULLETIN OF THE POLYTECHNIC INSTITUTE OF JASSY
Tome XLIII (XLVII), Fasc. 3–4 1997

Section III

ELECTROTECHNICS. ENERGETICS. ELECTRONICS

CONTENTS

Pp.

HUGO ROSMAN, Sur le concept de quadripôle général (French, Romanian summary) 7

RADU URSULEAN, Computing Differential Sensitivities for Linear Circuits: an Alternative Method for the Transient Response Case (English, Romanian summary) 15

DORIN BELAUS, Sur la possibilité de réaliser l'égalité des impédances équivalentes à la porte d'entrée, à vide et en court-circuit d'un quadripôle général linéaire non-autonome (French, Romanian summary) 19

VALERIU MUNTEANU and DANIELA TĂRNICERIU, Equivalence between Different Structures of Linear Time Varying Discrete Infinite Impulse Response Systems (English, Romanian summary) 27

DAMIAN IMBREA, N. COJAN and CLARISSA GÂTLAN, Identification of Undetectable Faults in Combinational Circuits Using Multiple-Stem Analysis (English, Romanian summary) 35

DANIELA TĂRNICERIU and VALERIU MUNTEANU, Modified Quadrature Mirror Filter Banks Based on Elliptic Filters of Even Order (English, Romanian summary) 41

CLAUDIA BONCIU et CRISTIAN BONCIU, Aspects concernant l'exploration 2D et 3D par ultrasons (French, Romanian summary) 49

LAURENŢIU DIMITRIU and LILIANA VORNICU, Frequency-meter with Microprocessor. Software Aspects. Period-Measuring Working (English, Romanian summary) 57

CRISTINA SCHREINER and ROMEO CIOBANU, Partial Discharge-Phenomena under Non-sinusoidal Electric Field of Some Composite Insulations for Special Electrical Machines (English, Romanian summary) 63

LIVIA COCIU, An Analytical Model of the Blown Film Process (English, Romanian summary) 71

I. SUCHAR, On the Reversibility of the D.C. Motors with Static Switching (English, Romanian summary) 79

COSTEL-EMIL TEODORU, Sur l'optimisation du fonctionnement du modulateur dans une installation d'essais de l'isolation des câbles HT (French, Romanian summary) 85

	Pp.
CRISTIAN DOMNIŞORU, Partial Magnetising Characteristic in DC Electrical Machine Design (English, Romanian summary)	93
PETRUŢ DUMA, CLARISSA GÂTLAN and LUMINIŢA SCRIPCARIU, One-Bit Digital Spatial Switch used in Low Capacity Electronic Telephone Exchange (English, Romanian summary)	103
EUGEN BÂRLĂDEANU and AL. POEATĂ, About the Optimal Development for the Electric Network considering Uncertain Information (English, Romanian summary)	109
DANIELA RĂDĂŞANU, M. GAVRILAŞ and GH. GEORGESCU, An Artificial Neural Network Approach for the Evaluation of Active Losses in Power Transmission Systems (English, Romanian summary)	115
JAN IGNAT and M. PROFIRE, Some Characteristics of the Two-Phase Ground Fault under Stabilized Conditions in the Supply System with Neural Earthing (English, Romanian summary)	123
CĂTĂLIN-D. GĂLĂŢANU and JAN IGNAT, Determination of the Variation Range of Some Parameters Specific to the Two-Phase Ground Fault (English, Romanian summary)	129
BOOK REVIEWS	135

BULETINUL INSTITUTULUI POLITEHNIC DIN IAŞI
Tomul XLIII (XLVII), Fasc. 3–4, 1997
Secţia III
ELECTROTEHNICĂ. ENERGETICĂ. ELECTRONICĂ

C.D. 612.392.5

SUR LE CONCEPT DE QUADRIPÔLE GÉNÉRAL

PAR
HUGO ROSMAN

On définit le quadripôle général comme un n-porte ayant deux portes d'accès avec l'extérieur et $n-2$ portes intérieures. En même temps on établit les équations d'un tel quadripôle, en le considérant linéaire, non-autonome et fonctionnant en régime permanent harmonique.

1. Introduction

La théorie des quadripôles en sens restreint (QSR) a constitué un instrument extrêmement utile pour aborder un grand nombre de problèmes concernant les circuits électriques. L'augmentation considérable du domaine concernant tels circuits, intervenue dans les dernières décennies, a exigé le perfectionnement de la théorie des quadripôles en introduisant le concept de quadripôle général (QG), proposé par V o r o n o v [2], P o u k h o v [3] et surtout S i g o r s k y [4]. Il s'agit de mettre en évidence, d'une façon explicite, dans les équations d'un quadripôle, outre les signaux aux portes d'accès, et ceux se référant à une porte supplémentaire qui réalise la liaison entre les deux portes d'accès (entrée, sortie).

Si les équation d'un QSR linéaire non-autonome (QSRLN) ont la forme bien connue (par ex. [1]):

$$\begin{bmatrix} \underline{U}_1 \\ \underline{I}_1 \end{bmatrix} = \begin{bmatrix} \underline{A}_{11} & \underline{A}_{12} \\ \underline{A}_{21} & \underline{A}_{22} \end{bmatrix} \begin{bmatrix} \underline{U}_2 \\ \underline{I}_2 \end{bmatrix}, \tag{1}$$

en établissant la liaison entre les signaux aux portes d'accès (Fig. 1 *a*), où $\underline{A}_{ij}$, $(i,j = 1,2)$, sont les paramètres fondamentaux du quadripôle respectif, les équations d'un QG de même linéaire et non-autonome (QGLN), sont celles préconisées par S i g o r s k y (*op. cit.*):

$$\begin{bmatrix} \underline{U}_1 \\ \underline{I}_1 \\ \underline{U}_3 \end{bmatrix} = \begin{bmatrix} \underline{A}_{11} & \underline{A}_{12} & \underline{A}_{13} \\ \underline{A}_{21} & \underline{A}_{22} & \underline{A}_{23} \\ \underline{A}_{31} & \underline{A}_{32} & \underline{A}_{33} \end{bmatrix} \begin{bmatrix} \underline{U}_2 \\ \underline{I}_2 \\ \underline{I}_3 \end{bmatrix}. \tag{2}$$

On observe aisément que dans ces équation interviennent, sauf les signaux aux portes d'accès du quadripôle $(\underline{U}_1, \underline{I}_1, \underline{U}_2, \underline{I}_2)$ et ceux de la porte $(\mathcal{3})$, $(\mathcal{3}')$, qui réalise le

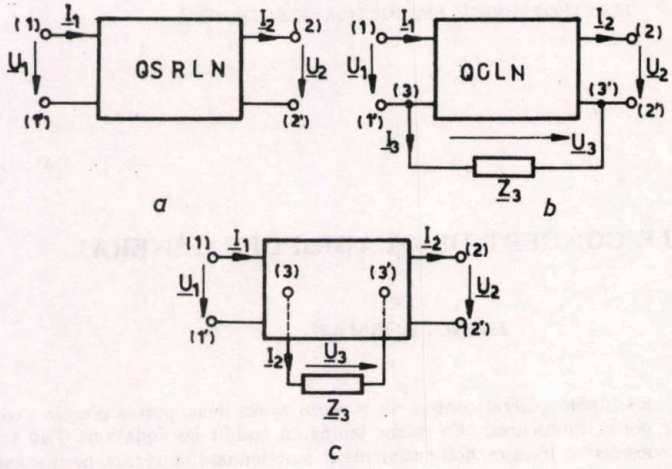

Fig. 1

couplage entre les deux portes d'accès (*1*), (*1'*), respectivement (*2*), (*2'*) (Fig. 1 *b*). Même dans ce cas $\underline{A}_{ij}$, $(i,j=1,2,3)$, représentent les paramètres fondamentaux du quadripôle (évidemment général).

Il est facile à constater que les équations (2) sont valables même pour le quadripôle représenté dans la Fig. 1 *c*, où la porte (*3*), (*3'*) est intérieure à celui-ci. Il s'ensuit que le quadripôle représenté dans la Fig. 1 *b* peut être accepté, aussi, comme un QGLN. On peut considérer ce résultat comme une première extension du concept de quadripôle général, tel qu'il a été introduit par S i g o r s k y.

Une autre extension de ce concept a été proposée dans une Note antérieure [5], où on a défini *le quadripôle en sens élargi* (QSE – Fig. 2).

Tel quadripôles que ceux représentés dans les Figs. 1 *b* et 2 sont utilisés avec succès dans l'étude de certains circuits électroniques ou d'autre nature (v. [6],...,[8]).

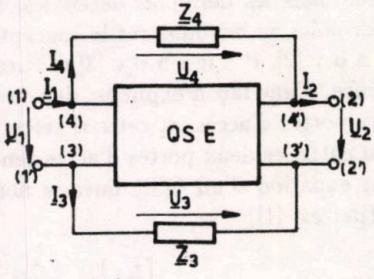

Fig. 2

Les équations d'un QSE ont la forme:

$$(3)\qquad \begin{bmatrix} \underline{U}_1 \\ \underline{I}_1 \\ \underline{U}_3 \\ \underline{U}_4 \end{bmatrix} = \begin{bmatrix} \underline{A}_{11} & \underline{A}_{12} & \underline{A}_{13} & \underline{A}_{14} \\ \underline{A}_{21} & \underline{A}_{22} & \underline{A}_{23} & \underline{A}_{24} \\ \underline{A}_{31} & \underline{A}_{32} & \underline{A}_{33} & \underline{A}_{34} \\ \underline{A}_{41} & \underline{A}_{42} & \underline{A}_{43} & \underline{A}_{44} \end{bmatrix} \begin{bmatrix} \underline{U}_2 \\ \underline{I}_2 \\ \underline{I}_3 \\ \underline{I}_4 \end{bmatrix},$$

où $\underline{A}_{ij}$, $(i,j=1,2,3,4)$, sont, même cette fois, les paramètres fondamentaux. Il est nécessaire à observer que les équations (3) ne sont pas indépendantes car, en régime quasistationnaire (v. Fig. 2):

$$(4)\qquad \underline{U}_1 + \underline{U}_3 - \underline{U}_2 - \underline{U}_4 = 0.$$

Pour passer d'un QSRLN à un QGLN il est nécessaire surtout d'introduire dans les équations de ce dernier les signaux au moins à une porte du quadripôle (évidemment intérieure). Afin de définir, dans la manière la plus générale, un QGLN, il s'avère nécessaire, selon ce qu'on pourra constater dans le § **2** de cette Note, à faire distinction entre les portes d'accès proprement dites du quadripôle ((*1*), (*1'*), respectivement (*2*), (*2'*)) et les autres portes prises en considération.

2. Portes des quadripôles généraux

Si un QSR est caractérisé seulement par deux portes – celle primaire (*1*), (*1'*) et celle secondaire (*2*), (*2'*) – un QG, tel que celui représenté dans les Figs. 1 *b*, 1 *c*, possède et une troisième porte, (*3*), (*3'*), qui n'est pas d'accès et qui remplit la fonction de *porte intérieure*. Dans le cas des QSE (Fig. 2) on peut distinguer, outre les portes d'accès (*1*), (*1'*), respectivement (*2*), (*2'*) et deux portes intérieures, (*3*), (*3'*) et (*4*), (*4'*). Il est nécessaire à faire distinction entre le rôle joué par les deux catégories de portes, par exemple, lors de l'établissement des conditions de réciprocité ou de symétrie du quadripôle, celles-ci caractérisant le quadripôle respectif seulement par rapport aux portes d'accès et pas du tout et par rapport aux celles intérieures Sinon les quadripôles perdraient la signification d'un tel circuit en devenant des triportes, etc.

Si le nombre des portes d'accès d'un QG est de deux (tout comme dans le cas d'un QSR), celui des portes intérieures peut être, au fond, quelconque, pas à tout prix une, comme dans le cas des QGLN (Figs. 1 *b*, 1 *c*) ou deux, pour les QSE (Fig .2). On arrive ainsi, à un élargissement du concept de quadripôle général, dans le sens qu'on peut considérer comme tels quadripôles ceux qui, outre deux portes d'accès, possèdent un nombre arbitraire de portes intérieures. Evidemment les signaux à ces dernières portes vont intervenir, inévitablement, dans les équations des QG.

3. Equations des quadripôles généraux

Si on considère un QG tel que celui représenté dans la Fig. 3, défini comme dans le § **2** de cette Note, ayant, évidemment, deux portes d'accès et $n-2$ portes intérieures, on peut écrire ses équations selon le modèle de celles précédentes (1),...,(3), à savoir:

$$\begin{bmatrix} \underline{U}_1 \\ \underline{I}_1 \\ \underline{U}_3 \\ \vdots \\ \underline{U}_k \\ \vdots \\ \underline{U}_n \end{bmatrix} = [\underline{A}] \begin{bmatrix} \underline{U}_2 \\ \underline{I}_2 \\ \underline{I}_3 \\ \vdots \\ \underline{I}_k \\ \vdots \\ \underline{I}_n \end{bmatrix}, \tag{4}$$

où

$$(5) \qquad [\underline{A}] = \begin{bmatrix} \underline{A}_{11} & \underline{A}_{12} & \cdots & \underline{A}_{1k} & \cdots & \underline{A}_{1n} \\ \underline{A}_{21} & \underline{A}_{22} & \cdots & \underline{A}_{2k} & \cdots & \underline{A}_{2n} \\ \cdots & \cdots & \cdots & \cdots & \cdots & \cdots \\ \underline{A}_{k1} & \underline{A}_{k2} & \cdots & \underline{A}_{kk} & \cdots & \underline{A}_{kn} \\ \cdots & \cdots & \cdots & \cdots & \cdots & \cdots \\ \underline{A}_{n1} & \underline{A}_{n2} & \cdots & \underline{A}_{nk} & \cdots & \underline{A}_{nn} \end{bmatrix}$$

représente la matrice des paramètres fondamentaux du QG. Evidemment on peut considérer un tel quadripôle comme un n-porte, sans négliger la fait que parmi les n portes de celui-ci, seulement deux sont d'accès.

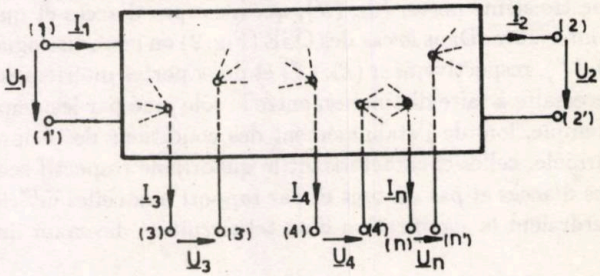

Fig. 3

Si on peut identifier dans la structure d'un QG des contours conducteurs fermés qui contiennent exclusif des portes (d'accès ou intérieures) du celui-ci, alors, en régime quasistationnaire sont satisfaites des relations de la forme:

$$(6) \qquad \sum_{(k)} \underline{U}_p = 0,$$

où p peut prendre quelques unes des valeurs 1, 2,..., n ou toutes et k représente le nombre d'ordre du contour conducteur fermé, $(k = 1, 2, ..., m)$. Dans ces conditions on constate aisément que les équations (4) ne sont pas indépendantes, le nombre des équations indépendantes en étant de $n - m$, $(m < n)$.

Dans quelques travaux antérieurs [9], [10] on a prouvé la possibilité d'attacher à un QGLN du type indiqué dans les Figs. 2*b* ou 2*c*, où à un QSE (Fig. 3), un quadripôle en sens restreint, denommé *primitif* (QSRP). Il s'avère que la connaissance du QSRP est extrèmement utile dans l'étude d'un grand nombre de problèmes, parmi les quels et ceux de la détermination des conditions de réciprocité ou de symétrie d'un QGLN ou QSE. Il y a la possibilité d'établir les équations du QSRP qui peut être attaché à un QG tel que celui représenté dans la Fig. 3. A savoir, considérant le cas simple où les branches (extérieures) incidentes aux portes intérieures (3), (3'); (4), (4'); ...; (n), (n') sont passives on peut écrire les équations:

$$(7) \qquad \underline{U}_3 = \underline{Z}_3\underline{I}_3, \quad \underline{U}_4 = \underline{Z}_4\underline{I}_4, \ldots, \underline{U}_n = \underline{Z}_n\underline{I}_n.$$

En éliminant des équations (4), (6), (7) les tensions $\underline{U}_3, \underline{U}_4, ..., \underline{U}_n$ et les courants $\underline{I}_3, \underline{I}_4, ..., \underline{I}_n$, on obtient un système ayant la forme:

$$\begin{bmatrix} \underline{U}_1 \\ \underline{I}_1 \end{bmatrix} = \begin{bmatrix} \underline{A}'_{11} & \underline{A}'_{12} \\ \underline{A}'_{21} & \underline{A}'_{22} \end{bmatrix} \begin{bmatrix} \underline{U}_2 \\ \underline{I}_2 \end{bmatrix}, \tag{8}$$

où $\underline{A}'_{ij}$, $(i,j = 1,2)$, représentent les paramètres fondamentaux du QSRP. Ils sont fonctions des paramètres fondamentaux $\underline{A}_{ij}$, $(i,j = 1,2,...,n)$, du QG et des impédances $\underline{Z}_3, \underline{Z}_4, ..., \underline{Z}_n$ incidentes aux portes intérieures.

On peut rencontrer des QG tels que celui représenté dans la Fig. 3, dans certains problèmes qui interviennent dans la théorie des circuits.

4. Généralisation d'un théorème

Il est bien connu le théoreme (établi par Blondel) selon le quel on peut écrire les équations (1) d'un QSRLN sous la forme:

$$\underline{U}_1 = \underline{U}_{10} + \underline{U}_{1cc}, \quad \underline{I}_1 = \underline{I}_{10} + \underline{I}_{1cc}, \tag{9}$$

qui mettent en évidence le fait que n'importe quel régime de fonctionnement d'un tel quadripôle peut être considéré comme résultant de la superposition d'un régime à vide ($\underline{U}_2$ ayant la valeur nominale) et d'un régime en court-circuit (avec $\underline{I}_2$ – la valeur nominale).

On peut élargir ce résultat même por le cas, plus général, d'un QG, dans un sens qui sera détaillé ci-dessous.

Soient $\underline{U}^{(k)}_{p0}, \underline{I}^{(k)}_{p0}$ la tension et le courant d'accès à la porte $p \neq k$ quand la porte k fonctionne à vide. Avec des significations analogues on peut définir $\underline{U}^{(k)}_{pcc}, \underline{I}^{(k)}_{pcc}$. Si la porte k est ouverte (fonctionne à vide) on peut écrire les équations (4) sous la forme:

$$\begin{bmatrix} \underline{U}^{(k)}_{10} \\ \underline{I}^{(k)}_{10} \\ \underline{U}^{(k)}_{30} \\ \vdots \\ \underline{U}_k \\ \vdots \\ \underline{U}^{(k)}_{n0} \end{bmatrix} = [\underline{A}] \begin{bmatrix} \underline{U}^{(k)}_{20} \\ \underline{I}^{(k)}_{20} \\ \underline{I}^{(k)}_{30} \\ \vdots \\ 0 \\ \vdots \\ \underline{I}^{(k)}_{n0} \end{bmatrix}, \tag{10}$$

tandis que lorsque la même porte est en court-circuit les équations du QG deviennent:

$$\begin{bmatrix} \underline{U}^{(k)}_{1cc} \\ \underline{I}^{(k)}_{1cc} \\ \underline{U}^{(k)}_{3cc} \\ \vdots \\ 0 \\ \vdots \\ \underline{U}^{(k)}_{ncc} \end{bmatrix} = [\underline{A}] \begin{bmatrix} \underline{U}^{(k)}_{2cc} \\ \underline{I}^{(k)}_{2cc} \\ \underline{I}^{(k)}_{3cc} \\ \vdots \\ \underline{I}_k \\ \vdots \\ \underline{U}^{(k)}_{ncc} \end{bmatrix}. \tag{11}$$

Vu que le QG considéré est linéaire (QGL) on peut appliquer le théorème de la superposition et effectuant la somme des relations (10) et (11) on obtient:

$$(12)\qquad \begin{bmatrix} \underline{U}_{10}^{(k)} + \underline{U}_{1cc}^{(k)} \\ \underline{I}_{10}^{(k)} + \underline{I}_{1cc}^{(k)} \\ \underline{U}_{30}^{(k)} + \underline{U}_{3cc}^{(k)} \\ \vdots \\ \underline{U}_k \\ \vdots \\ \underline{U}_{n0}^{(k)} + \underline{U}_{ncc}^{(k)} \end{bmatrix} = [\underline{A}] \begin{bmatrix} \underline{U}_{20}^{(k)} + \underline{U}_{2cc}^{(k)} \\ \underline{I}_{20}^{(k)} + \underline{I}_{2cc}^{(k)} \\ \underline{I}_{30}^{(k)} + \underline{I}_{3cc}^{(k)} \\ \vdots \\ \underline{I}_k \\ \vdots \\ \underline{I}_{n0}^{(k)} + \underline{I}_{ncc}^{(k)} \end{bmatrix}.$$

Si on compare les relations (4) et (12) il résulte que:

$$(13)\qquad \underline{U}_p = \underline{U}_{p0}^{(k)} + \underline{U}_{pcc}^{(k)}, \quad \underline{I}_p = \underline{I}_{p0}^{(k)} + \underline{I}_{pcc}^{(k)}, \quad (p \neq k).$$

Autrement dit on peut considérer le régime de fonctionnement d'un QGL comme résultant de la superposition d'un régime où la porte k est à vide et d'un régime où la même porte est en court-circuit, la tension $\underline{U}_k$ et le courant $\underline{I}_k$ ayant les valeurs nominales.

Evidemment on peut élargir le résultat obtenu même pour le cas plus général quand plusieures portes intérieures fonctionnent à vide ou en court-circuit, en obtenant les relations:

$$(14)\qquad \underline{U}_p = \underline{U}_{p0}^{(k,l,m,...)} + \underline{U}_{pcc}^{(k,l,m,...)}, \quad \underline{I}_p = \underline{I}_{p0}^{(k,l,m,...)} + \underline{I}_{pcc}^{(k,l,m,...)}, \quad (p \neq k, l, m, ...).$$

5. Conclusions

1° On définit le quadripôle général comme un n-porte ayant deux portes d'accès (avec l'extérieur) et $n-2$ portes intérieures. Le nombre minimum des portes intérieures est, évidemment, un, ce dernier cas étant celui étudié par S i g o r s k y (*op. cit*).

2° On établit les équations d'un quadripôle général, linéaire, non-autonome, en régime permanent harmonique.

3° On indique la possibilité d'attacher à un quadripôle général, un quadripôle en sens restreint, denommé primitif.

4° On propose une généralisation d'un quadripôle général linéaire non-autonome, résulté de la superposition d'un régime où la porte k est à vide et d'un régime où la même porte est en court-circuit, la tension $\underline{U}_k$ et la courant $\underline{I}_k$ ayant les valeurs nominales.

Reçue le 8 février 1997

Université Technique „Gh.Asachi", Jassy, Chaire d'Electrotechnique

BIBLIOGRAPHIE

1. Ş o r a C., *Cuadripolul electric*. Ed. Tehnică, Bucureşti, 1964.

2. V o r o n o v R.S., *Théorie générale des quadripôles et des multipôles* (en russe). Ed. Energ. d'Etat, Moscou, 1951.
3. P o u k h o v C.E., *Sur les bases d'une nouvelle théorie des quadripôles* (en russe). Trav. Sci., Inst. Polyt., Lvov, *5* (1949).
4. S i g o r s k y V.P., *Théorie générale des quadripôles*. Ed. Acad. Sci. Ukr., Kiev, 1955.
5. R o s m a n H., B e l a u s D., *Quadripôles linéaires en sens élargi, nonautonomes, en régime permanent harmonique*. Bul. Inst. polit., Iaşi, **XLIII (XLVII)**, *1-2*, s.III (1997) (sous presse).
6. D o b r e S., *Ecuaţiile generatorului Hall şi schemele echivalente în cadrul teoriei cuadripolului general*. Bul. Inst. polit., Timişoara, **14 (28)**, *2*, s. Electrot., 13-18 (1979).
7. Ş o r a C., D o b r e S., *Application of the General Quadripole Theory for the Investigation of Circuits Including a Hall Generator*. Rev. Roum. Sci. Techn., s. Electrot. et Energ., **24**, *1*, 15-22 (1979).
8. D o b r e S., *Analysis of Unidimensional Hall Generator Circuits Based on the General Quadripole Theory*. Bul. Inst. polit., Iaşi, **XXVI (XXX)**, *1-2*, s.III, 17-24 (1980).
9. R o s m a n H., *Sur les conditions de réciprocité et de symétrie d'un quadripôle général non-autonome en régime permanent harmonique*. Bul. Inst. polit., Iaşi, **XL (XLIV)**, *1-4*, s.III, 23-30 (1994).
10. R o s m a n H., *Quelques observations concernant les conditions de symétrie d'un quadripôle général linéaire, non-autonome, en régime permanent harmonique*. Bul. Inst. polit., Iaşi, **XLI (XLV)**, *1-2*, s.III, 15-19 (1995).

ASUPRA CONCEPTULUI DE CUADRIPOL GENERAL

(Rezumat)

Se defineşte cuadripolul general ca fiind un n-port având două porţi de acces (cu exteriorul) şi $n-2$ porţi interioare şi se stabilesc ecuaţiile unui astfel de cuadripol în cazul când acesta este liniar şi neautonom, iar regimul de funcţionare – permanent armonic.

Se indică posibilitatea de a ataşa oricărui cuadripol general astfel definit, un cuadripol în sens restrâns, numit primitiv.

Se extinde la cazul cuadripolilor generali o teoremă relativă la cuadripoli în sens restrâns, privitoare la faptul că orice regim de funcţionare rezultă din suprapunerea unui regim la gol şi a unuia în scurtcircuit.

BULETINUL INSTITUTULUI POLITEHNIC DIN IAŞI
Tomul XLIII (XLVII), Fasc. 3-4, 1997
Secţia III
ELECTROTEHNICĂ. ENERGETICĂ. ELECTRONICĂ

D.C. 538.551.21

COMPUTING DIFFERENTIAL SENSITIVITIES FOR LINEAR CIRCUITS: AN ALTERNATIVE METHOD FOR THE TRANSIENT RESPONSE CASE

BY
RADU URSULEAN

A method for computing the differential sensitivities suitable for any circuit representation is introduced. The method is based on the Jacobian, which is used for obtaining the steady state of the circuit. The only drawback is that sometimes the unknowns may be placed in different matrices.

1. Preliminaries

In what follows a method to compute differential sensitivities of linear circuits for the transient response case will be presented. A method suitable for linear circuits which admit the admittance type representation was given in [1]. The same subject was developed in the time domain in [2] and [3].

We begin from the following observations:

1° In the case of a real circuit only two types of sensitivities are needed: the sensitivity of a voltage due to the variations of all parameters and the sensitivity of all voltages due to the variations of one parameter.

2° To analyse a circuit, first a d.c. analysis is performed; this is the reason of knowing in advance the derivatives of the function of interest with respect to all parameters, also known as Jacobian. The Jacobian is in fact a matrix of sensitivities with respect to all parameters; without it, it is not possible to compute, using numerical methods, the d.c. state of the circuit.

3° In the case of the Jacobian, a column represents the differential sensitivity of all voltages (or currents) with respect to a single parameter; a row represents the differential sensitivities of one voltage (or current) with respect to all parameters.

The following system of linear equations

$$[A]_{(n,n)}[X]_{(n,m)} = [B]_{(n,m)} \tag{1}$$

has the solution

$$[X] = [A]^{-1}[B]. \tag{2}$$

If the j-th column of the $[X]$ matrix is needed, one must multiply it by $[e_j]$, a column vector having all elements zero, except the one in the j place, which is equal to 1:

$$[e_j] = [0, 0, ..., 0, \underset{j}{1}, 0, ..., 0]^{\mathrm{T}}, \tag{3}$$

where T symbolize the transpose. Denoting by $[X]^{\langle *,j\rangle}$ and $[B]^{\langle *,j\rangle}$ the j-th column of the matrices $[X]$ and $[B]$, then

$$[X]^{\langle *,j\rangle} = [X][e_j] = [A]^{-1}[B][e_j] = [A]^{-1}[B]^{\langle *,j\rangle}. \tag{4}$$

In the same manner, if the k-th row of the $[X]$ matrix, denoted by $[X]^{\langle k,*\rangle}$, is needed, let us multiply it by $[e_k]^{\mathrm{T}}$:

$$[X]^{\langle k,*\rangle} = [e_k]^{\mathrm{T}}[X] = [e_k]^{\mathrm{T}}[A]^{-1}[B]. \tag{5}$$

Denoting

$$[y_k]^{\mathrm{T}} = [e_k]^{\mathrm{T}}[A]^{-1}, \tag{6}$$

and transposing (6), we obtain:

$$[A]^{\mathrm{T}}[y_k] = [e_k]. \tag{7}$$

The last equality allows the vector $[y_k]$ to be computed using the transpose of $[A]$, and then to get $[X]^{\langle k,*\rangle}$, multiplying $[y]_k^{\mathrm{T}}$ by $[B]$.

2. The Proposed Method

In what follows we shall use an observation described in [4] and the above mentioned algorithm. We shall also use the Kirchhoff equations and the relation of definition for each circuit element, written for d.c. currents. Formally there is not any difference between this representation and the one involving an operational method which describes an a.c. circuit. In fact, the system of equations can be the one used to get the static functioning point of the circuit.

Let

$$[X_1] = \begin{bmatrix} V_G \\ I_R \end{bmatrix}, \tag{8}$$

$$[X_2] = \begin{bmatrix} V_{TG} \\ I_{LR} \end{bmatrix}, \tag{9}$$

$$[SI] = \begin{bmatrix} E \\ J \end{bmatrix}, \tag{10}$$

$$[W] = \begin{bmatrix} I_G \\ V_R \end{bmatrix}, \tag{11}$$

$$[SC(X_1)] = \begin{bmatrix} E(X_1) \\ J(X_1) \end{bmatrix}, \tag{12}$$

where V_G denotes the voltages across the circuit elements which admit the conductance representation; I_R – the currents flowing through the circuit elements which admit resistance type representation; I_G and V_R – the dual of these quantities; E

and J – independent voltage and current sources; $E(X_1)$ and $J(X_1)$ – the dependent sources.

Using the above notations the equations that describe the circuit are as follows:

$$[X_1] = [A_1][X_2] + [S][SI], \quad (14) \qquad [W] = [H(X_1)][X_1] + [SC(X_1)], \tag{13}$$

$$[0] = [A_1]^{\mathrm{T}}[W] + [A_2][X_2] + [Q][SI], \tag{15}$$

where A_1, S, A_2, Q are given by the circuit topology and $H(X_1)$ is a hybrid matrix due to the combined representation conductances–resistances.

If the parameter of interest is p, then

$$\frac{\mathrm{d}}{\mathrm{d}p}[X_1] = [A_1]\frac{\mathrm{d}}{\mathrm{d}p}[X_2] + [S]\frac{\mathrm{d}}{\mathrm{d}p}[SI], \tag{16}$$

$$\frac{\mathrm{d}}{\mathrm{d}p}[W] = \left(\frac{\partial}{\partial p}[W]\right)_p \frac{\mathrm{d}}{\mathrm{d}p}[X_1] + \left(\frac{\partial}{\partial p}[W]\right)_{[X_1]}, \tag{17}$$

$$[0] = [A_1]^{\mathrm{T}}\frac{\mathrm{d}}{\mathrm{d}p}[W] + [A_2]\frac{\mathrm{d}}{\mathrm{d}p}[X_2] + [Q]\frac{\mathrm{d}}{\mathrm{d}p}[SI]. \tag{18}$$

Substituting $\mathrm{d}[X_1]/\mathrm{d}p$ in (17) and $\mathrm{d}[W]/\mathrm{d}p$ in (18) we get

$$\begin{aligned} &\left[[A_1]^{\mathrm{T}}\left(\frac{\partial}{\partial X_1}\right)_p [A_1] + [A_2]\right]\frac{\mathrm{d}}{\mathrm{d}p}[X_2] = \\ &= -\left[[A_1]^{\mathrm{T}}\left(\frac{\partial}{\partial X_1}\right)_p [S] + [Q]\right]\frac{\mathrm{d}}{\mathrm{d}p}[SI] - [A_1]^{\mathrm{T}}\left(\frac{\partial}{\partial p}[W]\right)_{[X_1]}. \end{aligned} \tag{19}$$

The last equation can be solved in terms of $\mathrm{d}[X_2]/\mathrm{d}p$, as soon as all the matrices of the right term are known, since we supposed the Jacobian was computed in advance. Knowing $\mathrm{d}[X_2]/\mathrm{d}p$ and using (17) and (18), one can compute the matrices of the other sensitivities, namely $\mathrm{d}[X_1]/\mathrm{d}p$ and $\mathrm{d}[W]/\mathrm{d}p$.

If the sensitivity of one variable q_k with respect to all parameters is needed, one must compute the k-th row of the $\mathrm{d}[X_2]/\mathrm{d}p$ matrix. In this view let us solve first the equation:

$$\left[[A_1]^{\mathrm{T}}\left(\frac{\partial}{\partial p}[W]\right)_p [A_1] + [A_2]\right]^{\mathrm{T}} [y_k] = [e_k], \tag{20}$$

and then multiply to the left relation (19) with $[y_k]^{\mathrm{T}}$ to find the needed sensitivities.

Due to the chosen type of representation of the circuit there is a strong possibility to find some of the sensitivities of interest in different matrices; this is the price paid in order to be able to represent any type of circuit elements.

3. Conclusion

The presented method is suitable for calculating sensitivities of voltages and currents for any type of circuit representation. It involves the Jacobian matrix which is supposed to be computed from d.c. analysis. Using simple matrix manipulations any sensitivity of interest can be calculated. The main drawback is that, sometimes, depending on the chosen representation of the circuit, the unknown sensitivities can be found in different matrices.

Received, February 7, 1997

Technical University "Gh.Asachi", Jassy,
Department of General Electrotechnics
and Electrical Machines

REFERENCES

1. V l a c h J., S i n g h a l K., *Computer Methods for Circuit Analysis and Design.* Van Nostrand Reinhold, New York, 1983.
2. C h o j c a n J., I z y d o r c z y k J., *Computer-aided Time Domain Sensitivity Analysis of Linear Networks Using IZTIS Program.* Proc. of Internat. 1989 Brighton Conf. Signals & Systems, AMSE Press, **4**, 239-248.
3. B r a y t o n R.K., S p e n c e R., *Sensitivity and Optimization.* Elsevier Scientific, New York, 1980.
4. B r a n i n F.H., *Network Sensitivity and Noise Analysis Simplified.* IEEE Trans. Circuit Theory, **CT-20**, *3*, 285-288 (1973).

CALCULUL SENZITIVITĂŢII DIFERENŢIALE: O METODĂ ALTERNATIVĂ PENTRU CAZUL REGIMULUI TRANZITORIU

(Rezumat)

Se prezintă o metodă de calcul a senzitivităţilor diferenţiale valabilă pentru orice reprezentare de circuit. Calculul se bazează pe Jacobian, o matrice folosită în analiza punctului static de funcţionare a oricărui circuit. Unicul dezavantaj al metodei constă în faptul că, în unele cazuri, necunoscutele se pot afla în matrici diferite.

BULETINUL INSTITUTULUI POLITEHNIC DIN IAŞI
Tomul XLIII (XLVII), Fasc. 3-4, 1997
Secţia III
ELECTROTEHNICĂ. ENERGETICĂ. ELECTRONICĂ

C.D. 612.392.5

SUR LA POSSIBILITÉ DE RÉALISER L'ÉGALITÉ DES IMPÉDANCES ÉQUIVALENTES À LA PORTE D'ENTRÉE, À VIDE ET EN COURT-CIRCUIT D'UN QUADRIPÔLE GÉNÉRAL LINÉAIRE NON-AUTONOME

PAR
DORIN BELAUS

On détermine la valeur de l'impédance $\underline{Z}_3$ qui assure l'égalité des impédances équivalentes à la porte d'entrée, à vide et en court-circuit, d'un quadripôle général linéaire, non-autonome. Cette situation est réalisable seulement par de tels quadripôles qui sont nonrécipeoques.

1. Introduction

On considère un quadripôle général ayant le schéma proposé par V.P. S i g o r s k y [1], alimenté par la porte d'entrée (*1*), (*1'*), ayant à la porte de sortie (*2*), (*2'*) un récepteur passif dont l'impédance est $\underline{Z}_2$ (Fig. 1 *a*).

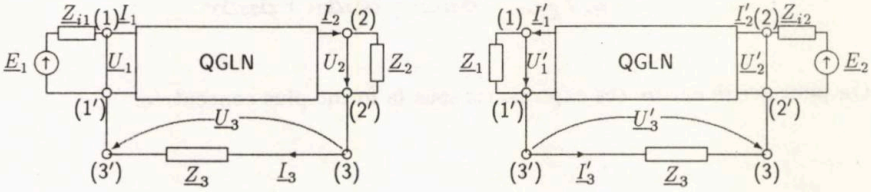

Fig. 1

L'impédance $\underline{Z}_3$, connectée aux bornes (*3*), (*3'*), ne doit pas être considérée comme un récepteur, car elle est un élément constitutif du quadripôle.

L'impédance équivalente à la porte d'entrée (1), $(1')$ est donnée par la formule (v. [2]):

$$(1) \qquad \underline{Z}_{e1} = \frac{(\underline{A}_{11}\underline{Z}_3 + \underline{A}_{13}\underline{A}_{31} - \underline{A}_{11}\underline{A}_{33})\underline{Z}_2 + \underline{A}_{12}\underline{Z}_3 + \underline{A}_{13}\underline{A}_{32} - \underline{A}_{12}\underline{A}_{33}}{(\underline{A}_{21}\underline{Z}_3 + \underline{A}_{23}\underline{A}_{31} - \underline{A}_{21}\underline{A}_{33})\underline{Z}_2 + \underline{A}_{22}\underline{Z}_3 + \underline{A}_{23}\underline{A}_{32} - \underline{A}_{22}\underline{A}_{33}}$$

si on considère le fonctionnement du quadripôle en régime permanent harmonique.

Les régimes de fonctionnement à vide et en court-circuit sont définis pour $\underline{Z}_2 \to \infty$, respectivement pour $\underline{Z}_2 = 0$. Ces régimes présentent de l'intérêt si on veut déterminer les constantes $\underline{A}_{ij}$, $(i,j = 1,2,3)$, de la matrice $[\underline{A}]$, ou bien le comportement du quadripôle dans les régimes extrèmes.

Ainsi on définit l'impédance équivalente à la porte d'entrée, avec la porte de sortie à vide par:

$$(2) \qquad \underline{Z}_{e10} = \left(\frac{\underline{U}_1}{\underline{I}_1}\right)_{\underline{Z}_2 \to \infty} = \frac{\underline{A}_{11}\underline{Z}_3 - \underline{A}_{11}\underline{A}_{33} + \underline{A}_{13}\underline{A}_{31}}{\underline{A}_{21}\underline{Z}_3 - \underline{A}_{21}\underline{A}_{33} + \underline{A}_{23}\underline{A}_{31}}$$

et l'impédance équivalente à la porte d'entrée, avec la porte de sortie en court-circuit, par:

$$(3) \qquad \underline{Z}_{e1cc} = \left(\frac{\underline{U}_1}{\underline{I}_1}\right)_{\underline{Z}_2 = 0} = \frac{\underline{A}_{12}\underline{Z}_3 - \underline{A}_{12}\underline{A}_{33} + \underline{A}_{13}\underline{A}_{32}}{\underline{A}_{22}\underline{Z}_3 - \underline{A}_{22}\underline{A}_{33} + \underline{A}_{23}\underline{A}_{32}}.$$

On peut écrire encore ces expressions sous la forme plus concentrée:

$$(4) \qquad \underline{Z}_{e10} = \frac{\underline{A}_{11}\underline{Z}_3 - \underline{a}_{22}}{\underline{A}_{21}\underline{Z}_3 - \underline{a}_{12}}, \qquad \underline{Z}_{e1cc} = \frac{\underline{A}_{12}\underline{Z}_3 - \underline{a}_{21}}{\underline{A}_{22}\underline{Z}_3 - \underline{a}_{11}},$$

en notant par $\underline{a}_{ij}$, $(i,j = 1,2,3)$, les mineurs du déterminant de la matrice $[\underline{A}]$.

2. Détermination de l'impédance $\underline{Z}_3$ pour laquelle les impédances équivalentes à vide et en court-circuit sont égales

On observe que dans les expressions (4) les impédances équivalentes $\underline{Z}_{e10}$ et $\underline{Z}_{e1cc}$ sont des fonctions complexes de la variable complexe $\underline{Z}_3$. On suppose seulement les cas où $\underline{Z}_{e10}$ et $\underline{Z}_{e1cc}$ sont différentes de zéro, ni tendant vers l'infini. Par suite on peut écrire l'égalité:

$$\underline{Z}_{e10} = \underline{Z}_{e1cc} \tag{5}$$

sous la forme:

$$\frac{\underline{A}_{11}\tilde{\underline{Z}}_3 - \underline{a}_{22}}{\underline{A}_{21}\tilde{\underline{Z}}_3 - \underline{a}_{12}} = \frac{\underline{A}_{12}\tilde{\underline{Z}}_3 - \underline{a}_{21}}{\underline{A}_{22}\tilde{\underline{Z}}_3 - \underline{a}_{11}}. \tag{6}$$

La solution $\tilde{\underline{Z}}_3$ vérifie l'équation du deuxième degré, à coefficients complexes:

$$(\underline{A}_{11}\underline{A}_{22} - \underline{A}_{12}\underline{A}_{21})\tilde{\underline{Z}}_3^2 - (\underline{a}_{11}\underline{A}_{11} + \underline{a}_{22}\underline{A}_{22} - \underline{a}_{21}\underline{A}_{21} - \underline{a}_{12}\underline{A}_{12})\tilde{\underline{Z}}_3 + \underline{a}_{11}\underline{a}_{22} - \underline{a}_{12}\underline{a}_{21} = 0. \tag{7}$$

On peut simplifier cette équation si on observe que:

$$\begin{gathered}\underline{A}_{11}\underline{A}_{22} - \underline{A}_{12}\underline{A}_{21} = |\tilde{\underline{A}}|, \quad \underline{a}_{11}\underline{A}_{11} + \underline{a}_{22}\underline{A}_{22} - \underline{a}_{21}\underline{A}_{21} - \underline{a}_{12}\underline{A}_{12} = |\underline{A}| + \underline{A}_{33}|\tilde{\underline{A}}|, \\ \underline{a}_{11}\underline{a}_{22} - \underline{a}_{12}\underline{a}_{21} = \underline{A}_{33}|\underline{A}|,\end{gathered} \tag{8}$$

où $|\tilde{\underline{A}}|$ est le déterminant de la matrice fondamentale du quadripôle en sens restreint et $|\underline{A}|$ – le déterminant de la matrice du quadripôle général. Par suite on peut écrire l'équation (7) sous la forme:

$$|\tilde{\underline{A}}|\tilde{\underline{Z}}_3^2 - (|\underline{A}| + \underline{A}_{33}|\tilde{\underline{A}}|)\tilde{\underline{Z}}_3 + \underline{A}_{33}|\underline{A}| = 0, \tag{9}$$

ayant les racines:

$$\tilde{\underline{Z}}_3^{\prime,\prime\prime} = \frac{|\underline{A}| + \underline{A}_{33}|\tilde{\underline{A}}| \pm \sqrt{(|\underline{A}| + \underline{A}_{33}|\tilde{\underline{A}}|)^2 - 4\underline{A}_{33}|\underline{A}||\tilde{\underline{A}}|}}{2|\tilde{\underline{A}}|} =$$

(10)

$$= \frac{|\underline{A}| + \underline{A}_{33}|\tilde{\underline{A}}| \pm (|\underline{A}| - \underline{A}_{33}|\tilde{\underline{A}}|)}{2|\tilde{\underline{A}}|},$$

à savoir:

(11) $$\tilde{\underline{Z}}_3^{\prime} = \underline{A}_{33}, \qquad \tilde{\underline{Z}}_3^{\prime\prime} = \frac{|\underline{A}|}{|\tilde{\underline{A}}|}.$$

La première solution n'est pas acceptable car, vu que $\underline{U}_3 = \underline{Z}_3\underline{I}_3$, la dernière des equations du QGLN [1]:

(12) $$\underline{U}_3 = \underline{A}_{31}\underline{U}_2 + \underline{A}_{32}\underline{I}_2 + \underline{A}_{33}\underline{I}_3,$$

conduit à

(13) $$\underline{A}_{31}\underline{U}_2 + \underline{A}_{32}\underline{I}_2 = 0.$$

Or, compte tenu que $\underline{Z}_2 = \underline{U}_2/\underline{I}_2$, peut avoir n'importe quelle valeur satisfaisant seulement la restriction $\Re e(\underline{Z}_2) \geq 0$, il s'ensuit que la relation (13) est valable seulement si $\underline{A}_{31}=0$, $\underline{A}_{32}=0$. Il est facile à constater que dans ce cas même $\underline{A}_{33}=0$ car si on se réfère au régime en courtcircuit avec $\underline{U}_2=0$, $\underline{U}_3=0$ il résulte de (12) que $\underline{A}_{32}\underline{I}_2 + \underline{A}_{33}\underline{I}_3=0$; compte tenu que $\underline{A}_{32}=0$ on déduit que dans ce cas est nécessaire que $\underline{A}_{33}$ soit nul.

On peut considèrer les QGLN dont les paramètres fondamentaux $\underline{A}_{31}$, $\underline{A}_{32}$, $\underline{A}_{33}$ sont nuls comme des quadripôles dégénéres de sorte que dans leur cas il n'est plus possible de les associer à des quadripôles (en sens réstreint) primitifs [3].

En même temps il faut observer que la seule solution acceptable de l'équation (7), à savoir $\underline{\tilde{Z}}_3'' = |\underline{A}|/|\underline{\tilde{A}}|$ (v. (11_2)), est spécifique aux quadripôles **nonrèciproques**. En effet si le quadripôle est réciproque [3], $|\underline{\tilde{A}}|=1$ et $|\underline{A}|=\underline{A}_{33}$, ce qui conduit à $\underline{\tilde{Z}}_3''=\underline{A}_{33}=\underline{\tilde{Z}}_3'$, valeur inacceptable comme on l'a prouvé ci-dessus. Par conséquent se sont seulement les QGLN nonréciproques qui rèalisent l'égalité des impédances équivalentes à vide et en court-circuit ($\underline{Z}_{e10}= \underline{Z}_{e1sc}$). Tels QGLN s'avèrent utils dans l'étude des quadripôles unidirectionnels ainsi qu'on le va prouver dans une Note subséquente.

Si on introduit la valeur (11_2) de l'impédance $\underline{\tilde{Z}}_3''$ dans l'une des expressions (2) ou bien (3) on obtient:

$$(14)\quad \underline{Z}_{e10}'' = \underline{Z}_{e1sc}'' = \frac{\underline{A}_{11}|\underline{A}| - \underline{a}_{22}|\underline{\tilde{A}}|}{\underline{A}_{21}|\underline{A}| - \underline{a}_{12}|\underline{\tilde{A}}|} = \frac{\underline{A}_{11}\underline{A}_{32} - \underline{A}_{12}\underline{A}_{31}}{\underline{A}_{21}\underline{A}_{32} - \underline{A}_{22}\underline{A}_{32}}, \quad (\underline{A}_{13}\underline{A}_{31} \neq \underline{A}_{11}\underline{A}_{23}).$$

Evidemment on peut étudier le cas similaire d'un quadripôle général linèaire, non-autonome, capable à rèaliser l'équalité des impédances équivalentes à vide et en court-circuit lorsqu'il est alimenté en sens inverse (par la porte (2), $(2')$). Dans ce cas il est facile à constater que

$$(15)\quad \underline{Z}_{e20}'' = \underline{Z}_{e2sc}'' = \frac{\underline{A}_{22}|\underline{A}| - \underline{a}_{11}|\underline{\tilde{A}}|}{\underline{A}_{21}|\underline{A}| - \underline{a}_{12}|\underline{\tilde{A}}|} = \frac{\underline{A}_{22}\underline{A}_{13} - \underline{A}_{12}\underline{A}_{23}}{\underline{A}_{21}\underline{A}_{13} - \underline{A}_{11}\underline{A}_{23}}, \quad (\underline{A}_{21}\underline{A}_{32} \neq \underline{A}_{22}\underline{A}_{31}).$$

En tenant compte des conditions de symétrie [3], il en résulte pour un quadripôle nonréciproque, mais symétrique si l'impédance $\underline{Z}_3''$ est donnée par la relation (11_2), sont satisfaites les équalités:

$$(16)\quad \underline{Z}_{e10}'' = \underline{Z}_{e1cc}'' = \underline{Z}_{e20}'' = \underline{Z}_{e2cc}''.$$

3. Détermination du quadripôle général dont les impédances équivalentes à vide et en court-circuit sont égales pour n'importe quelle valeur de l'impédance $\underline{Z}_3$

On poursuit, dans ce qui suit, à établir si l'égalité des impédances équivalentes à vide et en court-circuit est possible pour n'importe quelle valeur de l'impédance $\underline{Z}_3$. Ce cas est possible si les coefficients complexes de l'équation (9) sont simultanément nuls, à savoir:

$$|\tilde{\underline{A}}| = 0, \quad |\underline{A}| = 0. \tag{17}$$

On sait qu'un déterminant est nul lorsque les éléments de deux lignes ou de deux colonnes sont proportionnels. Si les termes des lignes 1 et 2 ou des colonnes 1 et 2 de la matrice $[\underline{A}]$ sont proportionnels, automatiquement est assurée l'égalité $|\underline{A}|$ 0 et en même temps l'égalité $|\tilde{A}| = 0$. On peut formuler, donc, la proposition suivante:

Si les coefficients $\underline{A}_{ij}$, $(i, j = 1, 2, 3)$, *d'un quadripôle linéaire, général, non-autonome, a les coefficients des deux premières colonnes (ou lignes) de la matrice* $[\underline{A}]$, *proportionnels, les impédances équivalentes à vide et en court-circuit sont toujours égales, indépendemment de la valeur de l'impédance* $\underline{Z}_3$.

Ce résultat est valable même dans le cas où le quadripôle général est alimenté par la porte (2), $(2')$, la porte (1), $(1')$ étant à vide ou en court-circuit.

4. Conclusions

On établit la valeur de l'impédance $\underline{Z}_3$ qui assure l'égalité des impédances équivalentes à vide et en court-circuit d'un quadripôle général linéaire non-autonome. Ce sont seulement des quadripôles nonréciproques qui sont capables à réaliser cette égalité.

L'égalité des impédances équivalentes à vide et en court-circuit est réalisée pour

n'importe quelle valeur de l'impédance $\underline{Z}_3$ si les paramètres fondamentaux $\underline{A}_{ij}$, $(i, j = 1, 2, 3)$, satisfont aux conditions (15).

Reçue le 10 avril 1997

Université Technique „Gh. Asachi", Jassy,
Chaire d'Electrotechnique
générale et Machines électriques

BIBLIOGRAPHIE

1. S i g o r s k y V.P., *Théorie générale des quadripôles* (en russe). Ed. Acad. Sci. Ukraïne, Kiev, 1955.

2. R o s m a n H., *Le domaine d'existence de l'impédance équivalente à la porte d'entrée d'un quadripôle général en régime permanent harmonique.* Mem. secţ. şt., Acad. Română, s. IV, **XI**, *1*, 193-206 (1988).

3. R o s m a n H., *Sur les conditions de réciprocité et de symétrie d'un quadripôle général nonautonome en régime permanent harmonique.* Bul. Inst. pol., Iaşi, **XL (XLIV)**, *1-4*, s. III, 25-30 (1994).

ASUPRA POSIBILITĂŢII DE REALIZARE A EGALITĂŢII IMPEDANŢELOR ECHIVALENTE LA POARTA DE INTRARE A UNUI CUADRIPOL GENERAL LINIAR, NEAUTONOM, LA FUNCŢIONAREA LA GOL ŞI ÎN SCURTCIRCUIT

(Rezumat)

Se demonstrează că este posibilă egalitatea impedanţelor echivalente la poarta de intrare a unui cuadripol general liniar, neautonom, la gol şi în scurtcircuit, pentru o anumită valoare a impedanţei $\underline{Z}_3$. Această egalitate este realizată numai de către cuadripoli nereciproci.

Se determină condiţia ca această egalitate să aibă loc indiferent de valoarea impedanţei $\underline{Z}_3$.

BULETINUL INSTITUTULUI POLITEHNIC DIN IAŞI
Tomul XLIII (XLVII), Fasc. 3–4, 1997
Secţia III
ELECTROTEHNICĂ. ENERGETICĂ. ELECTRONICĂ

D.C. 621.3.014.33

EQUIVALENCE BETWEEN DIFFERENT STRUCTURES OF LINEAR TIME VARYING DISCRETE INFINITE IMPULSE RESPONSE SYSTEMS

BY

VALERIU MUNTEANU and DANIELA TĂRNICERIU

This paper gives a new interpretation for a cascade of two infinite impulse response (IIR) all-pole filters with linear time varying (LTV) parameters and derives some characteristic properties of such architectures. The equivalence between a cascade of two IIR all-pole filters and a new structure, easier to be implemented, is developed. Simulation case studies prove the effectiveness of the proposed equivalence.

1. Introduction

In linear time varying (LTV) digital systems, the synthesis of a filter is one of the most difficult stages of the filter design procedure. In linear time invariant (LTI) systems [1] the realization of a filter that is described by a rational transfer function is a straightforward task. The rational function coefficients and the difference equation ones are identical [2]. In LTV systems [3],...,[5], this approach is called the frozen time approximation (FTA), because at any sampling instant the transfer function is frozen and the coefficients are used in a difference equation at that particular sampling instant. In [6], [7] the difficulty implied by the usage of the FTA has been shown, due to the fact that the authors chose to realize the LTV filter in the direct form 2 (DF2) structure. While this would certainly be a valid approximation, it is easily seen that DF2 structure does not realize the difference equation for a time varying filter. This is because the commutative property of cascaded filter sections, which is the basis for the DF2 structure, does not hold for LTV systems. The problem becomes more complicated when many filters are cascaded. This paper gives a new interpretation for a cascade of two infinite impulse response (IIR) all-pole filters and derives some characteristic properties of such an architecture. The equivalence between a cascade of two IIR all-pole filters and a new structure, easily to implement, is developed. In [8],...,[10] a similar problem, but for linear continuous systems with time varying parameters, has been studied. § **2** establishes the equivalence between different structures of IIR all-pole LTV discrete systems; some particular cases are considered. In § **3** simulation case studies are presented to prove the effectiveness of

the proposed equivalence. § 4 concludes the paper.

2. Equivalence between Structure of Discrete Linear Time Varying IIR Systems

In what follows two LTV discrete IIR all-pole cascaded filters are considered, as shown in Fig. 1. They are described by:

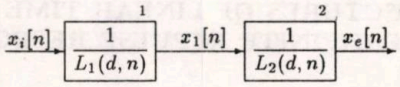

Fig. 1.– A cascade of two LTV discrete IIR all pole filters.

$$L_1(d,n)x_1[n] = x_i[n], \qquad L_2(d,n)x_e[n] = x_1[n], \tag{1}$$

where:

$$L_1(d,n) = \sum_{i=0}^{M} a_i[n]d^i, \qquad L_2(d,n) = \sum_{j=0}^{N} b_j[n]d^j, \tag{2}$$

are linear operators and d is a delay operator with the property:

$$d^i y[n] = y[n-i]. \tag{3}$$

Combining equations (1), one gets:

$$L_1(d,n)L_2(d,n)x_e[n] = x_i[n]. \tag{4}$$

To compose the two linear operators, two new delay operators are introduced. They are denoted by h and p, respectively, so that $d = h + p$ in $L_2(d,n)$ and $d = h$ in $L_1(d,n)$.

The following relations hold:

$$h^k\{a_i[n]x_e[n]\} = a_i[n]x_e[n-k], \tag{5}$$

$$p^k\{a_i[n]x_e[n]\} = a_i[n-k]x_e[n]. \tag{6}$$

With this notation, equation (4) becomes:

$$\left[\sum_{i=0}^{M} a_i[n](p+h)^i \sum_{j=0}^{N} b_j[n]h^j\right] x_e[n] = x_i[n]. \tag{7}$$

Relation (7) can be written as:

$$\left\{\sum_{i=0}^{M} a_i[n]\left[h^i + \sum_{k=1}^{i} C_i^k h^{i-k}p^k\right]\sum_{j=0}^{N} b_j[n]h^j\right\} x_e[n] = x_i[n], \tag{8}$$

where:

$$C_i^k = \frac{i!}{k!(i-k)!}. \tag{9}$$

An equivalent form of relation (8) is:

$$\left[\sum_{j=0}^{N}\sum_{i=0}^{M} a_i[n]b_j[n]h^{i+j}\right] x_e[n] + \left[\sum_{j=0}^{N}\sum_{i=0}^{M}\sum_{k=1}^{i} C_i^k a_i[n]b_j[n-k]h^{i+j-k}\right] x_e[n] = x_i[n]. \tag{10}$$

The first term of relation (10) represents the algebraic product of the operators:

$$L_1(h,n) = \sum_{i=0}^{M} a_i[n]h^i, \qquad L_2(h,n) = \sum_{j=0}^{N} b_j[n]h^j. \tag{11}$$

Let us consider the double sum:

$$S = \sum_{i=1}^{M}\sum_{k=1}^{i} C_i^k a_i[n]b_j[n-k]h^{i-k}, \tag{12}$$

which can be analytically manipulated as:

$$S = \sum_{i=1}^{M} a_i[n]b_j[n-i] + \sum_{i=2}^{M} C_i^{i-1} a_i[n]b_j[n-i+1]h + \tag{13}$$
$$+ \sum_{i=3}^{M} C_i^{i-2} a_i[n]b_j[n-i+2]h^2 + \cdots + \sum_{i=M}^{M} c_i^{i-M+1} a_i[n]b_j[n-i+M-1]h^{M-1}.$$

Assuming formally that:

$$b_j[n+k] = 0, \qquad (k = 0, 1, ..., M), \tag{14}$$

the sums in relation (13) can be considered from 1 to M:

$$S = \sum_{i=1}^{M} a_i[n]b_j[n-i] + \sum_{i=1}^{M} C_i^{i-1} a_i[n]b_j[n-i+1]h + \tag{15}$$
$$+ \sum_{i=1}^{M} C_i^{i-2} a_i[n]b_j[n-i+2]h^2 + \cdots + \sum_{i=1}^{M} c_i^{i-M+1} a_i[n]b_j[n-i+M-1]h^{M-1}.$$

Denoting:

$$\sum_{i=1}^{M} a_i[n]b_j[n-i] = M_j, \quad (j = 0, 1, ..., N), \tag{16}$$

$$b_j[n-i] = b_j^i[n], \tag{17}$$

the following relations can be written:

$$\begin{cases} \dfrac{\mathrm{d}M_j}{\mathrm{d}b_j} = 1!\displaystyle\sum_{i=1}^{M} C_i^{i-1} a_i[n]b_j[n-i+1], \\ \dfrac{\mathrm{d}^2 M_j}{\mathrm{d}b_j^2} = 2!\displaystyle\sum_{i=1}^{M} C_i^{i-2} a_i[n]b_j[n-i+2], \\ \cdots\cdots\cdots\cdots\cdots\cdots\cdots\cdots\cdots\cdots\cdots\cdots\cdots\cdots \\ \dfrac{\mathrm{d}^{M-1} M_j}{\mathrm{d}b_j^{M-1}} = (M-1)!\displaystyle\sum_{i=1}^{M} C_i^{i-M+1} a_i[n]b_j[n-i+M-1]. \end{cases} \tag{18}$$

Substituting (18) in (15), S can be expressed as:

$$S = \sum_{r=0}^{M-1} \frac{1}{r!} \cdot \frac{\mathrm{d}^r M_j}{\mathrm{d}b_j^r} h^r. \tag{19}$$

With (19), relation (10) becomes:

$$L_1(h,n)L_2(h,n)x_e[n] = x_i[n] - \left(\sum_{j=0}^{N} \sum_{r=0}^{M-1} \frac{1}{r!} \cdot \frac{\mathrm{d}^r M_j}{\mathrm{d}b_j^r} h^{r+j} \right) x_e[n]. \tag{20}$$

The relation above is implemented according to Fig. 2.

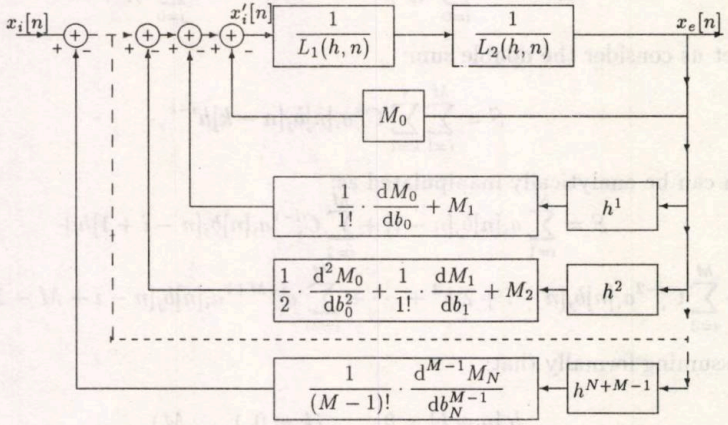

Fig. 2.– An equivalent block diagram for the cascade in Fig. 1.

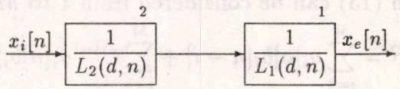

Fig. 3.– Another cascade of two LTV discrete IIR all pole filters.

The block diagrams in Figs. 1 and 2 are equivalent, because for the same input $x_i[n]$ the same output $x_e[n]$ is obtained. If in Fig. 1 the two blocks are interchanged, the structure in Fig. 3 results.

Following a similar procedure, one gets:

$$L_1(h,n)L_2(h,n)x_e[n] = x_i[n] - \left(\sum_{i=0}^{M} \sum_{r=0}^{N-1} \frac{1}{r!} \cdot \frac{\mathrm{d}^r N_i}{\mathrm{d}a_i^r} h^{r+i} \right) x_e[n], \tag{21}$$

where:

$$\sum_{j=1}^{N} b_j[n]a_i[n-i] = N_i, \quad (i = 0, 1, ..., M), \tag{22}$$

$$a_i[n-j] = a_i^j[n]. \tag{23}$$

The structure in Fig. 4 corresponds to relation (21).

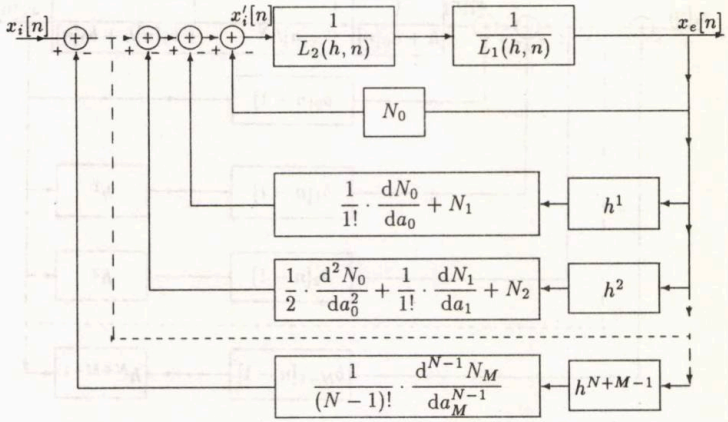

Fig. 4.– An equivalent block diagram for the cascade in Fig. 3.

The expressions $d^r N_i / da_i^r$, $(r=0,1,...,N-1)$, are computed as $d^r M_j / db_j^r$, $(r=0,1,..., M-1)$, from (18) considering that:

$$a_j[n+k]=0, \qquad (k=0,1,...,N). \tag{24}$$

3. Simulation Case Studies

E x a m p l e 1. Let there be a LTV discrete system with the block diagram represented in Fig. 5. The considered system is characterized by:

$$L_1(d,n)=d+a_0[n], \qquad L_2(d,n)=\sum_{j=0}^{N} b_j[n]d^j. \tag{25}$$

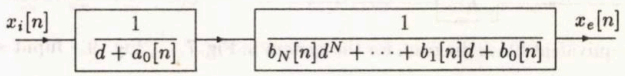

Fig. 5.– Block diagram of the system described in Example 1.

Then:

$$M_j=b_j[n-1], \qquad (j=0,1,...,N), \tag{26}$$

and relation (20) becomes:

$$\sum_{j=0}^{N}\sum_{i=0}^{1} a_i[n]b_j[n]x_e[n-i-j]+\sum_{j=0}^{N} M_j x_e[n-j]=x_i[n]. \tag{27}$$

Considering (26) and (27), the block diagram from Fig. 6 results.

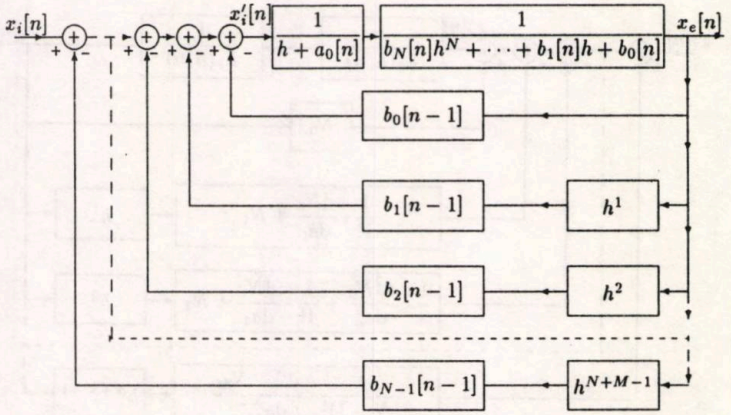

Fig. 6.– The equivalent block diagram for the system in Fig. 5.

E x a m p l e 2. Taking N=1 and $b_1[n]$=1, $a_0[n] = n$, $b_0[n] = n^2 - n + 1$ in Example 1, the block diagrams in Figs. 7 and 8 result. The responses $x_e[n]$ of the blocks depicted in these figures to an amplitude modulated input (presented in Fig. 9), are shown in Figs. 10 *a* and 10 *b*, respectively.

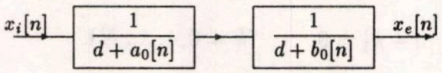

Fig. 7.– Block diagram of the system described in Example 2.

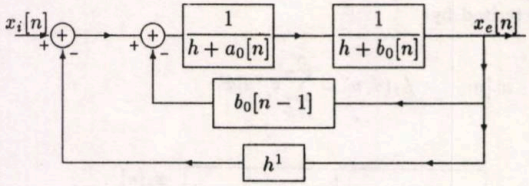

Fig. 8.– The equivalent block diagram for the system in Fig. 7.

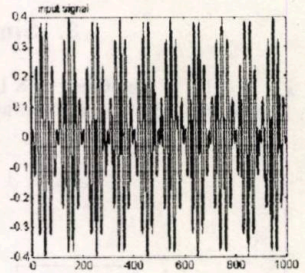

Fig. 9.– Input signal.

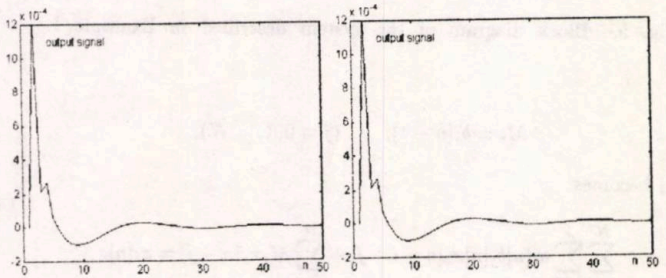

a *b*

Fig. 10.– Response of the block depicted in: *a* – Fig. 7; *b* – Fig. 8.

4. Conclusions

Based on the analysis presented above, the following conclusions may be drawn:

1° The block diagrams in Figs. 2 and 1 are equivalent and also those represented in Figs. 4 and 3, because at the same input signal $x_i[n]$, the same output signal $x_e[n]$ results.

2° The block diagrams in Figs. 2 and 4 differ only by feedback blocks.

3° For the block diagrams in Figs. 2 and 4 one can apply algebra of the discrete linear time invariant systems, because the delay operator h acts only on the output signal.

4° For the block diagrams in Figs. 2 and 4 one can apply the M a s o n's formula as for linear time invariant systems. So, the relationship between the output signal, $x_e[n]$, and the input one, $x_i[n]$, can be derived. Obviously, it is a difference equation of rank $N + M$.

5° The use of the M a s o n's formula in block diagrams in Figs. 2 and 4 allows one to obtain a new way to compose the linear operators.

6° Finite impulse response (FIR) LTV structures can be approached in a similar way.

Received, December 29, 1996

Technical University "Gh.Asachi", Jassy,
Department of Telecommunications

REFERENCES

1. K i r s z e m b l a t A., *Generalized Operational Calculus for Linear Parameter Systems.* Ann. des Telecom., France, *11-12* (1969).
2. P r o a k i s J.G., M a n o l a k i s A., *Digital Signal Processing.* McGraw-Hill, New York, 1990.
3. S t u b b e r u d A., *Linear Time Variable System Synthesis Techniques.* In *Modern Control Systems Theory*, C.T. L e o n d e s, McGraw-Hill, New York, 1965.
4. P e t e r s S.D., F a h m y M.M., *A Design Technique for Recursive Linear Time-varying Digital Filters.* Proc. ISCAS'88, 779-783.
5. L e o u T., A g g a r w a l J.K., *A Structure Independent Approach to the Analysis and Synthesis of Recursive Linear Time Variant Digital Filters.* IEEE Trans. Circ. Syst., **CAS-33**, 687-696 (1986).
6. L e o u T., A g g a r w a l J.K., *Recursive Implementation of LTV Filters – Frozen Time Transfer Function versus Generalized Transfer Function.* Proc. IEEE, **72**, 980-981 (1984).
7. O p p e n h e i m A., S c h a f f e r R., *Discrete Time Signal Processing.* Englewood Clifs, NJ, 1989.
8. M u n t e a n u V., A l e x a n d r u N., *Synthesis of Automatic Linear Systems with Time Varying Parameters* (I). Bul. Inst. polit., Iaşi, **XXI (XXV)**, *3-4*, s.III (1975).
9. M u n t e a n u V., A l e x a n d r u N., *Synthesis of Automatic Linear Systems with Time Varying Parameters* (II). Bul. Inst. polit., Iaşi, **XXII (XXVI)**, *3-4*, s.III (1976).
10. S e b a s t i a n L., M u n t e a n u V., *Considerations sur l'equivalence des structures des systèmes automatiques linéaires à paramètres variables dans le temps.* Automatisme, **XVII**, *1-2* (1972).

ECHIVALENŢA DINTRE DIFERITE STRUCTURI IIR ALE SISTEMELOR LINIAR-VARIANTE ÎN TIMP

(Rezumat)

Este prezentată o nouă interpretare pentru o cascadă de două filtre IIR all-pole, cu parametri liniar varianţi în timp şi sunt prezentate câteva proprietăţi caracteristice ale acestei arhitecturi. Se demonstrează echivalenţa dintre cascada sus amintită şi o nouă structură, uşor de implementat. Studiile de caz au testat corectitudinea echivalenţei propuse.

BULETINUL INSTITUTULUI POLITEHNIC DIN IAŞI
Tomul XLIII (XLVII), Fasc. 3–4, 1997
Secţia III
ELECTROTEHNICĂ. ENERGETICĂ. ELECTRONICĂ

D.C. 621.396.6

IDENTIFICATION OF UNDETECTABLE FAULTS IN COMBINATIONAL CIRCUITS USING MULTIPLE-STEM ANALYSIS

BY
DAMIAN IMBREA, N. COJAN and CLARISSA GÂTLAN

The analysis of reconvergence regions in combinational circuits based on implications of individual stems only, may not identify all redundant lines and gates. Some redundant lines and gates that resist to the single-stem analysis may be identified using multiple-stem analysis. A test pattern generation-based method may be used for the remaining redundancy. In this paper a multiple-stem analysis is introduced.

1. Definitions and Notations

D e f i n i t i o n 1. Let x denote an unspecified value. A path all of whose lines have value x is said to be an *x-path.*

D e f i n i t i o n 2. A path all of whose lines have binary values is said to be a *b-path.*

D e f i n i t i o n 3. Let G be a gate and s a line such that there are at least two disjoint paths from s to G; s is called a *reconvergent fanout stem* or simply a *stem*, and G is called a *reconvergence gate* of s.

A reconvergence gate may have more than one stem, and a stem may have more than one reconvergence gate.

D e f i n i t i o n 4. Let G be a reconvergence gate of stem s. The set of all gates on the paths from s to G (including G) and their input and output lines will be called *reconvergence region of s and G.* This will be denoted $R(s, G)$.

The reconvergence region of a set of stems S and a reconvergence gate G is given by:

$$R(S, G) = \bigcup_{s \in S} R(s, G). \tag{1}$$

D e f i n i t i o n 5. A line j is said to be a *dominator* of a line k if every path from k to the primary outputs passes through j.

Il line j is a dominator of the output of gate G then j dominates G.

D e f i n i t i o n 6. A line j is said to be *redundant* if setting it to binary value v does not change the function realized at the primary outputs of the circuit.

Let l be a dominator of a line j. If setting j to a binary value v does not change the function realized at the line l, then j is a redundant line.

2. Redundancy Identification

The following Lemma gives the basis for our multiple-stem analysis. In Fig. 1, C is a combinational circuit. The primary inputs of C are s, r, and X (vector) and the primary outputs of C are l and Z (vector). Suppose that there exist at least one path between s_1 and l, s_2 and l, r and l, not necessary disjoint; s_1 and s_2 are fanout branches of the stem s.

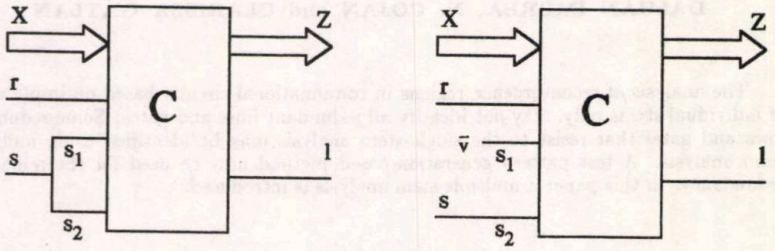

Fig. 1

L e m m a. *Suppose that in the circuit of Fig. 1a, the implication* $(r = u,\ s_2 = v) \Rightarrow (l = w)$ *is true, where* u, v, *and* w *are binary values. If there are no* x*-paths between* s_1 *and* l *while* $r = \overline{u}$, *then setting* s_1 *to the binary value* $\overline{v}$ *(s. Fig. 1b) does not change the function at the output* l.

P r o o f. Let $F(X, r, s_1, s_2)$ be the logic function realized at the output l while s_1 and s_2 are independent lines. We have to prove that

$$F(X, r, s_1, s_2)\,|_{s_1=s_2=s} = F(X, r, s_1, s_2)\,|_{s_1=\overline{v}, s_2=s}, \quad \forall (X, s). \tag{2}$$

Using the Shannon expansion of the function F, relation (2) becomes:

$$\begin{aligned} &\overline{r}\overline{s}F(X,0,0,0) + \overline{r}sF(x,0,1,1) + r\overline{s}F(X,1,0,0) + rsF(X,1,1,1) = \\ &= \overline{r}\overline{s}F(X,0,\overline{v},0) + \overline{r}sF(X,0,\overline{v},1) + r\overline{s}F(X,1,\overline{v},0) + rsF(X,1,\overline{v},1), \\ &\qquad \forall (X, r, s), \end{aligned} \tag{3}$$

$$\begin{cases} F(X,0,0,0) = F(X,0,\overline{v},0), \\ F(X,0,1,1) = F(X,0,\overline{v},1), \\ F(X,1,0,0) = F(X,1,\overline{v},0), \\ F(X,1,1,1) = F(X,1,\overline{v},1), \end{cases} \quad \forall X. \tag{4}$$

The relations (3) and (4) are equivalent. To prove (4) we consider four cases, namely vu=00, 01, 10 and 11.

2.1. Case vu=00

If v=0 then the second and the fourth parts of relation (4) are true. The implication $(r = 0,\ s_2 = 0) \Rightarrow (l = w)$ makes $F(X,0,0,0) = F(X,0,1,0) = w$ for every input vector X. Since there are no x-paths between s_1 and l while r=1, the line s_1 does not influence the output l while r=1. Therefore, $F(X,1,0,0) = F(X,1,1,0)$ for every input vector X.

Similar ways can be used for the others three cases.

O b s e r v a t i o n s. 1° The implication $(r = u,\ s = v) \Rightarrow (l = w)$ is a necessary condition for the implication $(r = u,\ s_2 = v) \Rightarrow (l = w)$ (s. Fig. 1 *a*).

2° The lines setted to binary values by implication $s_1 = \overline{v}$ (including s_1) and dominated by the output l, are redundant ones.

3° The above Lemma may be expanded to a stem s that have more than two fanout branches. Let $\{s_1, s_2, ..., s_p, s_q, ..., s_n\}$ be the fanout branches of the stem s. Suppose that there exist at least one path between s_i and l, for every i=1,...,n. If $(r = u,\ s_1 = s_2 = ... = s_p = v) \Rightarrow (l = w)$ and there are no x-path between s_i and l while $r = \overline{u},\ s_i \in \{s_q, ..., s_n\}$, then setting s_i to the binary value $\overline{v}$ does not change the function on line l.

T h e o r e m. *Let $G(c,i,g)$ be a reconvergence gate of stems s and r, where c, i and g are the controlling value, inversion and output of gate G, respectively. Suppose that there are no paths between s and r, and implication $(s = v,\ r = u) \Rightarrow (j = c)$ is true (v and u are binary values and j is an input of G). A fanout branch s_α of the stem $s(s_\alpha \in \mathbb{R}(s,G))$ setted to $\overline{v}$ does not change the logic function on line g if: a) there is no b-path between s_α and j while $(s = v,\ r = u)$ and b) there is no x-path between s_α and g while $r = \overline{u}$.*

P r o o f. Since $(s = v,\ r = u)$ does not produce any b-path between s_α and j, we may disconnect s_α from s without affecting the implication $(s = v,\ r = u) \Rightarrow (j = c)$. Because there is no x-path between s_α and g while $r = \overline{u}$, we may set the branch s_α to $\overline{v}$ and the function on line g does not change (s. Lemma).

E x a m p l e 1. In the circuit of Fig. 2 *a*, G_6 is a reconvergence gate of the stems s and r. Since $(r = 1,\ s = 1) \Rightarrow (f = 0)$ and there is no b-path between s_2 and f while $(r = 1,\ s = 1)$, and there is no x-path between s_2 and k while r=0, the function on line k does not change if we set s_2=0. Because $(s_2 = 0) \Rightarrow (e_1 = 1)$ and k is a dominator of e_1, line e_1 is redundant and may be removed. The resulting circuit is outlined in Fig. 2 *b*.

The above Theorem may be expanded to a set that has more than two stems in several ways. A possible extension is given by the following

C o r o l l a r y. *Let $G(c,i,g)$ be a reconvergence gate of the stems s, r, p (there are no paths between these stems). Suppose that implications $(s = v, r = u) \Rightarrow (g = c \oplus i)$ and $(r = \overline{u},\ p = w) \Rightarrow (g = c \oplus i)$ are true, where v, u, w are binary values. Let j be an input of G, setted to the binary value c by implication $(s = v,\ r = u)$. A fanout branch s_α of the stem $s(s_\alpha \in \mathbb{R}(s,G))$ setted to $\overline{v}$ does not change the function on line g if: a) there is no b-path between s_α and j while $(s = v,\ r = u)$, and b) there is no x-path between s_α and g while $(r = \overline{u},\ p = \overline{w})$.*

P r o o f. There is no x-path between s_α and g while $r = \overline{u}$. Thus, the conditions of the above Theorem are satisfied.

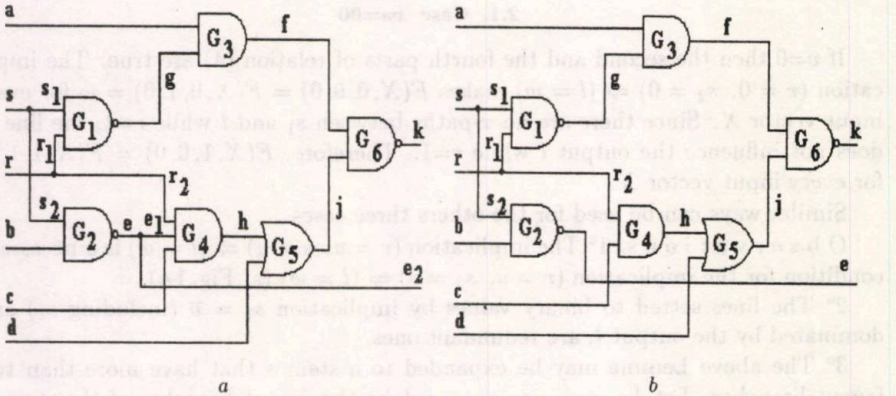

Fig. 2

E x a m p l e 2. In the circuit of Fig. 3 *a*, G_{10} is a reconvergence gate of the stems s, r and p. When $(s = 1, r = 1)$, the input j of gate G_{10} is setted to 0 and there are no b-path between s_2 and j. Also, $(r = 0, p = 1) \Rightarrow (g = 1)$. Since $(r = 0, p = 0) \Rightarrow (f = 1)$, there is no x-path between s_2 and g. Therefore, setting s_2 to 0 does not affect the function on line g. The line f_1 is redundant because $(s_2 = 0) \Rightarrow (f_1 = 1)$ and g is a dominator of f_1. After f_1 is removed, we obtain the circuit of Fig. 3 *b*.

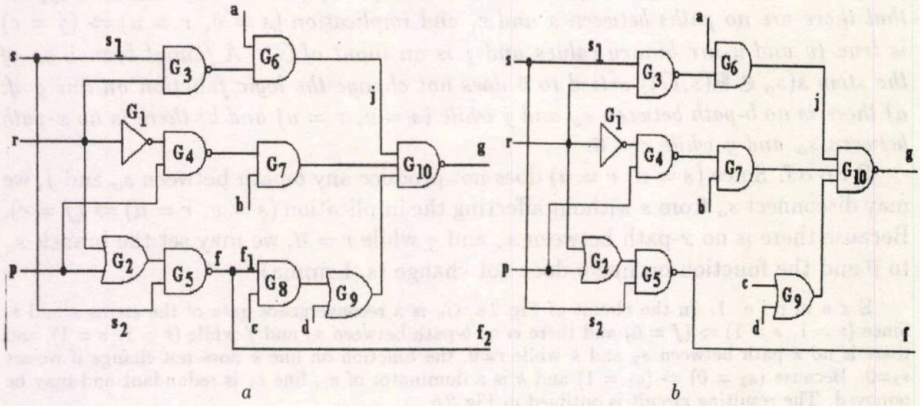

Fig. 3

3. Conclusions

The method of identifying redundancy in combinational circuits presented in this paper uses a multiple-stem analysis and identifies some redundant faults that multiple-stem analysis suggested in [3] cannot. This proposed method may be applied after single-stem analysis of reconvergence regions.

Received, August 21, 1996

Technical University "Gh.Asachi", Jassy,
Department of Applied Electronics

REFERENCES

1. Abramovici M., Breuer M.A., Friedman A.D., *Digital Systems Testing and Testable Design*. Computer Science Press, New York, 1990.
2. Harihara M., Menon P.R., *Identification of Undetectable Faults in Combinational Circuits*. Proc. ICCD, 290-293 (1989).
3. Menon P.R., Ahuja H., Harihara M., *Redundancy Identification and Removal in Combinational Circuits*. IEEE Trans. on CAD of IC's and Systems, **13**, *5*, 646-651 (1994).

IDENTIFICAREA DEFECTELOR NEDETECTABILE ÎN CIRCUITE COMBINAŢIONALE UTILIZÎND ANALIZA STEMURILOR MULTIPLE

(Rezumat)

Analiza regiunilor de reconvergenţă din circuitele combinaţionale, bazată pe implicaţii de stemuri individuale, poate să nu identifice toate conexiunile şi porţile redundante. Unele conexiuni şi porţi redundante rezistente la această analiză pot fi identificate utilizând implicaţii ale mai multor stemuri simultan. Se prezintă o astfel de metodă, mai eficientă decât altele, similare. Cele două exemple prezentate ilustrează modul de identificare a redundanţei cu metoda propusă.

BULETINUL INSTITUTULUI POLITEHNIC DIN IAŞI
Tomul XLIII (XLVII), Fasc. 3–4, 1997
Secţia III
ELECTROTEHNICĂ. ENERGETICĂ. ELECTRONICĂ

D.C. 621.318.7

MODIFIED QUADRATURE MIRROR FILTER BANKS BASED ON ELLIPTIC FILTERS OF EVEN ORDER

BY

DANIELA TĂRNICERIU and VALERIU MUNTEANU

A modified QMF (Quadrature Mirror Filter) bank shown in Fig. 2 is considered, when the filter $H_0(z)$ from the analysis bank is an elliptic one, of even order. Here we prove that the filter $H_1(z)$ from the analysis bank may be expressed according to the components $A(z)$ and $A_*(z)$ of $H_0(z)$, so that $H_0(z)$ and $H_1(z)$ are power complementary. The obtained components, $A(z)$ and $A_*(z)$, are not independent, the relation between them being established in this paper. Furthermore, an equivalent form for the allpass component $A(z)$ will be found. We also show that the polyphase components of $H_0(z)$ cannot be allpass. For the modified QMF bank from Fig. 2, the distortion function is found out. By using the above determined filter $H_1(z)$ in the synthesis bank, the amplitude distortion can be completely eliminated.

1. Introduction

In practice one often encounters signals with energy dominantly concentrated in a particular region of frequency. The signals are not band limited, but still have dominant frequency bands. So, we can split the signal in two frequency bands, using an analysis bank (filters $H_k(z)$ from Fig. 1 with $k = 0, 1$). The signal containing less energy can be encoded with fewer bits than the other. Thus, the signal will be split into two or more subbands, decimate each subband signal and allocate bits for samples in each subband, depending on the energy content. The reconstruction of the full band signal is done using the expanders and synthesis filters ($F_k(z)$ from Fig. 1 with $k = 0, 1$). The expanders restore the sampling rate and the filters $F_k(z)$ eliminate the images. Further, the modified Quadrature Mirror Filter (QMF) bank shown in Fig. 2 is considered, when the filter $H_0(z)$ from the analysis bank is an elliptic one, of even order. It is known that for a filter of even order, its transfer function may be written as [1]:

$$H_0(z) = \frac{A(z) + A_*(z)}{2}, \tag{1}$$

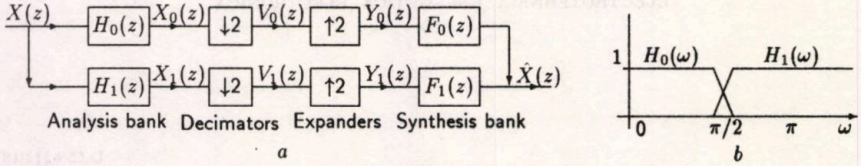

Fig. 1

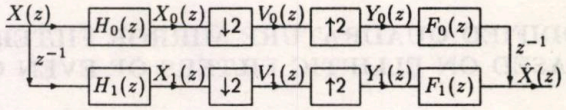

Fig. 2

where $A(z)$ is a unit magnitude allpass function of order $N/2$, with complex coefficients and $A_*(z)$ is obtained by conjugation of the coefficients of $A(z)$. Here we prove that the filter $H_1(z)$ from the analysis bank may be expressed according to the components $A(z)$ and $A_*(z)$ of $H_0(z)$, so that $H_0(z)$ and $H_1(z)$ are power complementary. The obtained components, $A(z)$ and $A_*(z)$, are not independent, the relation between them being established in this paper. Furthemore, an equivalent form for the allpass component $A(z)$ will be found. We also show that the polyphase components of $H_0(z)$ cannot be allpass. For the modified QMF bank from Fig. 2, the distortion function is found out. By using the above determined filter, $H_1(z)$, in the synthesis bank, the amplitude distortion can be completely eliminated.

2. Theoretical Preliminaries

Let us consider a typical QMF bank, as in Fig. 1 *a*, and the frequency characteristics of its component filters, as in Fig. 1 *b*, with

$$H_1(z) = H_0(-z). \tag{2}$$

The reconstructed signal $x(n)$ differs from $x(n)$ due to three reasons: aliasing, amplitude distortion and phase distortion. For obtaining $X(z)$, we get:

$$X_k(z) = H_k(z)X(z), \ (k = 0, 1), \tag{3}$$

$$V_k(z) = \tfrac{1}{2}\,[X_k(z^{1/2}) + Y_k(z^{-1/2})], \ (k = 0, 1), \tag{4}$$

$$Y_k(z) = V_k(z^2) = \tfrac{1}{2}\,[X_k(z) + X_k(-z)], \ (k = 0, 1), \tag{5}$$

$$\hat{X}(z) = F_0(z)Y_0(z) + F_1(z)Y_1(z) = T(z)H(z) + A(z)H(-z). \tag{6}$$

To avoid aliasing caused by the term $H(-z)$, one imposes:

$$A(z) = 0. \tag{7}$$

Thus the following choice cancels aliasing:

$$F_0(z) = H_1(-z), \quad F_1(z) = -H_0(z). \tag{8}$$

If aliasing is canceled, the system becomes linear time invariant (LTI) and has the transfer function, called also *distortion transfer function*, as follows:

$$T(z) = \tfrac{1}{2}\,[H_0(z)F_0(z) + H_1(z)F_1(z)]. \tag{9}$$

Unless $T(z)$ is allpass, (i.e. $|T(e^{j\omega})| = d \neq 0$ for all ω), we say that $X(e^{j\omega})$ suffers from *amplitude distortion*. Similarly, unless $T(z)$ has linear phase, $X(e^{j\omega})$ suffers from *phase distortion*.

If a QMF bank is free from aliasing, amplitude distortion and phase distortion, it is said to have the *perfect reconstruction* propriety. This is equivalent to the condition:

$$\hat{X}(z) = cz^{n_0}X(z), \quad \text{i.e.,} \quad \hat{x}(n) = cx(n - n_0), \quad c \neq 0, \quad c = \text{const.} \tag{10}$$

It is often advantageous to represent the analysis and synthesis banks in terms of *polyphase components* [2]:

$$H_0(z) = E_0(z^2) + z^{-1}E_1(z^2). \tag{11}$$

Using (2), we have:

$$H_1(z) = E_0(z^2) - z^{-1}E_1(z^2). \tag{12}$$

So, $T(z)$ becomes:

$$T(z) = 2z^{-1}E_0(z^2)E_1(z^2). \tag{13}$$

N o t a t i o n s. $(.)^*$ means complex conjugation, $(.)_*$ means the coefficient conjugation and tilde denotes paraconjugation.

D e f i n i t i o n s. $H_0(e^{j\omega})$ and $H_1(e^{j\omega})$ are *power complementary*, if:

$$|H_0(e^{j\omega})|^2 + |H_1(e^{j\omega})|^2 = 1. \tag{14}$$

Using (2) in (14), the *power symmetry* condition is obtained:

$$\tilde{H}_0(z)H_0(z) + \tilde{H}_0(-z)H_0(-z) = 1. \tag{15}$$

3. Basic Results

Let us consider the modified QMF bank shown in Fig. 2. When $H_0(z)$ is an IIR elliptic filter of even order, in [1] it is shown that it can be expressed as (1), where $A(z)$ is a unit magnitude allpass function of order $N/2$, with complex coefficients

and $A_*(z)$ is obtained by conjugation of the coefficients of $A(z)$. If $H_0(z)$ is power symmetric, we will prove first that $H_1(z)$ can be expressed according to $A(z)$ and $A_*(z)$, so that the bank is power complementary. In order to prove that $H_0(z)$ and $H_1(z)$ are power complementary, under the above conditions, we suppose $H_1(z)$ to have the following form:

$$H_1(z) = aA(z) + bA_*(z), \tag{16}$$

with a, b – complex numbers. With (2), (14) becomes:

$$\tilde{H}_0(z)H_0(z) + \tilde{H}_1(z)H_1(z) = 1. \tag{17}$$

Taking into account that:

$$\tilde{H}_0(z) = \frac{\tilde{A}(z) + \tilde{A}_*(z)}{2} = \frac{A_*(z^{-1}) + A(z^{-1})}{2} \tag{18}$$

and

$$\tilde{H}_1(z) = a^*A_*(z^{-1}) + b^*A(z^{-1}), \tag{19}$$

by replacing (1), (16), (18) and (19) in (17), we get:

$$\begin{aligned} &|A(z)|^2\left(aa^* + \tfrac{1}{4}\right) + \tilde{A}(z)\tilde{A}(z^{-1})\left(a^*b + \tfrac{1}{4}\right) + A(z)A(z^{-1})\left(ab^* + \tfrac{1}{4}\right) + \\ &+|A(z^{-1})|^2\left(bb^* + \tfrac{1}{4}\right) = 1. \end{aligned} \tag{20}$$

This implies:

$$aa^* + bb^* = \tfrac{1}{2}, \quad a^*b + \tfrac{1}{4} = 0, \quad ab^* + \tfrac{1}{4} = 0. \tag{21}$$

That is:

$$a = \frac{1}{\mathrm{j}2}, \quad b = -\frac{1}{\mathrm{j}2}. \tag{22}$$

So, $H_1(z)$ becomes:

$$H_1(z) = \frac{A(z) - A_*(z)}{\mathrm{j}2}. \tag{23}$$

If $H_0(z)$ is an elliptic lowpass filter, than $H_0(-z)$ is an elliptic highpass one and:

$$|H_1(e^{\mathrm{j}\omega})|^2 = |H_0(-e^{\mathrm{j}\omega})|^2. \tag{24}$$

From the uniqueness property of the elliptic filter [2], we get:

$$H_1(z) = \pm H_0(-z). \tag{25}$$

Under the above condition we can prove that $A(z)$ and $A_*(z)$ are not independent, the relation between them being established in what follows. Substituting $H_0(z)$ and $H_1(z)$ in (25) we get:

$$\frac{A(z) - A_*(z)}{\mathrm{j}2} = \pm\frac{A(-z) - A_*(-z)}{2}. \tag{26}$$

Denoting by a_k and a_{k^*} the coefficients of $A(z)$ and $A_*(z)$, respectively, by identification in (26) taken with sign "+", the coefficients of the even powers result:

$$a^*_{2k} = a_{2k}\frac{1-\mathrm{j}}{1+\mathrm{j}} = -\mathrm{j}a_{2k}. \tag{27}$$

By identification of the odd powers, it results:

$$a^*_{2k+1} = \mathrm{j}a_k. \tag{28}$$

From (27) and (28) we get:

$$A_*(z) = -\mathrm{j}A(-z). \tag{29}$$

Following a similar way for the "–" sign in (26), we have:

$$A_*(z) = \mathrm{j}A(-z). \tag{30}$$

Relations (29) and (30) may be compactly written as:

$$A_*(z) = \pm\mathrm{j}A(-z). \tag{31}$$

Because $A(z)$ is an allpass filter, it can be expressed as [3]:

$$A(z) = c_0\prod_{k=1}^{N}\frac{-\alpha^*_k + z^{-1}}{1-\alpha_k z^{-1}}, \tag{32}$$

with $|c_0| = 1$, thus $c_0 = \mathrm{e}^{\mathrm{j}\omega_c}$ and α_k are the poles of the filter. Substituting (32) in (31), after few mathematical manipulations, we get:

$$-\alpha_k = \alpha^*_k, \tag{33}$$

that is:

$$\alpha_k = \mathrm{j}\beta_k, \qquad \omega_c = \pm\frac{\pi}{4}. \tag{34}$$

So, $A(z)$ may be written as:

$$A(z) = \mathrm{e}^{\pm\mathrm{j}\frac{\pi}{4}}\prod_{k=1}^{N}\frac{-\mathrm{j}\beta_k + z^{-1}}{1+\mathrm{j}\beta_k z^{-1}}, \tag{35}$$

with $\beta_k \in [-1, 1]$, because $j\beta_k$ represents a pole.

In what follows we show that the polyphase components of $H_0(z)$ cannot be allpass, unlike the filter is of odd order. Using (1), (2), (11) and (12), we get:

$$2E_0(z^2) = \frac{A(z) + A_*(z)}{2} + \frac{A(z) - A_*(z)}{j2}, \tag{36}$$

that is:

$$E_0(z^2) = c_0 A(z) + c_0^* A_*(z), \tag{37}$$

where $A(z)$ and $A_*(z)$ are allpass functions and:

$$c_0 = \tfrac{1}{4}(1 - j). \tag{38}$$

In a similar way we prove that:

$$E_1(z^2) = c_1 A_1(z) + c_1^* A_{1*}(z), \tag{39}$$

with $A_1(z)$ and $A_{1*}(z)$ allpass and:

$$c_1 = \tfrac{1}{4}(1 + j). \tag{40}$$

It is known [2] that a sum of two allpass terms is not allpass, unless the terms are the same excepting a constant. Thus, because the polyphase components are sums of two allpass terms, they cannot be allpass. Further, the distortion function will be determined. With $H_1(z)$ as above obtained, the amplitude distortion has been eliminated. The complete QMF bank can be drawn in terms of $A(z)$, with reduced number of multiplications per unit (MPU) required to carry out the analysis bank. For the modified QMF bank from Fig. 1, aliasing is avoided for the following choice of filters:

$$H_1(z) = H_0(-z), \quad F_0(z) = H_0(z), \quad F_1(z) = H_1(z). \tag{41}$$

For the above bank, the intermediate signals are:

$$X_0(z) = H_0(z)X(z), \tag{42}$$

$$X_1(z) = z^{-1}H_1(z)X(z), \tag{43}$$

$$V_k(z) = \tfrac{1}{2}[X_k(z^{1/2}) + X_k(z^{-1/2})], \quad (k = 0, 1), \tag{44}$$

$$Y_k(z) = V_k(z^2) = \tfrac{1}{2}[X_k(z) + X_k(-z)], \quad (k = 0, 1), \tag{45}$$

$$Y_0(z) = V_0(z^2) = \tfrac{1}{2}[X(z)H_0(z) + X(-z)H_0(-z)], \tag{46}$$

$$Y_1(z) = V_1(z^2) = \tfrac{1}{2}[z^{-1}X(z)H_1(z) - z^{-1}X(-z)H_1(-z)], \tag{47}$$

$$\hat{X}(z) = z^{-1}F_0(z)Y_0(z) + F_1(z)Y_1(z) = T(z)H(z) + A(z)H(-z). \tag{48}$$

Substituting (46) and (47) in (48), we get:

$$A(z) = \tfrac{1}{2}z^{-1}[H_0(-z)F_0(z) - H_1(-z)F_1(z)], \tag{49}$$

$$T(z) = \tfrac{1}{2}z^{-1}[H_0(z)F_0(z) + H_1(z)F_1(z)]. \tag{50}$$

Having in view (41), it results:

$$A(z) = 0. \tag{51}$$

Thus, the system is free from aliasing. With (1) and (41), (50) becomes:

$$T(z) = \tfrac{1}{2}z^{-1}A(z)A_*(z). \tag{52}$$

Considering (31) and the fact that $A(z)$ and $A(-z)$ are allpass functions, it results:

$$|T(z)| = \text{const.} \tag{53}$$

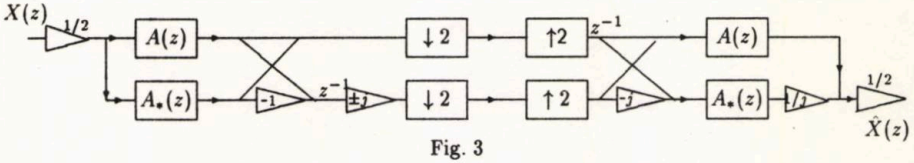

Fig. 3

So, the amplitude distortion is eliminated. The structure of the modified QMF bank in terms of $A(z)$ is shown in Fig. 3. If N denotes the even order of the filter, MPUs in the initial bank (Fig. 1) is $8N$ and MPUs from the modified bank in Fig. 1 is $4N + 8$, for complex coefficients.

4. Conclusions

A modified QMF bank with the filter $H_0(z)$ from the analysis bank being an elliptic one, of even order, is considered. For this case we prove that the filter $H_1(z)$ from the analysis bank may be expressed as function of the components $A(z)$ and $A_*(z)$ of $H_0(z)$, so that $H_0(z)$ and $H_1(z)$ are power complementary. The obtained components, $A(z)$ and $A^*(z)$, are not independent, the relation between them was been established in this paper. Furthermore, an equivalent form for the allpass component $A(z)$ was given. We have shown that the polyphase components of $H_0(z)$ cannot be allpass. For the modified QMF bank from Fig. 1, the distortion function was been found out. By using the determined filter $H_1(z)$ in the synthesis bank, the amplitude distortion can be completely eliminated. The structure of the modified QMF bank in terms of $A(z)$ results in less MPUs than the typical one.

Received, March 20, 1996

Technical University "Gh.Asachi", Jassy,
Department of Telecommunications

REFERENCES

1. Vaydianathan P.P., Nguyen T.Q., Doganata Z., Saramaki T., *Improved Technique for Design of Perfect Reconstruction FIR QMF Banks with Lossless Polyphase Matrices.* IEEE Trans. on Acoustics, Speech and Signal Proc., **ASSP-37**, 1042-1056 (1989).
2. Vaydianathan P.P., *Multirate Systems and Filter Banks.* Prentice Hall, Englewood Cliffs, New Jersey, 1993.
3. Tărniceriu D., Grigoraş V., *Sinteza filtrelor numerice.* Ed. „Gh. Asachi", Iaşi, 1995.

BANCURI QMF MODIFICATE REALIZATE CU FILTRE ELIPTICE DE ORDIN PAR

(Rezumat)

Este analizat un banc de filtre QMF modificat realizat cu filtre eliptice de ordin par. Considerând relaţia (1), se arată că $H_1(z)$ poate fi exprimat în funcţie de componentele lui $H_0(z)$, astfel încât bancul să fie complementar energetic (Power Complementary). Componentele polifazice ale lui $H_0(z)$ nu sunt de tipul trece tot. Se determină funcţia de distorsiune şi se arată că distorsiunile de amplitudine pot fi complet eliminate folosind filtrul $H_1(z)$ determinat.

4. Simulations de l'exploration d'un ellipsoïde avec la sonde tournante

Soit un ellipsoïde $E(x,y,z)$ défini par son centre $C(x_0,y_0,z_0)$, ses paramètres a,b,c et les angles d'Euler α,β,γ. Dans un système de coordonnées lié à l'ellipsoïde, $\Re_e(Cx_ey_ez_e)$, ses équations paramétriques sont:

$$E(x_e,y_e,z_e):\begin{cases} x_e = a\cos\theta\cos\varphi, & 0\le\theta\le\pi,\\ y_e = b\sin\theta, & 0\le\varphi\le 2\pi,\\ z_e = c\cos\theta\sin\varphi. \end{cases} \tag{11}$$

L'équation cartésienne implicite de l'ellipsoïde, dans le même système, a la forme:

$$\frac{x_e^2}{a^2}+\frac{y_e^2}{b^2}+\frac{z_e^2}{c^2}=1. \tag{12}$$

En supposant que la surface d'exploration, $S(x,y,z)$, intersecte à chaque instant l'ellipsoïde $E(x,y,z)$, nous allons déterminer l'intersection des deux surfaces. Afin de mettre l'équation précédente sous la forme cartésienne dans le système $\Re(Oxyz)$, on part de la relation:

$$\begin{bmatrix} x\\ y\\ z\end{bmatrix} = R\begin{bmatrix} x_e\\ y_e\\ z_e\end{bmatrix}+\begin{bmatrix} x_0\\ y_0\\ z_0\end{bmatrix}, \tag{13}$$

où R représente la matrice de rotation. R peut être exprimée en fonction des angles d'Euler α,β,γ, en considérant les rotations autour des axes OX,OY,OZ:

$$R = R_{\gamma|_{Oz}}R_{\beta|_{Oy}}R_{\alpha|_{Ox}}, \tag{14}$$

(15)
$$R=\begin{bmatrix}\cos\gamma & -\sin\gamma & 0\\ \sin\gamma & \cos\gamma & 0\\ 0 & 0 & 1\end{bmatrix}\cdot\begin{bmatrix}\cos\beta & 0 & \sin\beta\\ 0 & 1 & 0\\ -\sin\beta & 0 & \cos\beta\end{bmatrix}\cdot\begin{bmatrix}1 & 0 & 0\\ 0 & \cos\alpha & -\sin\alpha\\ 0 & \sin\alpha & \cos\alpha\end{bmatrix}=\begin{bmatrix}R_{00} & R_{01} & R_{02}\\ R_{10} & R_{11} & R_{12}\\ R_{20} & R_{21} & R_{22}\end{bmatrix},$$

où R_{mn} sont les éléments de la matrice de rotation.

La solution de l'équation matricielle (13) par rapport aux coordonnées x_e,y_e,z_e est:

$$\begin{bmatrix} x_e\\ y_e\\ z_e\end{bmatrix} = R^{-1}\begin{bmatrix} x-x_0\\ y-y_0\\ z-z_0\end{bmatrix} = f\left(\begin{bmatrix} x\\ y\\ z\end{bmatrix}\right), \tag{16}$$

où:

$$R^{-1}=R^{-1}_{\alpha|_{Ox}} * R^{-1}_{\beta|_{Oy}} * R^{-1}_{\gamma|_{Oz}} = R^T. \tag{17}$$

Les relations (12) et (16) permettent d'obtenir les coefficients de l'équation cartésienne de l'ellipsoïde dans le système $\Re(Oxyz)$:

$$a_1x^2+a_2y^2+a_3z^2+a_4xy+a_5xz+a_6yz+a_7x+a_8y+a_9z+a_{10}=0. \tag{18}$$

L'intersection de la surface d'exploration $S(x,y,z)$ avec l'ellipsoïde $E(x,y,z)$ (Fig. 4) est donnée par la solution du système d'équations:

$$E(x,y,z)=0, \quad S(x,y,z)=0, \tag{19}$$

qui peut être mis, encore, sous la forme:

$$\begin{aligned} &a_1x^2+a_2y^2+a_3z^2+a_4xy+a_5xz+a_6yz+a_7x+a_8y+a_9z+a_{10}=0,\\ &x=\rho\cos\theta\cos\varphi, && 0\le\rho\le D,\\ &y=\rho\sin\theta, && \tfrac{\pi-\theta_b}{2}\le\theta\le\tfrac{\pi+\theta_b}{2},\\ &z=\rho\cos\theta\sin\varphi, && \varphi_0\le\varphi\le\varphi_0+\Delta\varphi. \end{aligned} \tag{20}$$

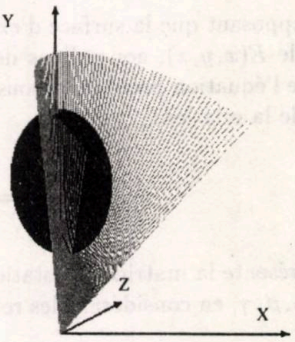

Fig. 4.– Intersection des surfaces $S(x,y,z)$ et $E(x,y,z)$.

En considérant un nombre n d'intervalles temporels dt équidistants, pendant la durée de balayage T_b du secteur échographique ($dt=T_b/n$), on peut écrire la solution discrète du système (20) sous la forme:

$$A\rho^2+B\rho+C=0, \quad A,B,C=f(\varphi(t),\theta(t)), \quad t=idt, \ i=0,\ldots,n-1, \tag{21}$$

où les coefficients A,B,C ont les expressions ci-dessous:

$$\begin{aligned} A=&\,a_1\cos^2\theta(t)\cos^2\varphi(t)+a_2\sin^2\theta(t)+a_3\cos^2\theta(t)\sin^2\varphi(t)+\\ &+a_4\cos\theta(t)\sin\theta(t)\cos\varphi(t)+a_5\cos^2\theta(t)\cos\varphi(t)\sin\varphi(t)+\\ &+a_6\cos\theta(t)\sin\theta(t)\sin\varphi(t),\\ B=&\,a_7\cos\theta(t)\cos\varphi(t)+a_8\sin\theta(t)+a_9\cos\theta(t)\sin\varphi(t),\\ C=&\,a_{10}. \end{aligned} \tag{22}$$

Comme application numérique on a simulé l'intersection d'une sonde tournante avec D=20 mm et θ_b=90° et un ellipsoïde de centre C(10,80,0), ayant les paramètres de forme a=20 mm, b=40 mm, c=25 mm et les angles d'Euler α=0°, β=5°, γ=10°.

La Fig. 5 présente les intersections successives obtenues. La reconstruction 3D de l'ellipsoïde, à partir des différentes sections coniques, est présentée dans la Fig. 6.

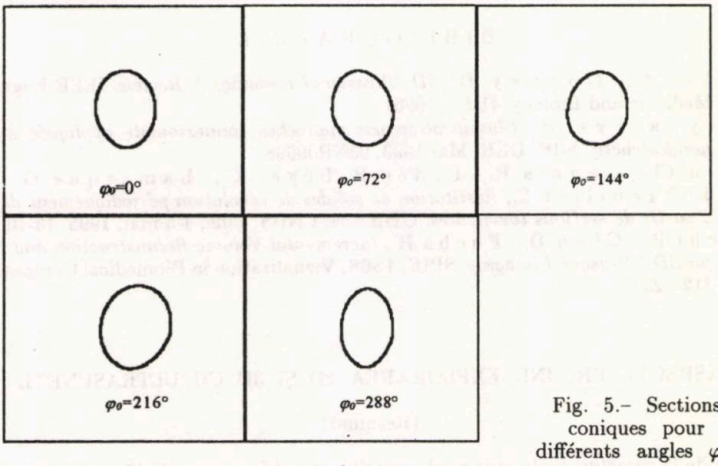

Fig. 5.– Sections coniques pour différents angles φ_0.

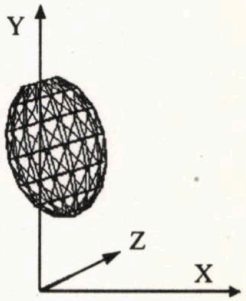

Fig. 6.– Représentation 3D des sections obtenues.

5. Conclusions

Les objets réels examinés par les systèmes à ultrasons sont, évidemment, beaucoup plus complexes que l'ellipsoïde étudié, mais les techniques de reconstruction 3D à partir des sections coniques doivent tenir compte de la complexité de la géométrie du système sonde tournante–objet exploré. Un système de reconstruction 3D en temps réel utilisant des coupes 2D doit être capable de traiter le maximum d'information utile dans un minimum de temps. Pour cela il est envisageable d'utiliser des encadrements elliptiques en 2D et ellipsoïdales en 3D, pour les objets d'intérêt [4], afin de réduire le volume d'informations.

Reçue le 11 avril 1997.

Université Technique „Gh.Asachi", Jassy,
Chaire d'Energetique,
Université d'Orléans (France),
Laboratoire d'Electronique,
Signaux, Images
et
Université Technique „Gh.Asachi", Jassy,
Chaire de Télécommunication

BIBLIOGRAPHIE

1. Fenster A., Downey D., *3D Ultrasound Imaging: A Review.* IEEE Engineering in Medicine and Biology, 41-51 (1996).
2. Lavayssière B., *Classification par approches connexioniste appliquée au contrôle nondestructif.* EdF, DER, Mai 1993, 93NB00098.
3. Bonciu Cl., Canàls R., Lédée R., Léger C., Lamarque G., Thiel J., Treuillet S., *Restitution de solides de révolution périodiquement déformables à partir de sections tournantes.* GDR 134, CNRS, Lille, 4-5 mai, 1995, 13-16.
4. Ohbuchi R., Chen D., Fuchs H., *Incremental Volume Reconstruction and Rendering for 3D Ultrasound Imaging.* SPIE, **1808**, Vizualization in Biomedical Computing, 1992. 312-323.

ASPECTE PRIVIND EXPLORAREA 2D ŞI 3D CU ULTRASUNETE

(Rezumat)

Plecând de la caracteristicile unei sonde rotative cu baleiere secvenţială, sunt studiate analitic şi numeric câteva aspecte ale geometriei sistemului sondă–obiect explorat, cu ajutorul unui volum elipsoidal de încadrare.

BULETINUL INSTITUTULUI POLITEHNIC DIN IAŞI
Tomul XLIII (XLVII), Fasc. 3–4, 1997
Secţia III
ELECTROTEHNICĂ. ENERGETICĂ. ELECTRONICĂ

C.D. 620.179.16

ASPECTS CONCERNANT L'EXPLORATION 2D ET 3D PAR ULTRASONS

PAR
CLAUDIA BONCIU et CRISTIAN BONCIU

En partant des caractéristiques d'une sonde tournante à balayage séquentiel, on étudie les aspects analytiques et numériques du système sonde–objet exploré, en considérant un volume ellipsoïdal d'encadrement.

1. Introduction

Au long du temps, des techniques de plus en plus sophistiquées ont été utilisées dans le cadre de la surveillance des processus industriels et biologiques. L'imagerie ultrasonore occupe dans ce domaine une place privilégiée compte tenu de son caractère nondestructif. C'est une technique en plein développement et ses applications sont nombreuses, car elle permet d'obtenir des images en temps réel. Les études effectuées depuis plusieurs années concernent la mise en oeuvre de méthodes de traitement adaptées aux images issues du contrôle de différents processus [1], [2].

Les principaux problèmes posés par ces images sont leur faible contraste, le bruit important, la variation des dimensions ou le mouvement dans l'espace des objets explorés. La solution de ce type de problèmes nécessite une recherche interdisciplinaire qui concerne l'acoustique, la science des matériaux, l'électronique et les algorithmes de traitement des images. On peut franchir les difficultés d'interprétation des images ultrasonores par une analyse complète du système sonde échographique–objet exploré [3].

Cet article est consacré à la simulation du mouvement 2D et 3D du faisceau ultrasonore, en vue de la reconstruction 3D. Une analyse complète et des simulations numériques concernant un système sonde tournante et un objet elliptique de synthèse sont présentées dans ce qui suit.

2. Encadrement du volume exploré dans le champ de balayage du faisceau ultrasonore

Dans une première étape il est très important d'étudier les possibilités d'exploration d'un volume donné avec une sonde ultrasonore 2D tournante. Dans ce

sens il faut rappeler que le faisceau ultrasonore est soumis à deux mouvements: le balayage et la rotation de la sonde.

Etant données la profondeur d'exploration du faisceau ultrasonore D et l'angle maximum θ_b du secteur échographique, le problème de déterminer les dimensions maximales du volume exploré se pose de manière qu'il puisse être encadré complètement dans l'espace balayé par la sonde.

On définit un repère convenable $\Re(Oxyz)$, tel que Oy représente l'axe de rotation de la sonde (Fig. 1). En considérant: ω_s – la vitesse angulaire de rotation de la sonde autour de son axe, ω_b – la vitesse de balayage du secteur échographique, T_s – la période de rotation de la sonde et T_b – la durée de balayage, avec les notations:

$$(1) \qquad \varphi = \omega_s t + \varphi_0, \quad \omega_s = \frac{2\pi}{T_s}; \qquad \theta = \omega_b t + \frac{\pi - \theta_b}{2}, \quad \omega_b = \frac{\theta_b}{T_b},$$

on peut définir la surface $S(x, y, z)$ d'exploration des ultrasons, pendant la première période de balayage, par les équations paramétriques:

$$(2) \qquad S(x,y,z): \begin{cases} x = \rho\cos\theta\cos\varphi, & 0 \le \rho \le D, \\ y = \rho\sin\theta, & \frac{\pi-\theta_b}{2} \le \theta \le \frac{\pi+\theta_b}{2}, \\ z = \rho\cos\theta\sin\theta, & \varphi_0 \le \varphi \le \varphi_0 + \Delta\varphi, \ \Delta\varphi = \frac{T_b}{T_s}\theta_b, \end{cases}$$

où φ_0 et $\Delta\varphi$ représentent la position initiale du plan de la sonde et, respectivement, l'angle de rotation de la sonde autour de son axe pendant le balayage complet du secteur échographique.

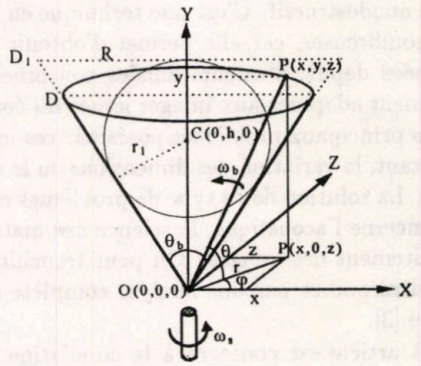

Fig. 1.– Déplacement du faisceau ultrasonore dans le système $\mathcal{R}(Oxyz)$.

Afin de déceler quelques conclusions concernant l'encadrement du volume exploré dans le champ de balayage du faisceau ultrasonore, on accepte une hypothèse simplificatrice en supposant que ce volume peut être inscrit, par exemple, dans une sphère de rayon r_1 et de centre $C(0, h, 0)$ (v. Fig. 1). Compte tenu de cette hypothèse on a les relations:

$$(3) \qquad R = D\,\mathrm{tg}\,\frac{\theta_b}{2}, \qquad (4) \qquad \frac{r_1}{R} = \frac{h}{D_1} = \frac{r_1 + h}{R + D_1} = \frac{D}{R + D_1},$$

d'où on peut exprimer le rayon et l'abscisse du centre de la sphère par les relations:

$$(5) \qquad r_1 = \frac{\sin\frac{\theta_b}{2}}{1+\sin\frac{\theta_b}{2}}D, \quad h = \frac{1}{1+\sin\frac{\theta_b}{2}}D.$$

En considérant les paramètres de la sonde, notamment la profondeur d'exploration des ultrasons, D et l'angle maximum du secteur échographique, θ_b, les relations ci-dessus permettent de calculer les dimensions maximales de la sphère dans laquelle doit être encadré l'objet exploré et, par conséquent, une première estimation des dimensions maximales des objets explorés.

3. Simulations du mouvement 2D et 3D du faisceau ultrasonore

Dans ce qui suit on utilise les notations: $f_b = 1/T_b$ - fréquence de balayage du secteur échographique et $f_s = 1/T_s$ - fréquence de rotation de la sonde. Afin de réaliser le modèle de la surface d'exploration on suppose que le faisceau est déterminé par l'origine $O(0,0,0)$ et son extrémité, $P(x,y,z)$, et qu'il est soumis à deux mouvements: le balayage et la rotation de la sonde (Fig. 1). Ainsi, dans la première partie, ce paragraphe est consacré aux équations des trajectoires $P(x,0,z)$ et, finalement, à la génération des surfaces d'explorations du faisceau ultrasonore. Ces surfaces coniques ont comme sommet l'origine $O(0,0,0)$ et comme base, les trajectoires du point $P(x,y,z)$.

3.1. Cas 2D ($\omega_s = 0$)

Si la sonde est immobile ($\omega_s = 0$), le faisceau ultrasonore se déplace dans un plan Oxy, perpendiculaire au plan Oxz. La trajectoire du point $P(x,y,z)$ de la Fig. 1 représente, dans le plan Oxy, un arc de cercle, pendant que sa projection sur l'axe Ox, $P(x,0,z)$, est linéaire. Les équations paramétriques, en coordonnées polaires, de cette trajectoire linéaire ont la forme:

$$(6) \qquad r = R\left(1-\frac{2}{T_b}t\right) = D\,\mathrm{tg}\,\frac{\theta_b}{2}\left(1-\frac{2}{T_b}t\right), \quad \text{pour } \omega_s = 0;\ \varphi = \varphi_0.$$

En coordonnées cartésiennes, les équations précédentes deviennent:

$$(7) \quad x = r\cos\varphi_0 = D\,\mathrm{tg}\,\frac{\theta_b}{2}\left(1-\frac{2}{T_b}t\right)\cos\varphi_0, \quad z = r\sin\varphi_0 = D\,\mathrm{tg}\,\frac{\theta_b}{2}\left(1-\frac{2}{T_b}t\right)\sin\varphi_0.$$

3.2. Cas 3D ($\omega_s \neq 0$)

Nous allons étudier l'effet du mouvement de rotation de la sonde sur la surface balayée par le faisceau. Si $\omega_s \neq 0$, le faisceau ultrasonore se déplace sur une surface conique, dont le sommet se trouve dans l'origine $O(0,0,0)$ du système $\mathcal{R}(Oxyz)$ et la base est donnée par la trajectoire du point $P(x,y,z)$. Pour déterminer la trajectoire du point $P(x,0,z)$, qui représente la projection du point $P(x,y,z)$ dans le plan Oxz,

nous allons considérer un intervalle de temps égal à la première période de balayage, T_b. En tenant compte du rapport:

$$n = \frac{T_s}{T_b} = \frac{f_b}{f_s}, \tag{8}$$

les coordonnées polaires de la projection du point $P(x, y, z)$ dans le plan Oxz, soit $P(x, 0, z)$, sont:

$$r = R\left(1 - \frac{2}{T_b}t\right) = D \operatorname{tg}\frac{\theta_b}{2}\left(1 - \frac{2}{T_b}\right), \quad \varphi = \omega_s t + \varphi_0 = \frac{2\pi}{nT_b}t + \varphi_0. \tag{9}$$

En coordonnées cartésiennes, les équations paramétriques ont la forme:

$$\begin{cases} x = r\cos(\omega_s t + \varphi_0) = R\left(1 - \frac{2}{T_b}t\right)\cos\left(\frac{2\pi}{nT_b}t + \varphi_0\right), \\ z = r\sin(\omega_s t + \varphi_0) = R\left(1 - \frac{2}{T_b}t\right)\sin\left(\frac{2\pi}{nT_b}t + \varphi_0\right). \end{cases} \tag{10}$$

De la Fig. 2 on peut remarquer que lorsque le rapport $n = f_b/f_s$ augmente, à la limite ($n \to \infty$), la surface d'exploration du faisceau ultrasonore s'approche du plan „méridien". Au contraire, lorsque le rapport n diminue, la surface d'exploration du faisceau s'écarte du plan „méridien" et devient une surface conique, avec un rayon de plus en plus petit.

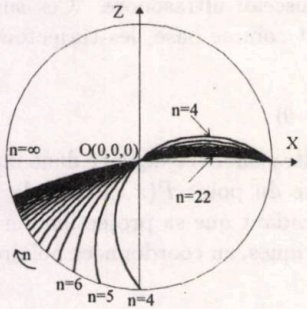

Fig. 2.– Trajectoire du point $P(x, 0, z)$ en fonction de $n = T_s/T_b$, pour une période T_b.

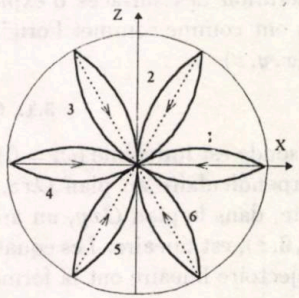

Fig. 3.– Trajectoire du point $P(x, 0, z)$ pour $n = T_s/T_b = 6$ et pour une période T_b.

Dans la Fig. 3 sont présentées les trajectoires du point $P(x, 0, z)$, pendant une rotation complète de la sonde autour de son axe Oy, pour un rapport $n = 6$.

Les surfaces d'exploration du faisceau ultrasonore dans l'espace 3D sont déterminées en considérant que le faisceau a l'origine dans $O(0, 0, 0)$ et la projection de son extrémité, $P(x, y, z)$, dans le plan Oxz, $P(x, 0, z)$, glisse sur une courbe dont la forme est présentée dans la Fig. 2. Ainsi, les surfaces successives de balayage du faisceau ultrasonore sont générées par l'origine $O(0, 0, 0)$ et les trajectoires successives de la Fig. 3.

Il faut souligner que, en raison du fait que la rotation de la sonde n'est pas exactement uniforme en temps, en réalité, les trajectoires correspondantes sont légèrement modifiées par rapport aux celles présentées dans la Fig. 3.

BULETINUL INSTITUTULUI POLITEHNIC DIN IAŞI
Tomul XLIII (XLVII), Fasc. 3–4, 1997
Secţia III
ELECTROTEHNICĂ. ENERGETICĂ. ELECTRONICĂ

D.C. 621.317.761

FREQUENCY-METER WITH MICROPROCESSOR. SOFTWARE ASPECTS. PERIOD-MEASURING WORKING

BY

LAURENŢIU DIMITRIU and LILIANA VORNICU

A frequency-meter with a large range of measuring (0.01 Hz,...,1 MHz), based on the programmable counters utilization, is presented. The main software problems for the period-meter working (0.01 Hz,...,100 Hz) are shown. The used principle allows the substantially reducing of the measuring circuit's working time with the microprocessor, a useful feature in real time applications.

1. Introduction

In some real time applications of microprocessors has be solved the optimal working time problems. This working time can be increased in measurement circuits of process parameters and it could appear the risk of loosing control by the microprocessor.

This kind of situation is presented in the following lines. It is considered a microprocessor system in a specific application, also to measure and to display the frequency of some signals in a large range of values (0.01 Hz,...,1 MHz). The utilization of standard hardware resources allows solving the problem of measuring and frequency display in such a range, but it needs a complex software, increasing significantly microprocessor's working time. For the range of 100 Hz,...,1 MHz a direct frequency measurement method was used. For very low frequency (0.01 Hz,...,100 Hz) the signal's period is measured and the frequency is obtained using a dividing operation [1]. The working time for a dividing subroutine and a hexadecimal to decimal result conversion subroutine can be significant in this situation. To reduce the working time with the microprocessor a specific hardware structure is used, based on the 8253 type programmable counters resources [2], [3]. Finally a simplified software is obtained.

The paper presents specific software for period-measuring working.

2. Working Algorithm with Period Measurement

In Fig. 1 the schematic diagram of the frequency-meter with microprocessor is presented. All specific circuits are shown and the modality of interconnection with the microprocessor system is specified.

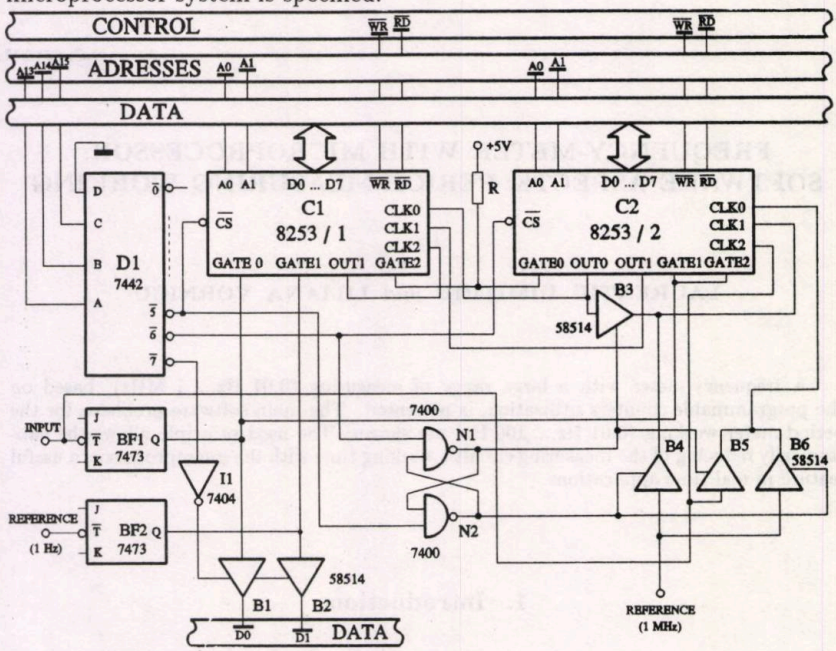

Fig. 1

The programme of period-meter working consists in two distinct blocks. In the first the section COUNTER *0* of $C1$ circuit (8253/1) is controlled to assure period measurement. In the second the sections COUNTER *1* and COUNTER *2* of $C1$ circuit work to achieve the transformation of the period numeric value in frequency value.

All data transfers in the system are effected only on LOW level of GATE control signals of counters, to assure data stability. The commands will be immediately executed when a LOW level of measured signals is detected. How we don't know the necessary time of specific operations, the commands are done immediately when a transition to LOW level is detected. The detection is achieved by comparing the signal value in the testing moment, read from the PORT A, in the memory space at E000H address, with his previous value (obtained in the previous test and memorized), located in a memory identified by PORT P.

Two bits of PORT A and PORT P are interesting: b_0 – containing the logic value of the 0.5 Hz time reference and b_1 – containing the logic value of the pulse signal for which the period are measured. The other bits of PORT P are used for specific decisions, as follows.

The logic diagram of the programme is presented in the Figs. 2 *a* and 2 *b*.

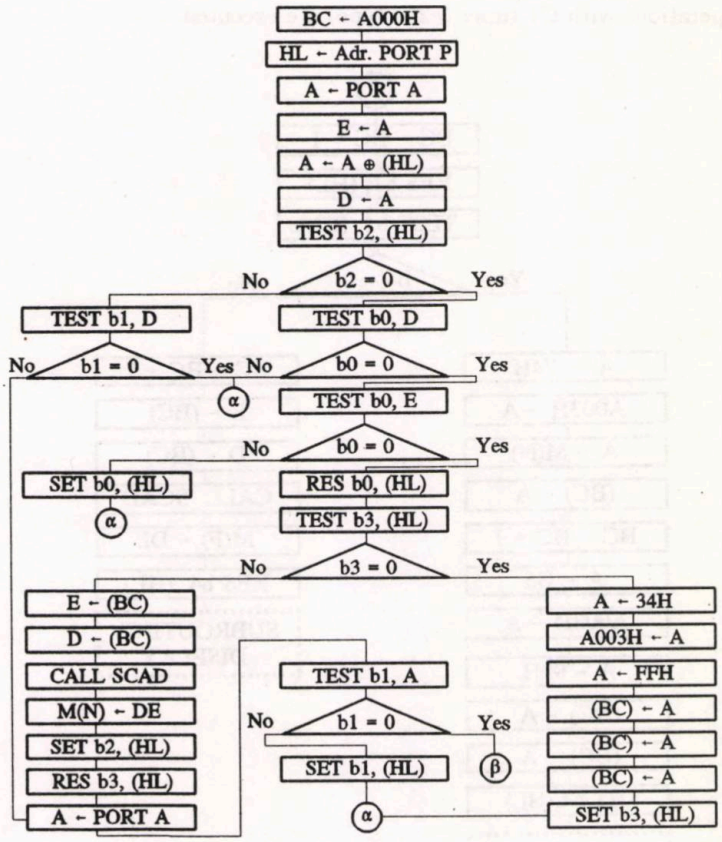

Fig. 2 *a*

In the beginning of the programme, the addresses of used memory locations will be written in specific registers. So, in the BC register is written A000H value, representing the address of the section COUNTER *1* from $C1$ (8253 type), and in HL register the address of PORT P location. The identification of signals level modification in PORT A is done using a XOR – operation with the memorized value of PORT P, the result being placed in D register. If a modification is identified, the bit b_2 of PORT P will be tested. If the bit has logic value "1", this means that a period measurement was done and the conversion to frequency value operation is necessary. If $b_2 = 0$, the period of the signal must be measured.

Then the bit b_0 of D register is tested. If $b_0 = 0$, means that the present value of the signal, reported to the previous value, is unmodified. The situation is not interesting, the system continuing to work in the main programme. If $b_0 = 1$, a modification of measured signal is identified. To see the value of measured signal

the bit b_0 of E register is tested. The logic value "1" is not interesting and a return to main programme is effected. If $b_0 = 0$, the interesting situation, allowing period measuring, is detected. The logic value "0" of bit b_0 is load in PORT P location. Then the operations with $C1$ timer (8253 type) are executed.

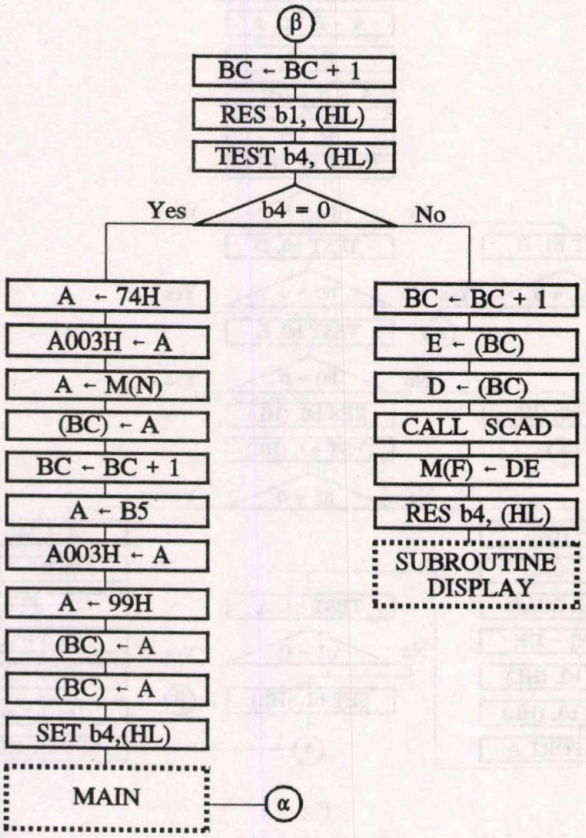

Fig. 2*b*

For a measurement execution, COUNTER *0* section must be first programmed and then loaded with FFFFH initial value. Then the measurement is effected, and finally the content of the section is read. In this way, every measurement begins from the same initial value (FFFFH), to simplify the computing. To respect this operation order, the bit b_3 of PORT P is tested. If $b_3 = 0$, writing operations with the timer are necessary. After these operations, $b_3 = 1$ is written in PORT P. If $b_3 = 1$, means that the clock pulses were counted for a time equal to measured signal period and the result can be read. The content of COUNTER *0* ($C1$) timer is transferred in the DE register. Then a subtracting operation from FFFFH value is effected, using a subroutine (SCAD), the result being loaded in the memory location $M(N)$. The bit

b_2 of PORT P is set to mark the end of period measurement operation and the bit b_3 is reset to signalize the necessity to initialize again the timer COUNTER *0* (*C*1). Then follows the conversion programme from the period to frequency form.

How the counters used to assure the conversion are enabled by 0.5 Hz reference signal, they are commanded only when LOW level is detected. The level is tested using the bit b_1 of PORT A and the commands are initiated using the bit b_1 of PORT P. Two groups of operation are effected: the mode control writing and loading of COUNTER *1* (*C*1) and COUNTER *2* (*C*1) timers, respectively reading of the results to calculate the frequency. To select a specific branch of the programme, the bit b_4 of PORT P is used. If $b_4 = 0$, the control words and necessary initial values of the programmable counters sections are written, respectively: in COUNTER *1* (*C*1) is loaded the determined period value, and in COUNTER *2* (*C*1), the 9999H value. If $b_4 = 1$, the content of COUNTER *2* (*C*1) is read, and using a subtracting operation from 9999H, assured by a subroutine (SCAD), the value of frequency is obtained. To prepare the return in the main programme, the bits b_2 and b_4 of PORT P are reset.

3. Conclusions

Using the circuit shown in the Fig. 1 and a software structured as is shown in the Figs. 2*a* and 2*b*, very low frequency measurement is possible using an extremely reduced working time with the microprocessor. The operations with the microprocessor are only reading, writing, bits testing and manipulation and two subtracting without borrow operations.

Received, October 21, 1996

Technical University "Gh.Asachi", Jassy,
Department of Applied Electronics

REFERENCES

1. V o r n i c u L. *et al., Frequency-meter with Microprocessor.* Bul. Inst. polit., Iaşi, **XLIII (XLVII)**, *1-2*, s.III (1997).
2. C ă p ă ţ î n ă O. *et al., Proiectarea sistemelor cu microprocesoare.* Editura Dacia, Cluj-Napoca, 1983.
3. D i m i t r i u L. *et al., Circuit pentru împărţirea a două numere întregi (Two Integer Numbers Divider Circuit).* Patent RO *106301* (1993).

FRECVENŢMETRU CU MICROPROCESOR. ASPECTE SOFTWARE. FUNCŢIONAREA CU MĂSURAREA PERIOADEI

(Rezumat)

Se prezintă un frecvenţmetru cu gamă extinsă de măsurare (0.01 Hz,...,1 MHz) utilizând numărătoare programabile. Măsurarea se efectuează în patru subgame, pentru două (la capătul inferior al domeniului) măsurând perioada. Rezultatul este, în final, afişat în Hz, impunând o operaţie de împărţire pentru subgamele cu măsurarea perioadei, efectuată de un circuit original, bazat pe numărătoare programabile 8253. Se prezintă modul specific de utilizare a numărătoarelor programabile pentru efectuarea măsurării şi a împărţirii. Programul de lucru face apel la operaţiuni simple, cu durată redusă de execuţie: scrieri, citiri, testări şi manipulări la nivel de bit şi scăderi

fără împrumut. Timpul de lucru cu microprocesorul a circuitului de măsurare se reduce substanţial, asigurând avantaje însemnate pentru aplicaţii de timp real.

BULETINUL INSTITUTULUI POLITEHNIC DIN IAŞI
Tomul XLIII (XLVII), Fasc. 3–4, 1997
Secţia III
ELECTROTEHNICĂ. ENERGETICĂ. ELECTRONICĂ

D.C. 537.529; 621.313.39

PARTIAL DISCHARGE-PHENOMENA UNDER NON-SINUSOIDAL ELECTRIC FIELD OF SOME COMPOSITE INSULATIONS FOR SPECIAL ELECTRICAL MACHINES

BY

CRISTINA SCHREINER and ROMEO CIOBANU

The theme of partial discharges in the specific insulation of linear induction motors is briefly described and some experimental data are interpreted.

Specific phenomena occur especially at low frequencies that leads to a new concept in insulation designing, till now ignored in insulation coordination calculus.

The application is considered as original and concerns all the power motors using pulse convertors as feeding sources.

1. Introduction

The different applications of electrical machines, requesting variable speeds or forces, imply a detailed analysis of the behaviour of their insulation under periodic non-sinusoidal electric field, due to the main use of pulse convertors feeding systems.

The partial discharges (P.D.) phenomena occurrence is more probable at this type of machines, if the insulation system is not correlated to the frequency and voltage regime. Besides the feeding problems and the usual incompatibilities (especially at low frequences) between the electrical machine and convertor, other specific causes can determine P.D.'s occurrence, such as [1]: a) the dielectric lamination and coils impregnation technology; b) the existance of open and hard to be compacted magnetic slots; c) the transient state (providing, e.g., stops and sense changings) specific to the manipulator applications, that generates transient overvoltages; d) the pulse regime of convertors, that implies also peak current overcharges for electrical machines, with seccondary thermal effects, leading to aging phenomena and to local microclimate conditions that can favour P.D.'s occurrence; e) the specific behaviour of $\mathrm{tg}\,\delta$ factor of the insulation, under the above mentioned thermal conditions, due also to the non-sinusoidal state of applied voltage, that can favour synergically the P.D. phenomenon; f) the high local magnetic field that, especially at high frequencies, can maintain the P.D.'s when long discharge distances are also involved [2], [3]; g) the possibility of attracting moisture and/or dust in the uncompacted slots under high frequency electromagnetic field, that can accentuate the insulation aging and

create new opportunities in surface P.D.'s occurrence.

This study was not conceived to outline separately the complicated above mentioned influence of every involved factor, but mainly to model the insulation behaviour under the most probable regime, that cummulates the actions of these causes. Such service regimes can be found at many applications of electrical machines, in particular to a power linear motor, part of a manipulator, providing oscillatory movements.

2. The Measuring Method and Apparatus

A special measuring cell was designed and tested during the experiments, being attached to an open magnetic circuit, in order to model the behaviour of the insulation part of a power linear motor. The slot-insulation was a multilayer of electrotechnical board [4] and a (0.06 mm thin) PEHD for electrical purposes [2]. Silicon resin for electrical purposes [2] was needed to model the impregnation proceeding and mainly to avoid accidental surface discharges or Corona phenomenon around and between the copper and iron edges. Ground guard rings were also used to shield the surface effects and homogenize the electric field. A special device was designed to provide, during the measurements, a constant pressure on the dielectric samples, that had different thicknesses. Another device was used to outline separately the a.c. magnetic field value (till a maximum value of 1.5 T, that was experimentally obtained).

When the applied voltage is high enough, P.D. occurs due to the ionisation processes in the gas-filled microcavities within the insulation (in particular due to the porous and multilayer structure). The most usual way is to be measured the electrical strength of an insulation configuration by increasing slowly the applied a.c. voltage, till the P.D. phenomenon occurs.

In order to avoid the influence of the secondary thermal effects during the measurement period, to detect more accurately the voltage threshold specific to every composite configuration and to make simultaneously the very necessary statistical processing of the experimental data (requested also by the high frequency conditions), the measurement were carried out using a computer-controlled setup, as briefly presented in Fig. 1 and described at length in [5], [6]. This used resonance step-up transformers in order to provide a frequency output till 500 kHz. The detected P.D. pulses were coupled out by special high-pass filters, matched to a 50 Ω output-impedance. A digital storage oscilloscope (100 MHz bandwidth) was used to detect P.D. pulses and calculate the apparent charge by digital integration. All measured values of P.D.-(inception and extinction) electric fields are here presented as peak values. The characteristic presentation using electric fields, instead of the correspondent voltages, was here prefered because the secondary effect of samples thickness is so minimised and the results are presented in a more accurate way. All that presumed statistical interpretation and specific correlations was made using the "Windows-Mathcad-Statistica 6.0"-programme.

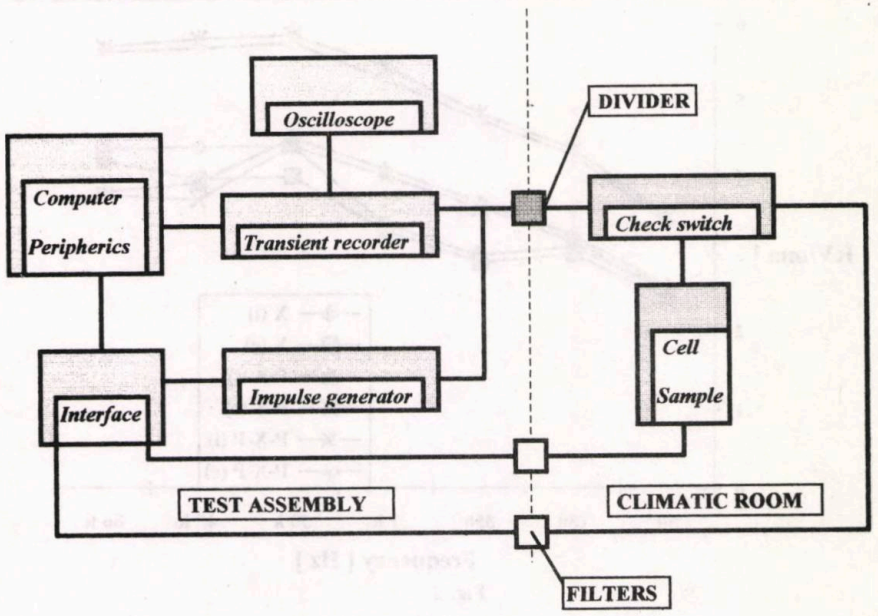

Fig. 1

3. Results and Discussion

The experimental characteristics are presented in Figs. 2,...,4, outlining the frequency influence on P.D. phenomena for different types of composite insulators, where: X – electrical board [7], in order: (*1*) – 1 mm thin, (*2*) – 2 mm thin and (*3*) – 2 mm thin after 10,000 service hours; $P-X$ – electrical board +1 sheet PEHD, to the iron side; $P-X-P$ – electrical board +2 sheets PEHD, to the iron and copper sides; index i indicates the P.D.-inception electric field characteristic; index e indicates the P.D.-extinction electric field characteristic.

The obtained results are, generally, in good agreement with some previous ones [8], [9], but many other new aspects were also noticed, leading finally to some peculiar conclusions.

In Fig. 2, where the thinest electrical board is involved, there can be observed that only a sheet of PEHD brings no important improving at low frequency, but it can lead to severe problems at frequency values over 200 Hz, because of the unsymmetry of the electrical field within the insulating structure. This effect dissapears at the two-sheets structure, that behaves itself better under high frequency electric field. An increased slope of this characteristic could be noticed, due to the specific interfacial-dipolar polarisation process.

A bulker electrical board (Fig. 3) trends similarly versus frequency, but some nuanced aspects need to be outlined namely: a) when alone, it leads to lower values of electrical fields (comparing to Fig. 2), especially at low frequency (under 1 kHz); b) when a single PEHD sheet is involved, it brings no essential improving to the

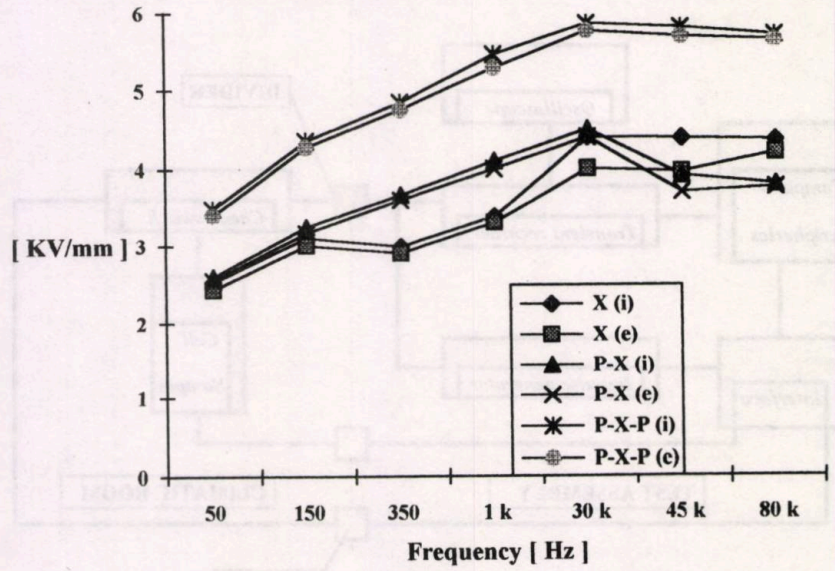

Fig. 2

electrical characteristics, but such a structure can be used without problems at high frequencies; comparing to Fig. 1, the unsymmetry problems are here very attenuated; c) when two PEHD sheets are used, the structure behaves itself very good and leads unexpectedly to higher values of electrical fields (comparing to Fig. 2), that proved a better compatibility of components under the variable electrical stress.

That finally means that a composite structure needs to be well dimensioned (regarding the electrical stress), but also to be designed regarding the secondary physical and chemical aspects, in order to increase the compatibility between the components under the P.D. processes, especially when variable frequencies are involved.

Because more than 90% of applications for electrical machines of such insulation types are referring to frequencies up to 1 kHz, the aspects suggested from this study should recommend: a) not to use a very thin porous dielectric; b) the porous dielectric to have a minimal air content and a very high homogeneity (that can be obtained also after the impregnation process); c) the porous dielectric to be bordered on both sides by well dimensioned plastic laminates; d) the contact surfaces to be realised, as possible, without technological defects (meaning especially contact voids).

In Fig. 4 the influence of aging was taking into account, the physical structures being in fact similar to those described in Fig. 3. Lower values for all these characteristics, comparing to Fig. 3, are noticed. Aging process reduces the capability of a dielectric structure to overtake the electric stress and favours the P.D.'s occurrence, especially at low frequencies. At high frequencies, over 30 kHz, the P.D. process is very accentuated in the porous material due to the secondary thermal aspects in aged cellulose. This effect is only partially avoided when only one PEHD sheet is added, but dissapears when two sheets are used (Fig. 4). Once again the plastic laminate

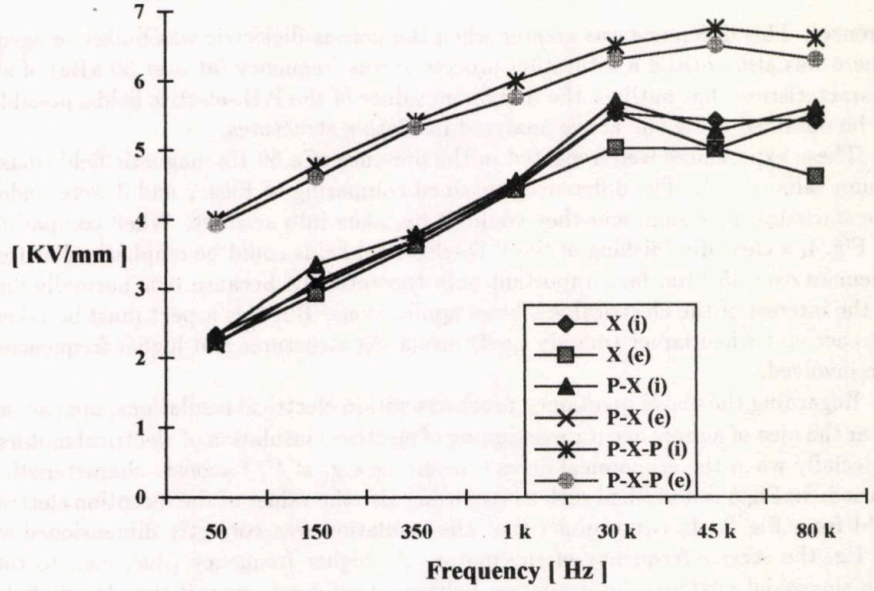

Fig. 3

presence was decisive in assessing a higher reliability of these insulators type.

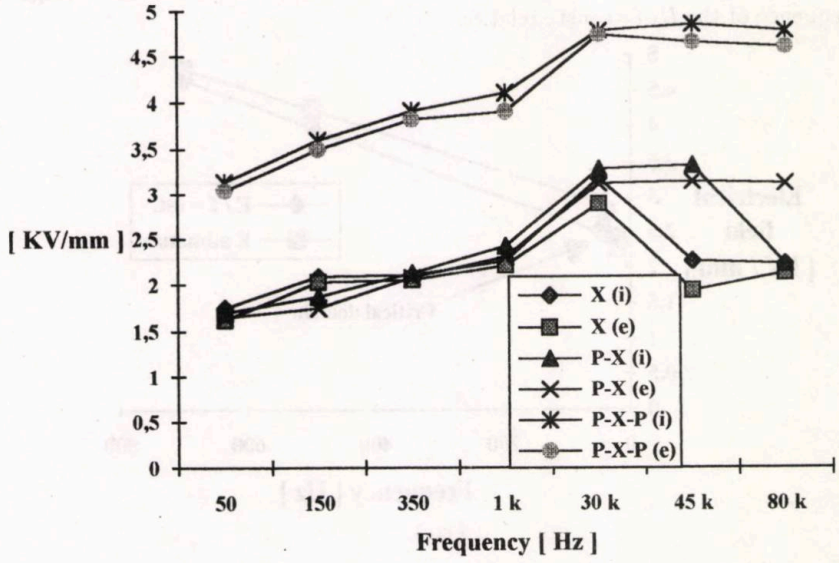

Fig. 4

As a final comment, there could be noticed very close values of inception and extinction electric fields for every type of dielectric structure (a maximum 10% dif-

ference). This difference was greater when the porous dielectric was bulker or aged. There was also noticed a saturation process versus frequency (at over 30 kHz) of all characteristics, that outlines the maximum values of the P.D.-electric fields, possible to be obtained using the above analysed insulating structures.

These experiences were repeated in the presence of a 50 Hz magnetic field (maximum value 1.5 T). The differences obtained comparing to Figs. 2 and 3 were under the statistical precision, and they couldn't be taken into account. When comparing to Fig. 4, a clear diminishing of the P.D.-electrical fields could be emphasised at frequencies over 45 kHz, fact important only theoretically, because it is normally out of the interest of the electrical machines applications. But this aspect must be taken into account when larger (mainly aged) insulating structures and higher frequencies are involved.

Regarding the above mentioned processes within electrical insulations, appears as clear the idea of a more accurate designing of electrical insulation of electrical motors, especially when the economical drive (presuming e.g. a U/f=const. characteristic) is used. In Fig.5 is described such a case, using also the values of the inception electric field from Fig. 2. It is presumed that the insulation was correctly dimensioned at 50 Hz, the service frequency of the motor. At higher frequency (due, e.g., to the non-sinusoidal charge), the insulation behaves itself good, even if the electric field value is lower, because the distortion regime is usually very carefully controled. The case is similar when the service frequency is increased, if the breakdown strength of the insulation was previously correlated to the new value of the service voltage, as consequence of the U/f=const. relation.

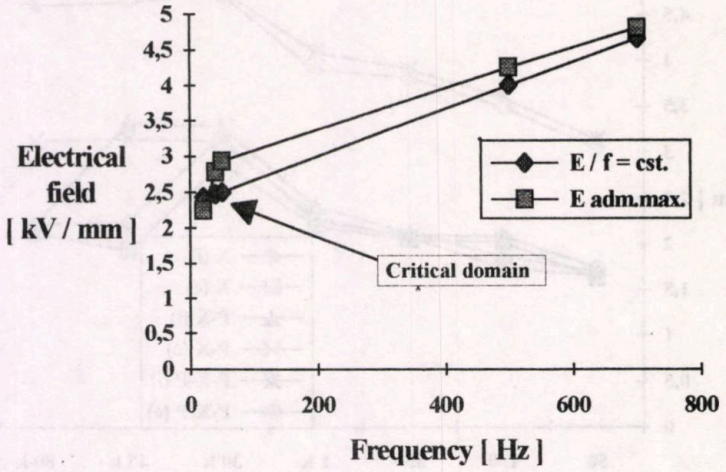

Fig. 5

The problem appears when the frequency is decreased, in order to obtain improved parameters (e.g., a greater force at a linear motor). Till now, this domain wasn't taken into account, because there were considered as sufficient the breakdown strength cautions, as previously designed at the service voltage, and the P.D.'s

should not occur. But, according to Fig. 4, the slope of the inception electric field is normally 2...5 times greater than the slope of the U/f characteristic, base of the initial designing. That finally means that the P.D.-process can appear (and age very accentuately the insulation) at much lower values of the service electric fields (e.g., at 20 Hz, at less than 40% of the correspondent breakdown strength), even if the dielectric structure was considered as correctly dimensioned regarding the voltage range. This phenomenon is now considered as a novelty and it can generally occur in all types of composite structures, working under variable frequency conditions. The effect is more accentuated if the materials can provide at low frequency a high dielectric permitivity, due, e.g., to a specific interfacial polarisation process, as shown in [9].

4. Conclusions

The designing of the insulation of the electrical machines, working under variable voltages and frequencies conditions (e.g., according to the U/f = const. characteristic), must take into account not only the possible overvoltages (leading to accidental breakdowns), but also the premature aging, due to the specific P.D.-phenomena, that occur with a greater probability at low frequencies.

The composite insulations (e.g., multilayer or impregnated structures) can be used reliablely till 1 kHz only if an adequate dimensioning is assumed, especially under the circumstances when the interfacial polarisation plays an important role.

The correct use of a porous dielectric at low frequency implies a previous double side lamination under a severely controlled electrotechnical technology. The extended analysis of P.D. phenomena versus frequency can be also used, under these circumstances, as an indirect qualitative method in characterising the behaviour and/or technology of complex electrical insulations.

Especially when a composite structure is submitted to special service charges (e.g., non-sinusoidal electric field) and/or is working under a U/f=const. characteristic, the dimensioning base needs to be accorded to the following observations:

1° When the frequency increases, the nominal service voltage must be designed 2...3 times lower comparing to the breakdown one, that is according to every involved frequency. This is usually not a simple operation, because the applications presume a continuous increase of the service voltage, under the circumstances when the breakdown voltage decreases very much versus frequency [2]. Here the P.D.-phenomena in dielectric can be ignored.

2° When the frequency decreases, the nominal service voltage must be designed lower as the P.D.-extinction voltage, that is according to every involved frequency. This operation is needed in applications using frequencies up to 50 Hz, at that the P.D.-inception voltage is normally under 40% of the breakdown one. The probability of an accidental breakdown in this frequency interval is very low, but the aging phenomena of the dielectric are very accentuated.

The influence of the magnetic field on the P.D.-phenomena can be neglected, in

ordinary conditions.

A c k n o w l e d g e m e n t. The obtained results are part of a research program, financially supported by A.v. Humboldt-Stiftung, Bonn, Germany, and technically attended by Technische Hochschule, Darmstadt.

Received, March 6, 1996

Technical University "Gh.Asachi", Jassy,
Department of Industrial Utilizations,
Electric Drives and Automation
and
Department of Electrical Measurements

REFERENCES

1. S c h r e i n e r C., *Contribuţii privind realizarea mişcărilor oscilante cu ajutorul motoarelor liniare de inducţie.* Ph. D. Diss., Technical University "Gh. Asachi", Jassy, 1997.
2. I f r i m A., N o t i n g e r P., *Materiale Electrotehnice.* Ed. Did. şi Ped., Bucureşti, 1979.
3. K ö n i g D., N a r a y a n a - R a o Y., *Partial Discharges in Power Apparatus.* VDE-Verlag, Berlin, 1993.
4. . * . *Specifications for Laminates of Plastic Film and Kraft Paper for Electrical Purposes.* VDE 0316/07.67.
5. H u n d R., P f e i f f e r W., R e i n h a r d H., S c h e u r e r F., *Partial Discharge Testing of Components for Low-voltage Equipment at High Frequencies.* CEIDP, Pocono Manor, 1990, 261-266.
6. H u n d R., P f e i f f e r W., *Insulation of Low Voltage Equipment at High Frequencies.* CEIDP, Pocono Manor, 1993, 514-519.
7. . * . *Laminated Pressboard for Electrical Purposes.* VDE 0314, Teil 200/04.87.
8. C i o b a n u R., P f e i f f e r W., *The Specific Behaviour of Electrotechnical Papers under H.F.-P.D.'s.* IEEE Int. Symp. on Electr. Insul., Montreal, Canada, June 16-19, 1996.
9. C i o b a n u R., P f e i f f e r W., *The Influence of Electrotechnical Papers Technology on the Specific P.D.-Inception Electric Field.* IEEE Int. Conf. on Dielectric Measurement and Applications, Bath, U.K., Sept. 23-26, 1996.

FENOMENE DE DESCĂRCĂRI PARŢIALE ÎN CÂMP ELECTRIC NESINUSOIDAL, SPECIFICE IZOLAŢIILOR COMPOZITE ALE UNOR MAŞINI ELECTRICE SPECIALE

(Rezumat)

Dimensionarea sistemelor de izolaţii destinate maşinilor electrice speciale, care funcţionează la frecvenţă variabilă sau în regim nesinusoidal, presupune, pe lângă verificarea pas cu pas a rigidităţii dielectrice, şi analiza fenomenelor specifice de descărcări parţiale, care în special la joasă frecvenţă pot produce o îmbătrânire accentuată a dielectricului.

Fenomenul de descărcări parţiale depinde prioritar de structura şi tehnologia producerii dielectricului (în special dacă polarizarea interfacială joacă un rol important) şi poate fi favorizat de prezenţa câmpului magnetic dacă distanţele de izolaţie sunt mari şi dielectricul puternic degradat.

Se fac referiri la trei tipuri de structuri electroizolante, evidenţiindu-se particularităţile fiecăreia şi se fac observaţii necesare proiectării sistemelor de izolaţii destinate unor astfel de aplicaţii.

BULETINUL INSTITUTULUI POLITEHNIC DIN IAŞI
Tomul XLIII (XLVII), Fasc. 3–4, 1997
Secţia III
ELECTROTEHNICĂ. ENERGETICĂ. ELECTRONICĂ

D.C. 621.3.07; 678.027.3

AN ANALYTICAL MODEL OF THE BLOWN FILM PROCESS

BY
LIVIA COCIU

A blown film size control system in the plastic extruders is proposed. The aim of the paper is to develop the most appropriate process model to be used in the system optimization. It is clearly shown how the model parameters depend on the operating conditions and which are the elements of interest. The model simplifications are specified, so that the essential process behaviour to be captured.

1. Introduction

In blown film processes a thin film is produced by means of the extrusion of a polymer melt through an annular die, as schematically shown in Fig. 1.

The molten tube, exiting from die, is drawn upward by a take-up device. To inflate and cool the tube, air is admitted inside through a duct and then removed through another one concentric with the first. The height above the die at which solidification occurs is the so-called freezeline. The solidified thin film is flattened into a double layered sheet by nip rolls. To maintain a constant circumference of the finished tube, it is necessary to control the volume of air inside by using a feedback system. The plastic tube represents the controlled process for which a primary model has been proposed in [1].

Taking into account the control strategy adopted in [2] for better performances at a reduced cost an appropiate model adapted to industrial operation conditions is necessary. To achieve this aim, in what follows the region of interest for modelling the film blowing process extends from the die exit to the nip rolls and the influence of the operating conditions on the parameters is determined.

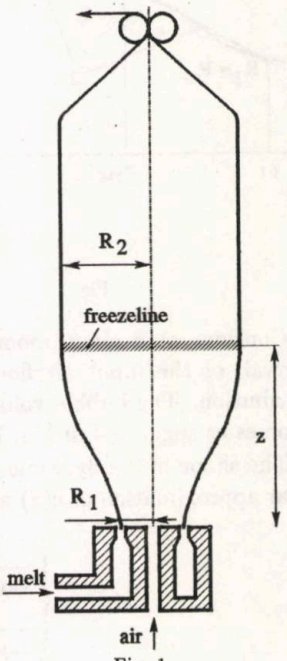

Fig. 1

Even though the system is nonlinear, its nonlinearity can be disregarded as the system is operating with small deviations about a fixed operating point, so that a linearized model can be developed. Thus, the process model is described by a transfer function relating the bubble radius deviation, $r(z,t)$, from its steady-state value, $R(z)$, to the difference of the input and output air flow, $q(t)$, where $R(z)$ is considered to be known [3] and z – the axial height above the die. If the operating conditions change $R(z)$ can change as well. These changes represent only the modifications of the initial conditions. The dynamic modelling is based on the assumption that any temporal sample of the family $r(z,t)$ can be linearized with respect to z.

2. Theoretical

Let us consider the region in which the film can undergo deformations. The variation of the bubble radius R with the axial distance z is shown in Fig. 2, curve *1*. $R_1 = R(z_1)$ is the bubble radius about the die exit and $R_2 = R(z_2)$ – the radius at and beyond the freezeline, where the film deformation is negligible.

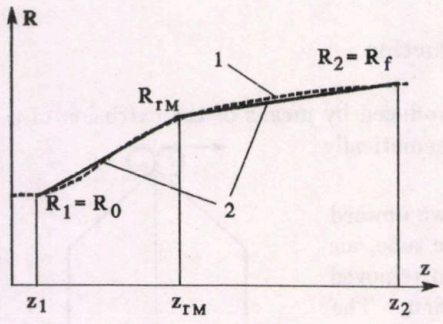

Fig. 2

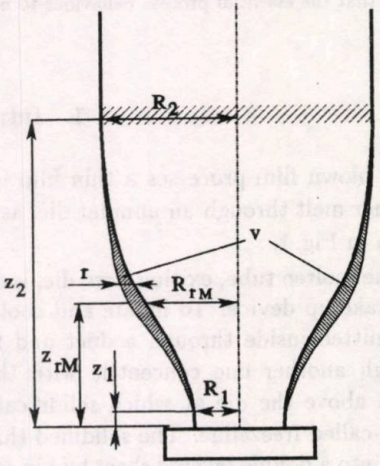

Fig. 3

Consider at a given moment a sudden increase, for an extremely short time interval, of the input air flow. This variation of q will be modelled by a Dirac distribution. The bubble volume increases and, in the very next moment its profile becomes as suggested in Fig. 3.

The shape of the dynamic radius $r(z)$ is shown in Fig. 4 – curve *1*. Curve *2* is the linear approximation of $r(z)$ at fixed moments:

$$(1) \qquad r(z) = \begin{cases} \dfrac{r_M}{z_{rM} - z_1}(z - z_1), & z_1 \le z \le z_{rM}, \\ \dfrac{r_M}{z_{rM} - z_2}(z - z_2) + r_2, & z_{rM} < z \le z_2, \end{cases}$$

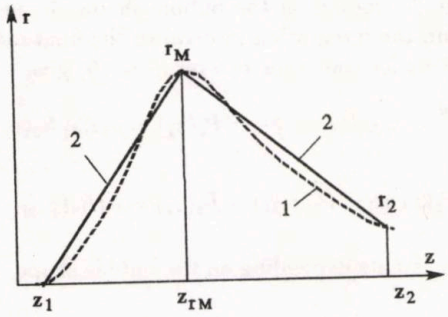

Fig. 4

where r_M is the maximum value of $r(z)$. Note that only r_2 and r_M vary with time, while the deformation shape does not.

It is well known that in the steady-state the bubble volume in the deformable region is:

$$V_0 = \pi \int_{z_1}^{z_2} R^2(z)\,\mathrm{d}z. \tag{2}$$

After the air flow variation:

$$\begin{aligned} V &= \pi \int_{z_1}^{z_2} [R(z) + r(z)]^2\,\mathrm{d}z = \\ &= \pi \int_{z_1}^{z_2} R^2(z)\,\mathrm{d}z + 2\pi \int_{z_1}^{z_2} R(z)r(z)\,\mathrm{d}z + \pi \int_{z_1}^{z_2} r^2(z)\,\mathrm{d}z \simeq V_0 + v. \end{aligned} \tag{3}$$

Neglecting the term due to r^2 the volume variation is identified to be:

$$v = 2\pi \int_{z_1}^{z_{rM}} R(z)r(z)\,\mathrm{d}z + 2\pi \int_{z_{rM}}^{z_2} R(z)r(z)\,\mathrm{d}z = v_1 + v_2. \tag{4}$$

In the range $[z_1, z_{rM}]$:

$$v_1 = 2\pi \frac{r_M}{z_{rM} - z_1} \left[\int_{z_1}^{z_{rM}} R(z)z\,\mathrm{d}z - z_1 \int_{z_1}^{z_{rM}} R(z)\,\mathrm{d}z \right]. \tag{5}$$

Integrating by parts the first term and substituting into (5) gives:

$$v_1 = 2\pi \frac{r_M}{z_{rM} - z_1} \left[zP_1(z)\Big|_{z_1}^{z_{rM}} - \int_{z_1}^{z_{rM}} P_1(z)\,\mathrm{d}z - z_1 P_1(z)\Big|_{z_1}^{z_{rM}} \right], \tag{6}$$

where $P_1(z)$ denotes the antiderivative of $R(z)$.

It makes good sense to express v_1 in terms of variables whose value can be experimentally determined, such as the final radius R_2 and the integration interval. Thus the third term of (6) becomes:

$$P_1(z)\Big|_{z_1}^{z_{rM}} \doteq P_1(z_{rM}) - P_1(z_1) = R_{\mathrm{med1}}(z_{rM} - z_1) = a_3 R_2 (z_{rM} - z_1), \tag{7}$$

where a_3 is a constant depending on the bubble shape, defined as the ratio of the average radius R within the integration interval to the final radius R_2.

Similar considerations for the other two terms of (6) give:

$$zP_1(z)\Big|_{z_1}^{z_{rM}} = z_{rM}P_1(z_{rM}) - z_1P_1(z_1) = a_1z_{rM}R_2(z_{rM} - z_1),$$

$$\int_{z_1}^{z_{rM}} P_1(z)\,\mathrm{d}z = P_2(z_{rM}) - P_2(z_1) = a_2R_2(z_{rM} - z_1)^2, \tag{8}$$

where a_1, a_2 are also constants depending on the bubble shape. Substituting (7) and (8) into (6) gives:

$$v_1 = 2\pi r_{rM}R_{rM}[a_1z_{rM} - a_2(z_{rM} - z_1) - a_3z_1] = 2\pi r_{rM}R_2a(z_{rM} - z_1). \tag{9}$$

In the same way, the expression for v_2 may be shown to be:

$$\begin{aligned} v_2 &= 2\pi r_{rM}R_{rM}[-b_1z_{rM} + b_2(z_2 - z_{rM}) + b_3z_2] + 2\pi r_2R_2c(z_2 - z_{rM}) = \\ &= 2\pi r_{rM}R_2b(z_2 - z_{rM}) + 2\pi r_{rM}R_2c(z_2 - z_{rM}) = \\ &= 2\pi R_2(z_2 - z_1)[br_M(t) + cr_2(t)]. \end{aligned} \tag{10}$$

Finally the incremental volume $v(t)$ can be evaluated as:

$$\begin{aligned} v(t) &= 2\pi c_1R_2(z_2 - z_1)r_M(t) + 2\pi c_2R_2(z_2 - z_1)r_2(t) = \\ &= 2\pi R_2(z_2 - z_1)[c_1r_M(t) + c_2r_2(t)]. \end{aligned} \tag{11}$$

Eq. (11) shows the manner in which $v(t)$ depends on the height of the deformable region $z_2 - z_1$, the final radius R_2 and the maximum dynamic deformation $r_M(t)$; c_1 and c_2 are shape coefficients determining the weight each transversely section affects the total volume variation.

To evaluate c_1 and c_2 let consider the linear approximation of $R(z)$ as in Fig. 4, curve *2*:

$$R(z) = \begin{cases} \dfrac{R_{rM} - R_1}{z_{rM} - z_1}(z - z_1) + R_1, & z_1 \le z \le z_{rM}, \\ \dfrac{R_{rM} - R_2}{z_{rM} - z_2}(z - z_2) + R_2, & z_{rM} < z \le z_2. \end{cases} \tag{12}$$

Substituting into (5) gives:

$$v_1 = 2\pi r_{rM}R_2\left(\frac{R_{rM}}{3R - 2} + \frac{R_1}{6R_2}\right)\alpha(z_2 - z_1), \tag{13}$$

where α locates the height of the maximum deformation within the deformable region limits:

$$\alpha = \frac{z_{rM} - z_1}{z_2 - z_1}. \tag{14}$$

Its values are in the range of 1 – the upper limit, to 0 – the lower one.

In the same way v_2 is readily shown to be:

$$(15)\quad v_2 = 2\pi r_M R_2 \left(\frac{R_{rM}}{3R_2} + \frac{1}{6}\right)(1-\alpha)(z_2 - z_1) + 2\pi r_2 R_2 \left(\frac{R_{rM}}{6} + \frac{1}{3}\right)(z_2 - z_1).$$

Then it follows that:

$$(16)\quad \begin{aligned} v &= 2\pi r_M R_2 (z_2 - z_1)\left(\frac{2R_{Rm}}{R_2} + \alpha\frac{R_1}{R_2} + 1 - \alpha\right) + \\ &+ 2\pi R_2 (z_2 - z_1)\left(\frac{R_{rM}}{6R_2} + \frac{1}{3}\right) = 2\pi R_2 (z_2 - z_1)[c_1 r_M(t) + c_2 r_2(t)]. \end{aligned}$$

Finally:

$$(17)\quad c_1 = \frac{1}{6}\left(\frac{2R_{rM}}{R_2} + \alpha\frac{R_1}{R_2} + 1 - \alpha\right), \quad c_2 = \frac{1}{6}\left(\frac{R_{rM}}{R_2} + 2\right).$$

3. Dynamic Modelling

Consider a time interval $\mathrm{d}t$ during which the film is moved upward with $\mathrm{d}z = v_f\,\mathrm{d}t$ distance. Then r_2 varies with the value $\mathrm{d}r_2 = -m\,\mathrm{d}z$; m denotes the slope of the streightline *2* (Fig. 4) which approximates $r(z)$ in the range $[z_{rM}, z_2]$. Hence:

$$(18)\quad \frac{\mathrm{d}r_2}{\mathrm{d}t} = \frac{r_M - r_2}{(1-\alpha)(z_2 - z_1)} v_f.$$

On the other hand:

$$(19)\quad v(t) = \int_{-\infty}^{t} r(t)\,\mathrm{d}t.$$

From (16), (18) and (19) the system which describes the dynamic behaviour of the process results as follows:

$$(20)\quad c_1\frac{\mathrm{d}r_M}{\mathrm{d}t} + c_2\frac{\mathrm{d}r_2}{\mathrm{d}t} = \frac{1}{2\pi(z_2 - z_1)R_2}q, \quad \frac{(1-\alpha)(z_2 - z_1)}{v_f}\cdot\frac{\mathrm{d}^2 r_2}{\mathrm{d}t^2} + \frac{\mathrm{d}r_2}{\mathrm{d}t} = \frac{\mathrm{d}r_M}{\mathrm{d}t}.$$

Solving w.r.t. $r_M(t)$ the equation relating the variation of $r_M(t)$ to the input, air flow $q(t)$ is found to be:

$$(21)\quad \begin{aligned} &\frac{(1-\alpha)(z_2 - z_1)}{v_f}\cdot\frac{c_1}{c_2}\cdot\frac{\mathrm{d}^2 r_M}{\mathrm{d}t^2} + \left(1 + \frac{c_1}{c_2}\right)\frac{\mathrm{d}r_M}{\mathrm{d}t} = \\ &= \frac{1}{2\pi(z_2 - z_1)R_2 c_2}\left[\frac{(1-\alpha)(z_2 - z_1)}{v_f}\cdot\frac{\mathrm{d}q}{\mathrm{d}t} + q\right]. \end{aligned}$$

The Laplace transform gives:

$$(22)\quad H_{zrM}(s)=\frac{\mathcal{L}(r_M(t))}{\mathcal{L}(q(t))}=\frac{1}{2\pi(z_2-z_1)R_2(c_1+c_2)}\cdot\frac{s\frac{(1-\alpha)(z_2-z_1)}{v_f}+1}{s\left[s\frac{(1-\alpha)(z_2-z_1)}{v_f}\cdot\frac{c_1}{c_1+c_2}+1\right]}.$$

Similarly, solving (20) w.r.t. $r_2(t)$, the differential equation relating $r_2(t)$ to $q(t)$ is obtained:

$$(23)\quad \frac{c_1(1-\alpha)(z_2-z_1)}{v_f}\cdot\frac{\mathrm{d}^2r_2}{\mathrm{d}t^2}+(c_1+c_2)\frac{\mathrm{d}r_2}{\mathrm{d}t}=\frac{1}{2\pi(z_2-z_1)R_2}q.$$

Hence:

$$(24)\quad H_{zr2}(s)=\frac{\mathcal{L}(r_2(t))}{\mathcal{L}(q(t))}=$$
$$=\frac{1}{2\pi(z_2-z_1)R_2(c_1+c_2)}\cdot\frac{1}{s\left[s\frac{c_1}{c_1+c_2}\cdot\frac{1}{v_f}(1-\alpha)(z_2-z_1)+1\right]}.$$

At this point the final model of the process is easy to be found. Thus, rewriting (1) in the range $[z_{rM},z_2]$ and defining:

$$(25)\quad \beta=\frac{z-z_{rM}}{z_2-z_{rM}},$$

it results:

$$(26)\quad r(z,t)=r_M\frac{z_1-z}{z_2-z_{rM}}+r_2\frac{z-z_{rM}}{z_2-z_{rM}}=r_M(t)(1-\beta)+r_2(t)\beta.$$

Taking into account the linearity property of the Laplace transform, the relation

$$(27)\quad H_z(s)=(1-\beta)H_{zrM}(s)+\beta H_{zr2}(s)$$

may be written, so that:

$$(28)\quad H_z(s)=(1-\beta)k_P\frac{s\tau_1+1}{s(s\tau_2+1)}+\beta\frac{k_P}{s(s\tau_2+1)}=k_P\frac{s\tau_1(1-\beta)+1}{s(s\tau_2+1)}.$$

The desired model which can predict the dynamic behaviour of the blown film process in the range $[z_{rM},z_2]$ is now obtained. It is of no interest for practical applications to model the process in the region below z_{rM} (even though it is easy to be found) since the transducer is, on no account, placed there.

It is important to note that, except the upper limit ($z=z_2$), the aspect of $H_z(s)$ is the same for any z, namely of second order with a pole at the origin and a zero. The time constants have been directly determined from (22) and (26) as follows:

$$(29)\quad \begin{cases} k_P=\dfrac{1}{\tau}=\dfrac{1}{2\pi(z_2-z_1)R_2(c_1+c_2)}, \\ \tau_1=\dfrac{(1-\alpha)(z_2-z_1)}{v_f},\quad \tau_2=\dfrac{(1-\alpha)(z_1-z_2)}{v_f}\cdot\dfrac{c_1}{c_1+c_2}=\tau_1\dfrac{c_1}{c_1+c_2}. \end{cases}$$

The most surprising result is that the zero time constant $\tau_1(1-\beta)$ depends on the axial position z, while the poles time constants do not. The fact plays an important role in system optimization, such as allowing a precise evaluation of the pole and zero position.

A complete description of the extrusion process implies to extend its model beyond the freezeline, where the bubble radius $r(z,t)$ is a delayed version of the final radius $r_2(t)$. The delay of the response has been treated separately and could be added back to the transfer function $H_z(s)|_{z=z_2}$ as a dead time. If setting $z = z_2$, then β results to be equal to 1. Substituting into (28) we obtain:

$$H_{zr2} = k_P \frac{s\tau_1(1-\beta)+1}{s(s\tau_2+1)}\bigg|_{\beta=1} = \frac{k_P}{s(s\tau_2+1)}. \tag{30}$$

It follows that:

$$H_z(s) = \frac{k_P}{s(s\tau_2+1)} e^{-s\tau_T}, \quad z > z_2, \tag{31}$$

where:

$$\tau_T = \frac{z-z_2}{v_f}. \tag{32}$$

Eqs. (28) and (30) represent the model of the controlled process in the region where the film size is justified to be measured (i.e., between maximum deformation line and nip rolls).

4. Conclusions

A complete model which describes the blown film process in its entire existence (i.e., between die exit and nip rolls) has been developed in order to be used in optimization of the film size control systems. Two transfer functions, one for the deformable film region and another for that beyond the frezeeline, have been found. The parameters have been identified and the factors which they determine have been pointed out.

Received, April 29, 1997

Technical University "Gh.Asachi", Jassy,
Department of General Electrotechnics
and Electrical Machines

REFERENCES

1. Cociu L., Cociu R., *Dynamic Behaviour of the Blown Film Process.* Proc. Sci. Sess. "85 years from Setting up of the Industrial Electricity School", Jassy, 1995.
2. Cociu L., Cociu R., Goraş L., *Procedeu şi instalaţie pentru menţinerea diametrului balonului din polietilenă în instalaţii de extrudere, în cazul răcirii interioare.* Patent Romania, *99014* (1989).

3. F a n g S., C h e n L., Z h u F., *Studies on the Theory of Single Screw Plasticating Extrusion* (Part II). Polymer Eng. and Sci., **31**, *15* (1991).
4. R o s a r i o E., B r e t a s S., G r a n a d o C., *Simulation of the Extrusion of HDPE Blends*. Eur. Polym. J., **29**, *6* (1993).

UN MODEL ANALITIC AL PROCESULUI DE EXTRUDERE A FOLIILOR DIN POLIETILENĂ

(Rezumat)

Se studiază un sistem de reglare autonomă a lăţimii foliilor din polietilenă, utilizat în instalaţiile de extrudere. Scopul urmărit este cel de a modela procesul reglat în vederea utilizării sale în optimizarea sistemului, în corelaţie cu strategia de reglare adoptată. Modelul propus oferă o descriere completă a procesului, stabilindu-se modul în care parametrii săi depind de condiţiile de operare. Se determină mărimile de interes şi cele al căror efect poate fi neglijat, precum şi ipotezele simplificatoare adecvate scopului propus, aspectele esenţiale fiind menţinute.

BULETINUL INSTITUTULUI POLITEHNIC DIN IAŞI
Tomul XLIII (XLVII), Fasc. 3–4, 1997
Secţia III
ELECTROTEHNICĂ. ENERGETICĂ. ELECTRONICĂ

D.C. 621.313.2; 621.313.047

ON THE REVERSIBILITY OF THE D.C. MOTORS WITH STATIC SWITCHING

BY

I. SUCHAR

Because of their construction, the d.c. motors with static switching don't allow the changing of the direction of rotation by reversing the inductor magnetic flux or the sense of the current through the induced winding.

A novel procedure for reversing the direction of rotation, suitable for the motor studied in [1], is presented.

1. Introduction

If in the case of the conventional d.c. motor all the parts are gathered under the same mechanical structure, in the case of d.c. motors with solid-state commutation the role of the collector and the brushes is taken by a solid-state switch and a transducer for the position of the rotor; these parts are placed separately from the d.c. motor itself.

Because we refer to a d.c. motor with solid-state commutation studied in detail in [1], whose induced winding, placed on the stator, is made of three identical sections, the electronic circuitry for switching consists of three identical modules denoted in Fig. 1 by *I, II, III.* Every module contains:

a) a series ferroresonant circuit R_0, C_0, L which constitute the fixed part of the transducer for the position of the rotor, with the nonlinear coil orthogonally driven by the field produced by the permanent magnet *1*, which is the moving part of the transducer, as in [1] and [3];

b) a transistorized switch, CT, made by the coupling circuit CC with the transistor T_1 and C, the switch itself, obtained by means of the power transistor T_2 whose collector circuit has one of the sections S_1, S_2 or S_3 of the induced winding of the motor M. The rotor of the d.c. motor is a bipolar magnet (*8*), diametrically magnetized, with the role of the inductor.

The transducer is powered from the audiofrequency generator *2*. The CT switch and the d.c. motor M are powered by a d.c. power supply, *3*. Switching off the C switch is provided by the power supply *4*.

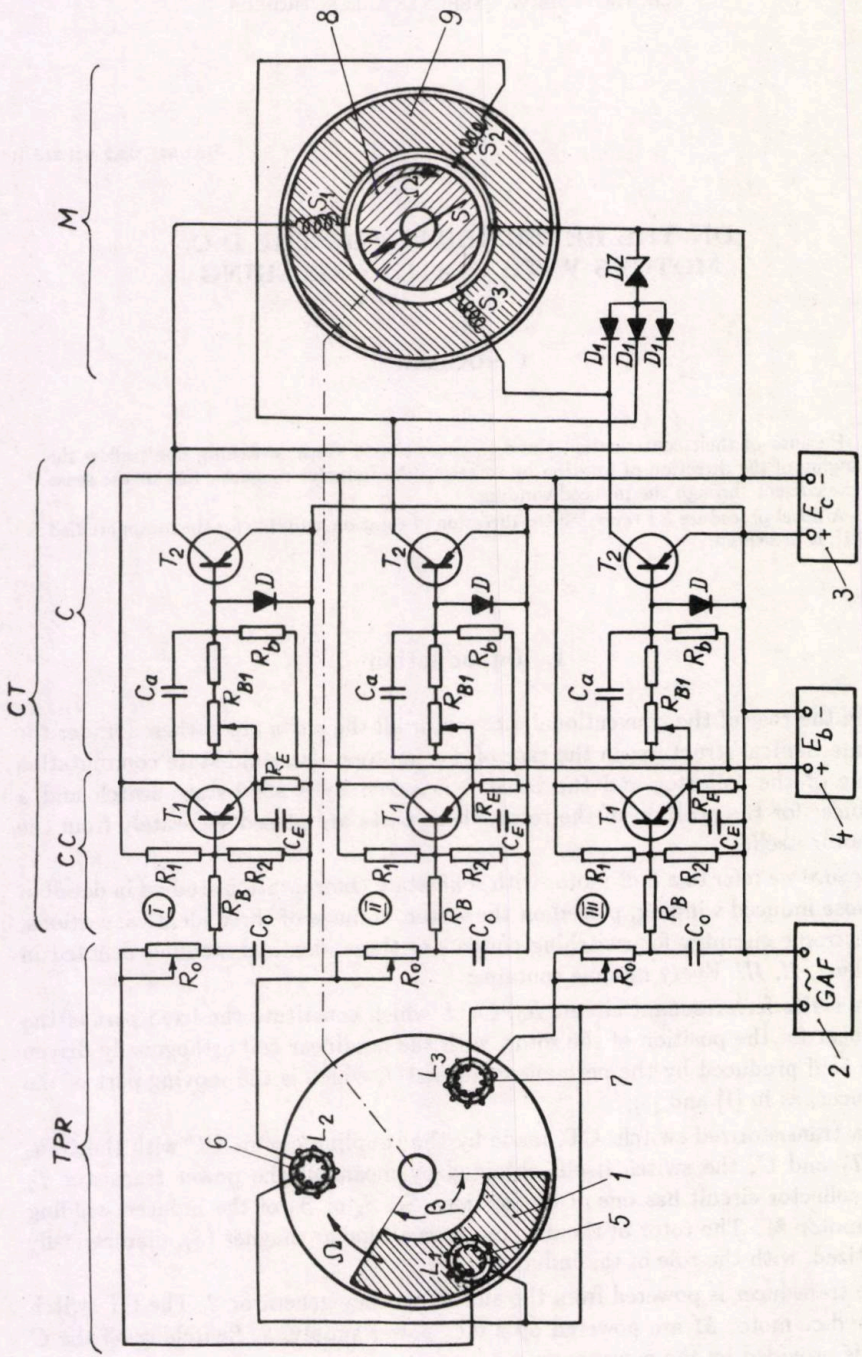
M
CT
C
CC
TPR
8
9
S1
S2
S3
W
DZ
D1
T2
T1
D
Ca
RB1
Rb
RE
CE
R1
R2
RB
Co
Ro
I
II
III
Ec
Eb
GAF
2
3
4
5
6
7
L1
L2
L3
Ω
β

Fig. 1

2. The Principle of Functioning of a D.C. Motor with Solid-state Commutation

Two conditions must be obeyed, [2], to obtain an electromagnetic torque from the d.c. motor we are studying:

a) the angle ρ between the N–S axis of the poles of the inductor *8* and the bisectrix Δ of the angle of the sector of the signal β must be constant and equal to 90°;

b) the three nonlinear coils satisfying the equality $L_1=L_2=L_3$ (the sensitive elements for the position of the rotor) must be placed on the frontal shield of the d.c. motor so that between the radial direction of the each ferrite *5, 6, 7* and the plane of the corresponding section S_1, S_2 and S_3 of the induced winding, placed on the stator *9*, must be an angle $\gamma_1=120°$ or $\gamma_2=60°$.

The mechanism which produces the torque is explained in Fig. 2.

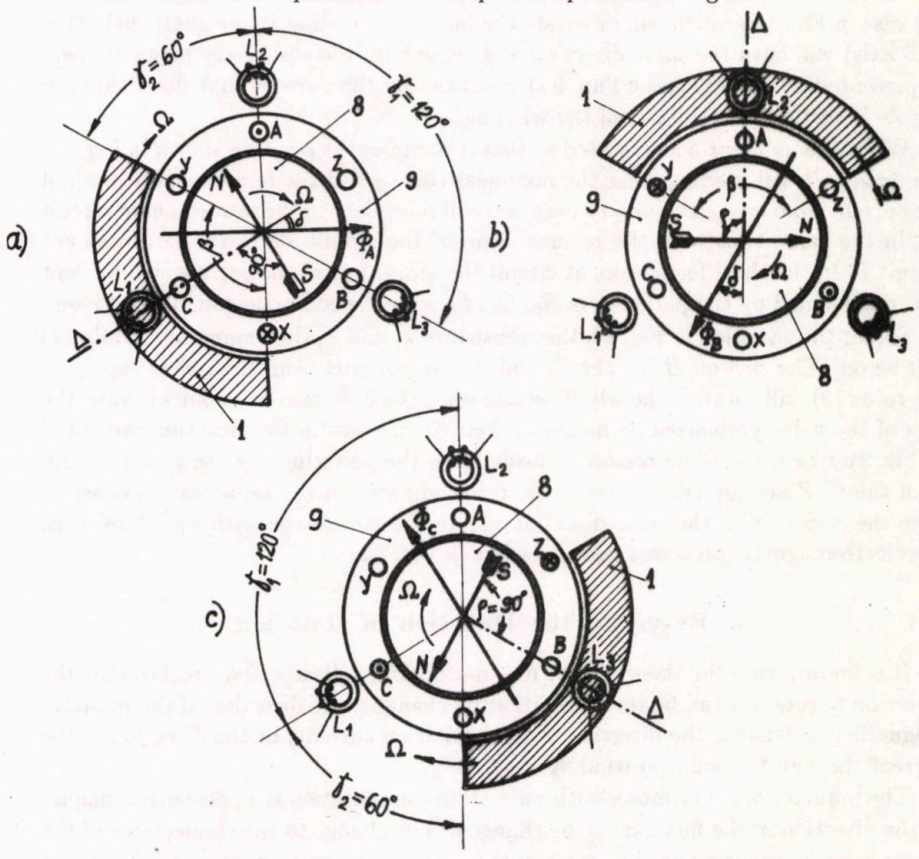

Fig. 2

Let us suppose that in the moment of the starting of the d.c. motor the magnet *1* of the transducer, placed on the inductor *8*, is in the position shown in Fig. 2*a*.

In this situation only the nonlinear coil L_1 of the ferroresonant circuit from the first switching module of the CT switch is orthogonally driven. As a consequence, the ferroresonant jump of the current from the low value of the amplitude to the high one will take place only in the I ferroresonant circuit which contains R_0, C_0 and L_1. In the circuits II and III the ferroresonance doesn't occur, the amplitude of the currents will be kept at minimum because the nonlinear coils L_2 and L_3 are not premagnetized by the magnet *1*.

The voltage drop on the capacitor C_0 will have the adequate shape and amplitude to turn on the transistor T_1, followed by the turning on of T_2 and therefore the load current will flow only through the section S_1 of the winding of the d.c. motor. All the other transistors will be off because their base to emitter voltage is lower than the one needed for conduction.

An electromagnetic torque will spin the polarized rotor, *8*, (in horarly direction in the case in Fig. 2 *a*) which will orientate the inductor *8* so that its magnetic field (the N–S axis) will have the same direction and sense with the stationary magnetic field (represented by the magnetic flux Φ_A) produced by the current that flows through the A–X section (the coil S_1) of the winding.

When the inductor *8* has rotated so that it occupies the position shown in Fig. 2 *b*, the magnet *1* will premagnetize the nonlinear coil L_2 and the ferroresonant jump of the current from a small value to a high one will take place in the ferroresonant circuit II, in the same time with the reverse jump of the amplitude in the ferroresonant circuit I. In the third ferroresonant circuit the amplitude of the current will be kept low, determined by the parameters R_0, C_0, L_3 with the coil orthogonally undriven.

So, for the situation in Fig. 2 *b*, the transistors T_1 and T_2 (belonging to module II) will be on. The section B–Y (the S_2 coil) being powered from the power supply *3*, the rotor (*8*) will rotate in hourly direction until the N–S axis will coincide with the axis of the field symbolized by means of Φ_B. We are now in the situation presented in Fig. 2 *c* when, the same reasoning leads us to the powering, by the power supply *3*, of the C–Z section (the S_3 coil); the rotor will spin in the same way in order to have the N–S axis on the same direction and in the same sense with Φ_C. After this, the electromagnetic processes continues like in Fig. 2 *a*.

3. Reversing the Direction of Rotation

It is known from the theory of the d.c. motor with collector and brushes that the direction of rotation can be reversed either by changing the direction of the inductor magnetic flux (that is the direction of the excitation current) or the direction of the current through the induced winding.

The inductor of a d.c. motor with solid-state commutation is a permanent magnet so the direction of the flux cannot be changed. The change to the connections of the power supply cannot be used because of the presence of the transistors in the circuit of the induced winding. On the other way, the changing of the connections of the three sections is not recommended because the already existing arrangement of the would be modified.

The direction of rotation of a d.c. motor with solid-state commutation depends on the order in which the connections of the power supply to the sections of the induced windings are made. This particularity is used in what follows.

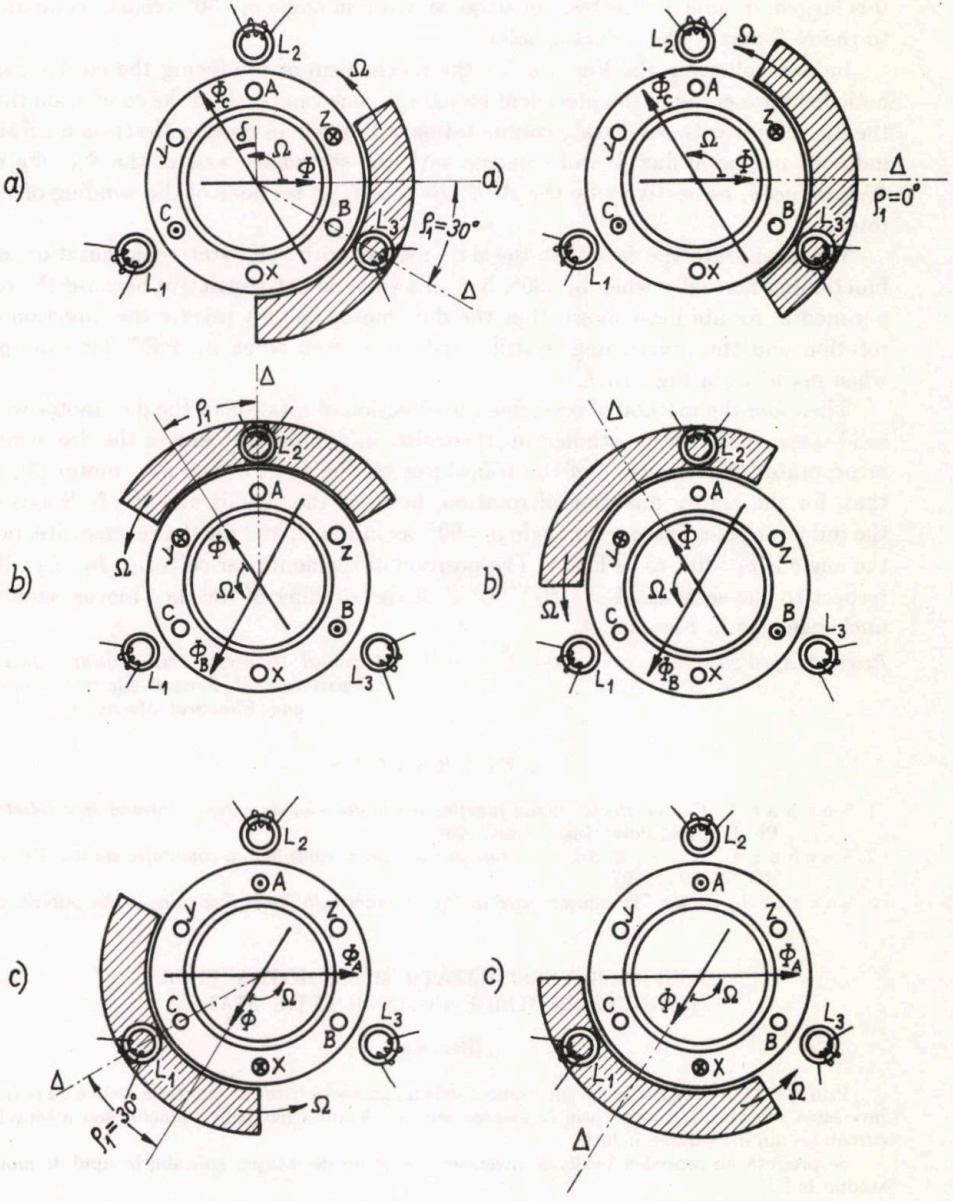

Fig. 3

Fig. 4

So, maintaining unchanged (as in Fig.2) the position on the stator of the nonlinear coils L_1, L_2, L_3 with respect to the sections A–X, B–Y, C–Z of the induced winding, the d.c. motor will develop a strong torque, with well determined direction of rotation even when the symmetry axis (the bisectrix) Δ of the angle of the sector of the signal β is lagged, in hourly direction, in advance, with an angle $\rho_1=30°=$const., compared to the N–S axis of the inductor poles.

Indeed, following the Figs. 3 a, b, c the mechanism of producing the electromagnetic field presented in the precedent paragraph, one can reach to the conclusion that the d.c. motor with solid-state commutation will rotate in reverse direction until the inductor magnetic flux Φ will coincide with the stationary axis of the Φ_A, Φ_B or Φ_C produced, respectively by the A–X, B–Y or C–Z sections of the winding of the rotor.

We must state the fact that the d.c. motors with solid-state commutation are functioning normally when $\rho_1=30°$, but this value is not restrictive because the experimental results have shown that the d.c. motor doesn't reverse the direction of rotation and the functioning is still satisfactory even when $\rho_1 \neq 30°$, for example when $\rho_1=0°$ as in Figs. 4 a, b, c.

Therefore the method of reversing the direction of rotation of the d.c. motor with solid-state commutation studied in [1] consists in a different fixing of the disc which incorporates the magnet *1* of the transducer on the shaft of the d.c. motor [3], so that, for the hourly direction of rotation, between the Δ axis and the N–S axis of the inductor poles there is an angle $\rho_1=90°$, as in Fig. 2, and for the reverse direction the angle is $\rho_1=30°$, as in Fig. 4. The position of the nonlinear coils L_1, L_2, L_3 with respect to the sections A–X, B–Y, C–Z of the winding of the d.c. motor remains unchanged, as in Figs. 2,...,4.

Received, April 30, 1997

Technical University "Gh.Asachi", Jassy,
Department of General Electrotechnics
and Electrical Machines

REFERENCES

1. S u c h a r I., *Contribuţii la studiul funcţionării motoarelor de curent continuu fără colector.* Ph. D. Diss., Polyt. Inst., Jassy, 1981.
2. S u c h a r I., C r e ţ u Ad., *Electromotor de curent continuu cu comutaţie statică.* Patent, RO, *74350* (1980).
3. S u c h a r I., *On the Transducers used in D.C. Motors with Static Switching* (to be published).

ASUPRA REVERSIBILITĂŢII MICROMOTOARELOR MAGNETOELECTRICE CU COMUTAŢIE STATICĂ

(Rezumat)

Prin specificul construcţiei lor, micromotoarele magnetoelectrice cu comutaţie statică nu permit inversarea sensului de rotaţie prin inversarea sensului fluxului magnetic inductor sau a sensului curentului din înfăşurarea indusă.

Se prezintă un procedeu inedit de inversare a sensului de rotaţie, aplicabil la tipul de motor studiat în [1].

BULETINUL INSTITUTULUI POLITEHNIC DIN IAŞI
Tomul XLIII (XLVII), Fasc. 3–4, 1997
Secţia III
ELECTROTEHNICĂ. ENERGETICĂ. ELECTRONICĂ

C.D. 621.396.21; 621.315.62.001.4

SUR L'OPTIMISATION DU FONCTIONNEMENT DU MODULATEUR DANS UNE INSTALLATION D'ESSAIS DE L'ISOLATION DES CÂBLES HT

PAR

COSTEL-EMIL TEODORU

L'essai des câbles à isolation en polyéthylène, sous tension continue, n'offre pas des informations complètes sur l'état de l'isolation et en plus détermine le vieillissement prématuré de celle-ci. Le comportement de l'isolation du câble à la fréquence de 50 ou 60 Hz et pour forme d'onde sinusoïdale sont largement connus. La difficulté est représentée par le grand gabarit des sources d'essai. Pour éliminer cet inconvénient on utilise l'essai à tension de basse fréquence (0,1 Hz), mais dans ce cas le problème principal est représenté par la difficulté d'obtenir une onde de tension à fréquence tellement basse.

On présente quelques aspects concernant l'amélioration du fonctionnement d'un modulateur qui constitue la principale source qui fournit la tension de 50 Hz, modulée à une fréquence de 0,1 Hz.

1. Introduction

Depuis nombre d'années déjà, beaucoup de recherches ont été effectuées pour développer des méthodes d'essai des câbles, qui offrent des informations utiles sur l'état de l'isolation. Les efforts des recherches ont été orientés dans différentes directions (l'essai par tension oscillante – onde oscillante de tension; l'essai par circuit résonant; l'essai par tension à basse fréquence). Toutes les méthodes d'essai ont été élaborées pour éliminer la possibilité de polariser, sous courant continu, les câbles testés [1],...,[4], [6].

La Fig. 1 présente le schéma électrique de principe d'une installation d'essai à basse tension. Ce schéma contient les sous-ensembles suivants: le modulateur de 0,1 Hz, le commutateur de polarité, des transformateurs HT et le démodulateur HT, de 50 Hz à 0,1 Hz. Le commutateur assure l'application de la tension modulée, successivement, aux deux transformateurs survolteurs et aux démodulateurs associés à ceux-là.

Basé sur ce schéma on a réalisé un modèle expérimental du modulateur et on a conçu le fondement théorique de la solution proposée.

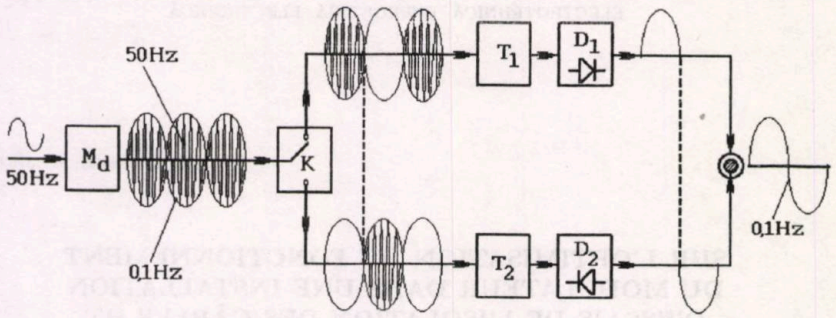

Fig. 1

2. Considérations générales sur le fonctionnement du modulateur

Le modulateur inclu dans l'installation d'essai de l'isolation des câbles HT, à une tension ayant une fréquence extrêmement basse doit assurer à la sortie, pour l'alimentation du transformateur survolteur, une tension de 50 Hz, modulée par une onde ayant une fréquence de 0,1 Hz. Dans ce but on a adopté comme modulateur un transformateur rotatif (Fig. 2), dont la construction ressemble à celle des machines asynchrones à rotor bobiné [5]. Sur le stator et le rotor sont disposés deux enroulements monophasés, caractérisés par une inductance mutuelle entre ceux-ci ayant la forme d'une fonction cosinusoïdale de l'angle formé par les axes des deux enroulements. L'angle α est variable par rapport au temps:

$$\alpha = \Omega t, \tag{1}$$

où Ω représente la vitesse angulaire de rotation du rotor. Pour la solution proposée il est avantageux que les deux enroulements soient réalisés avec une seule paire de pôles (p=1), pour obtenir l'efficience maximale dans la modulation désirée.

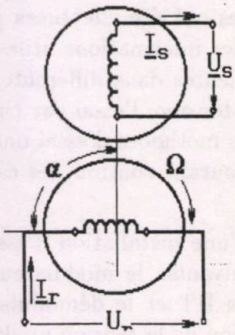

Fig. 2

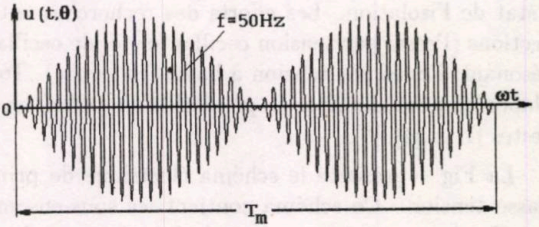

Fig. 3

Dans la situation où l'enroulement rotorique est alimenté avec la tension:

$$u_r = U_{r\max} \sin \omega t \tag{2}$$

et le rotor est entraîné à une vitesse angulaire Ω, tenant compte du fait que l'induction mutuelle, M_{rs}, varie d'une manière cosinusoïdale par rapport à l'angle α:

$$M_{rs} = M \cos \alpha, \tag{3}$$

il est évident que la tension électromotrice induite dans l'enroulement statorique, dans le cas du fonctionnement à vide, varie selon une loi sinusoïdale:

$$E_{s0} = E_{s\,\max} \sin \alpha. \tag{4}$$

M définit la valeur maximale de l'inductance mutuelle entre les deux enroulements, lorsque $E_{s\,\max}$ représente la valeur maximale de la tension induite dans l'enroulement statorique.

Dans le cas du fonctionnement à vide on obtient, dans le stator, une tension modulée ayant la forme:

$$e_{r0}(t) = E_{r\,\max} \cos \Omega t \, \sin \omega t \tag{5}$$

et dont le mode de variation est représenté dans la Fig. 3. Dans cette figure on a noté par T_m la période de l'onde modulatrice à basse fréquence et par f – la fréquence de l'onde modulée à 50 Hz, l'onde résultante étant $u_s(t)$.

Pour écrire les équations des tensions et des courants et pour étudier les conditions de fonctionnement on peut considérer le cas du modulateur idéal où les harmoniques supérieures des courbes de repartition des densités linéïques du courant manquent; la courbe de repartition de l'inductance magnétique est sinusoïdale; le circuit magnétique n'est pas saturé; l'entrefer est parfaitement constant; la symétrie magnétique radiale est réalisée; les pertes dans le fer sont négligeables.

Si l'enroulement statorique est couplé à l'impédance de charge Z_e on obtient les équations:

$$e_{\mathrm{st}} = u_s + R_s i_s, \qquad u_r = -e_{rt} + R_r i_r, \tag{6}$$

où R_s, R_r sont les résistances des enroulements; $e_{\mathrm{st}} = -\,\mathrm{d}\Psi_s/\,\mathrm{d}t$; $e_{rt} = -\,\mathrm{d}\Psi_r/\,\mathrm{d}t$ – les tensions induites dans les deux enroulement et u_s – la tension aux bornes de la charge.

On note par θ l'angle de rotation entre l'axe de l'enroulement rotorique et l'axe perpendiculaire sur celui de l'enroulement statorique; donc $\theta = 90° - \alpha$. Les flux totaux pour le stator et le rotor sont donnés par les équations:

$$\Psi_s = L_s i_s + M_{sr} i_r, \quad \Psi_r = L_r i_r + M_{rs} i_s, \tag{7}$$

où $L_s = L_{su} + L_{s\sigma}$ et $L_r = L_{ru} + L_{r\sigma}$ représentent les sommes des inductances utiles et des celles de fuites, lorsque:

$$M_{rs} = M_{sr} = M \sin \theta. \tag{8}$$

On peut exprimer les inductances en fonction du nombre de spires N_s, N_r et de la réluctance du circuit magnétique, R_m:

$$L_{us} = \frac{N_s^2}{R_m}, \quad L_{ru} = \frac{N_r^2}{R_m}, \quad M = \frac{N_s N_r}{R_m}. \tag{9}$$

Si l'on tient compte des équations (7) et (8) on peut écrire les équations (6) sous la forme complexe:

$$\begin{aligned} \underline{E}_s &= \underline{U}_s + \mathrm{j}\omega L_{s\sigma}\underline{I}_s + \mathrm{j}\omega M\underline{I}_r \sin\theta + R_s\underline{I}_s, \\ \underline{U}_r &= -\underline{E}_r + \mathrm{j}\omega L_{r\sigma}\underline{I}_r + \mathrm{j}\omega M\underline{I}_s \sin\theta + R_r\underline{I}_r, \end{aligned} \tag{10}$$

où $\underline{E}_s = -\mathrm{j}\omega L_{su}\underline{I}_s$ et $\underline{E}_r = -\mathrm{j}\omega L_{ru}\underline{I}_r$.

Si on considère que le modulateur fonctionne à vide ($\underline{I}_s = 0$) et le courant rotorique est $\underline{I}_{r0}$ le système est plus simple, en devenant:

$$\underline{U}_{s0} = \mathrm{j}\omega M\underline{I}_{r0}\sin\theta, \quad \underline{U}_r = -\underline{E}_{r0} + (R_r + \mathrm{j}\omega L_{rs})\underline{I}_{r0}. \tag{11}$$

On peut déterminer le rapport de transformation du modulateur:

$$K_m = \frac{E_{r0}}{E_{s0}} \cong \frac{U_r}{U_{s0}} = \frac{N_r}{N_s \sin\theta} = \frac{K}{\sin\theta}, \tag{12}$$

où $K = n_r/N_s$, identique avec le rapport de transformation pour le transformateur classique.

On observe que le rapport de transformation du modulateur dépend autant du rapport du nombre des spires, que de l'angle de rotation θ. Pour $\theta = 90°$ il résulte $K = K_m$. On peut déterminer donc la tension à vide:

$$U_{s0} = \frac{U_r \sin\theta}{K}. \tag{13}$$

Dans le cas du modulateur on peut rapporter les valeurs statoriques au rotor tout comme dans le cas du transformateur classique:

$$U_s' = KU_s, \quad I_s' = \frac{1}{K}I_s, \quad R_s' = K^2R_s, \quad X_s' = K^2X_s, \quad L_{s\sigma}' = K^2L_{s\sigma}. \tag{14}$$

L'équation (13) indique le fait que pour le fonctionnement à vide la tension obtenue dépend d'une manière sinusoïdale de l'angle θ.

Quand le modulateur fonctionne en charge, la dépendance idéale de la tension U_{s0} est modifiée puisque la réaction de la charge détermine la modification du flux utile.

Pour déterminer l'influence de la charge sur la forme de la tension statorique on multiplie la deuxième équation du système (10) par N_r/N_s et on tient compte des relations (9) et (14); le système (10) devient alors:

$$\begin{cases} -\underline{U}_s' = (R_s' + \mathrm{j}\omega L_{s\sigma}')\underline{I}_s + \mathrm{j}\omega\left(\dfrac{N_r^2}{R_m}\right)\underline{I}_r \sin\theta + \mathrm{j}\omega\left(\dfrac{N_r^2}{R_m}\right)\underline{I}_s', \\ \underline{U}_r = (R_r + \mathrm{j}\omega L_{r\sigma}')\underline{I}_r + \mathrm{j}\omega\left(\dfrac{N_r^2}{R_m}\right)\underline{I}_s' \sin\theta + \mathrm{j}\omega\left(\dfrac{N_r^2}{R_m}\right)\underline{I}_r. \end{cases} \tag{15}$$

Si on introduit les réactances (on note avec $\omega L_{ru} = X_m$ la réactance de magnétisation) et les impédances, le système (15) devient:

$$(16) \qquad -\underline{U}'_s = (\underline{Z}_s + \mathrm{j}X_m)\underline{I}'_s + \mathrm{j}\underline{X}_m\underline{I}_r \sin\theta, \quad \underline{U}_r = (Z_r + \mathrm{j}X_m)\underline{I}_r + \mathrm{j}X_m\underline{I}'_s \sin\theta.$$

Compte tenu de l'équation de charge dans le circuit statorique:

$$(17) \qquad \underline{U}'_s = \underline{Z}'_e\underline{I}'_s,$$

où Z'_e représente l'impédance de charge statorique rapportée au rotor, le système d'équations (16) devient:

$$(18) \qquad 0 = \mathrm{j}X_m\underline{I}_r \sin\theta + (\underline{Z}'_s + \underline{Z}'_e + \mathrm{j}X_m)\underline{I}'_s, \quad \underline{U}_r = (\underline{Z}_r + \mathrm{j}X_m)\underline{I}_r + \mathrm{j}\underline{X}_m\underline{I}'_s \sin\theta.$$

A l'aide de ce système on déduit l'expression du courant statorique rapporté:

$$(19) \qquad \underline{I}'_s = -\frac{\mathrm{j}X_m\underline{U}_r \sin\theta}{(\underline{Z}_r + \mathrm{j}X_m)(\underline{Z}'_s + \underline{Z}'_e + \mathrm{j}X_m) + X_m^2 \sin\theta}$$

et celle de la tension aux bornes de la charge:

$$(20) \qquad \underline{U}'_s = -\frac{\underline{U}_r \sin\theta}{\left(1 - \dfrac{\mathrm{j}\underline{Z}_r}{X_m}\right)\left(1 + \dfrac{\underline{Z}'_s + \mathrm{j}X_m}{\underline{Z}'_e}\right) - \dfrac{\mathrm{j}X_m}{\underline{Z}'_e} + \dfrac{\mathrm{j}X_m}{\underline{Z}'_e}\cos^2\theta}.$$

De l'analyse de l'équation (20) on constate que la valeur de la tension aux bornes de la charge est proportionnelle avec $\sin\theta$ (au numérateur) et influencée par $\cos^2\theta$ (au dénominateur). Pour éliminer ou diminuer cet inconvénient on utilise des méthodes diverses de compensation.

3. L'amélioration du fonctionnement du modulateur

Puisque dans le cas du modulateur classique la forme de la tension en charge est influencée par la valeur de la charge, par l'intermédiaire d'un terme qui dépend de $\cos^2\theta$, on cherche à diminuer l'influence de celui-là sur la forme de la tension statorique.

La méthode la plus répandue dans la littérature de spécialité est la symétrisation du modulateur par l'introduction d'un enroulement supplémentaire pour le stator et le rotor.

De l'équation (20) on constate que le terme qui contient $\cos^2\theta$ contient aussi X_m et Z'_e. On peut réduire, donc, ce terme si on diminue la réactance de magnétisation X_m et on agrandit l'impédance Z'_e. Cette observation nous a conduit à adopter la solution de surdimensionner le modulateur. Dans cette situation on diminue la valeur de la réactance de magnétisation et le régime de fonctionnement en charge est proche du celui à vide si la loi de variation prévue par l'équation (13) est respectée, ce qui représente un avantage pour le refroidissement.

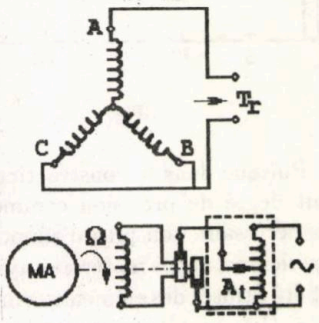

Fig. 4

Un autre inconvénient de la présence des enroulements monophasés est l'impossibilité d'anihiler la présence des harmoniqes de rang 3 qu'on les peut annuler dans le cas de l'enroulement triphasé. En prenant cette considération comme point de départ, on a adopté, pour l'enroulement statorique, un enroulement triphasé connecté tout comme dans la Fig. 4, l'inducteur étant alimenté à courant alternatif monophasé par un autotransformateur. On diminue ainsi, dans le stator, l'harmonique de rang 3 et, tout en utilisant dans le rotor un enroulement à répartition triangulaire, les valeurs des coefficients de réduction des harmoniques de rang 5 et 7 sont extrêmement réduites (moins de 0,5%). Dans les Fig. 5 et 6 sont présentées les formes du champ magnétique pour un enroulement triphasé et, respectivement, un enroulement monophasé, disposés sur une armature à 24 encoches. Par analyse harmonique on a déterminé le contenu d'harmoniques pour chaque onde (Fig. 7 et 8) et on a constaté des valeurs plus grandes de leurs amplitudes dans le deuxième cas.

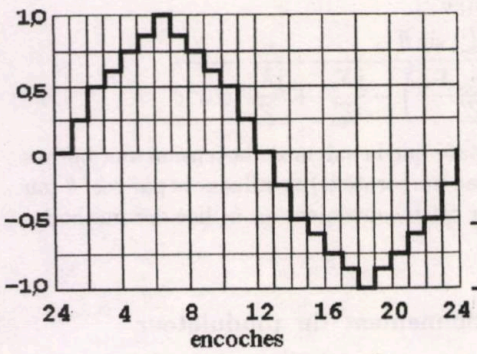

Fig. 5

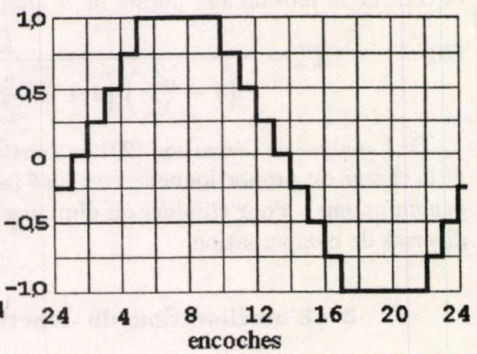

Fig. 6

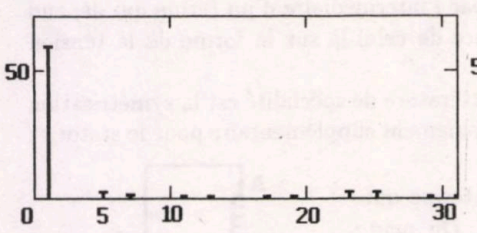

Fig. 7

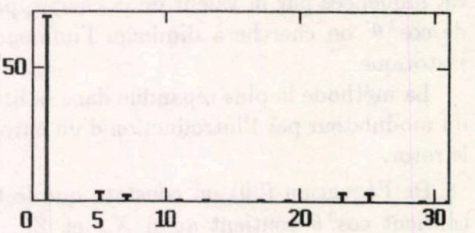

Fig. 8

Puisque dans la construction du modulateur il n'est pas nécessaire d'obtenir un haut degré de précision comme dans le cas des transformateurs rotatifs, il n'est pas nécessaire non plus d'adopter ou respecter certaines technologies de fabrication supérieures, ni des matériaux ayant des qualités spéciales. Pour réaliser le modulateur ont été utilisés des éléments composants des moteurs asynchrones de la production de série. Cette option assure le degré de précision voulu, en choisissant correctement les enroulements, les nombres d'encoches et le degré de saturation du circuit magnétique.

4. L'installation d'entraînement du modulateur

La principale difficulté qu'on doit surmonter dans le processus d'obtention de l'onde modulée de tension est représentée par la fréquence extrêmement basse (0,1 Hz) et la nécessité de la maintenir constante.

Pour réaliser ces desiderata il est nécessaire d'entraîner le rotor du modulateur par un servomoteur de courant continu, alimenté par l'intermédiaire d'un pont redresseur monophasé commandé. Le schéma de principe de l'installation de l'entraînement du modulateur est représenté dans la Fig. 9.

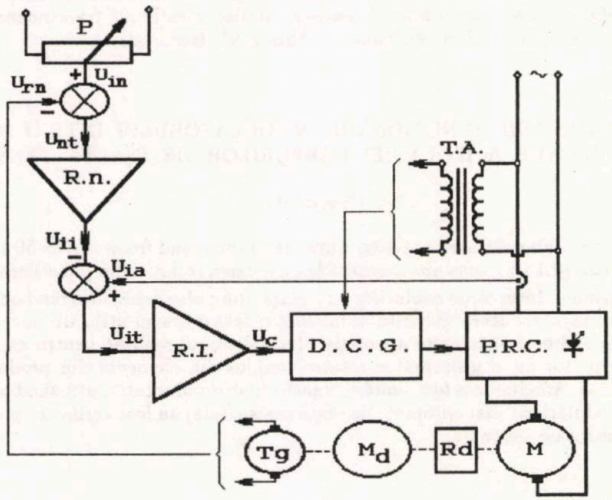

Fig. 9

Pour obtenir un couple actif suffisamment grand à une vitesse réduite de rotation de l'enroulement rotorique du modulateur, on introduit entre le servomoteur et le modulateur le réducteur R_d. On peut obtenir ainsi, facilement, la valeur de la vitesse de rotation nécessaire pour une onde modulée à une fréquence de 0,1 Hz.

5. Conclusions

L'utilisation du modulateur sous la forme constructive proposée, dans les installations d'essai à basse fréquence des cables HT à isolation en polyéthylène, assure une grande fiabilité en exploitation et, en plus, l'installation est facilement transportable grâce à son gabarit réduit.

À la réalisation du modulateur dans la variante proposée on peut utiliser des composantes des moteurs de construction classique, ce qui conduit à des dépenses réduites.

Reçue le 31 mars 1997

Université Technique „Gh. Asachi", Jassy,
Chaire d'Electrotechnique
générale et Machines électriques

BIBLIOGRAPHIE

1. Farnetti F., Ombello F., Bertani E., Mosca W., *Génération d'ondes oscillantes pour l'essai après pose des liaisons HT en câble à l'isolation extrudée.* CIGRE, 1990.
2. Kalkner W., Bach R., Plath R., *Les différentes méthodes d'essai pour les câbles après pose.* Jicable'91.
3. Ward B.H., Steiner J.P., *An Alternative to DC Testing of Installed Polymetic Power Cables.* Internat. Symp. High-Voltage, Dresden, 1991.
4. Gronefeld P., *Elektrische Prüfung von Kunststoffen mit Spannungen unterschiedlicher Form.* Diss., TU Hannover, 1986.
5. Simion Al., *Maşini electrice speciale pentru automatizări.* Universitas Chişinău, 1993.
6. Teodoru E., Groza D., Hajdău C., *Installation d'essais des câbles à isolation en polyéthylène à tension à basse fréquence.* Atelier scientifique franco-canadiano-roumain „Matériaux pour l'Electrotechnique", MmdE'97, Bucureşti.

STUDIUL OPTIMIZĂRII FUNCŢIONĂRII MODULATORULUI ÎNTR-O INSTALAŢIE DE ÎNCERCARE A IZOLAŢIEI CABLURILOR DE ÎNALTĂ TENSIUNE

(Rezumat)

Se abordează problema obţinerii practice a unei tensiuni având frecvenţa de 50 Hz cu o undă de frecvenţă foarte joasă (0,1 Hz), tensiune necesară la încercarea izolaţiei din polietilenă a cablurilor de medie şi înaltă tensiune. Încercările cablurilor cu izolaţie din polietilenă, utilizând o frecvenţă foarte joasă, prezintă avantajul reducerii gabaritului instalaţiei faţă de cazul utilizării unei frecvenţe de 50 Hz şi elimină pericolul de îmbătrânire a izolaţiei. La prototipul realizat pentru astfel de încercări s-a folosit ca modulator un transformator rotativ compus din elemente din producţia de serie a motoarelor asincrone. Ameliorarea funcţionării transformatorului rotativ, utilizând soluţiile propuse (obţinerea unei modulări cât mai apropiate de unda sinusoidală) au fost verificate şi confirmate prin încercările experimentale efectuate.

BULETINUL INSTITUTULUI POLITEHNIC DIN IAŞI
Tomul XLIII (XLVII), Fasc. 3–4, 1997
Secţia III
ELECTROTEHNICĂ. ENERGETICĂ. ELECTRONICĂ

D.C. 621.313; .001.13

PARTIAL MAGNETISING CHARACTERISTIC IN DC ELECTRICAL MACHINE DESIGN

BY

CRISTIAN DOMNIŞORU

A part of a DC electrical machine design made using the MATHCAD software is presented. This application is intended to be a classroom tool for teaching electrical machines design in electrotechnical curriculum. The main subject of the paper is to present a way to compute and to represent the partial magnetising characteristic of a DC machine using the MATCHAD capabilities. Also is presented a solution to replace the traditional computation of certain values using "graphical calculation of surfaces" with a more modern approach, a definite integral. Using this way we can compute the ampere-turns of the excitation winding in load keeping on the one hand the traditional design algorithm and on the other hand using a powerful software tool.

1. Introduction

In order to teach students electrical machine design several books [2],...,[4] are available. All these books presents the DC electrical machines design in a traditional way without any connection to computers and programmes. However, in [4] are presented some applications in Fortran but not related to a DC machine. Also in [1] are presented applications relative to several electrical machines but, unfortunately, unusable for a teaching purpose. In order to use, in the classroom together the traditional electrical machines design and the newer computers generation we may use a traditional language like Fortran, Turbo Pascal or C. The result is usually a programme difficult to update with a little interactivity. Also the formulas which are the basis of the calculus are hidden in the programme and the students can learn probably to use these programmes but not to design an electrical machine. Another solution can be to ignore in the classroom the computer programmes and to left in the students task to make programmes. The most attracting approach seems to be the use of a powerful tool like MATHCAD. With a short effort the students can use this tool and can develop powerful applications.

At several stages the traditional way of design in electrical machines contain the necessity of solving transcendent equations. Usually this is done using graphical equalities between certain surfaces. An example is the calculation of the magnetomotive force of the transversal reaction of the armature which must be compensated

by the magnetomotive force F_{aq}. The traditional algorithm require that a point on the partial magnetic characteristic to be translated till two surfaces became equals. The solution in MATHCAD is relative simple and use a definite integral with variable limits of integral domain, depending on a variable, u. The equation describing the condition of equality between the surfaces involved is solved using the appropriate feature in MATHCAD (given . . . find).

In what follows, a part of a MATHCAD application is presented being directly taken from the MATHCAD environment.

The presented example is taken from [2] in order to prove the advantages MATHCAD is used in electrical machines design.

2. Magnetomotive Force of the Main Pole

2.1. The Leakage Flux

If the DC machine has auxiliary poles k=4.5, for machines without auxiliary poles k=4; we adopt k:=4.5 and consequently

$$\Phi_\sigma := \frac{k l_m b_m}{\tau}(U_{m\delta} + U_{md} + U_{ma} + U_{mdc}) \times 10^{-6} = \begin{bmatrix} 0 \\ 0.124 \\ 0.175 \\ 0.204 \\ 0.243 \\ 0.301 \\ 0.415 \\ 0.645 \end{bmatrix} \times 10^{-2}, \quad [\text{Wb}].$$

The magnetic flux in the main pole is:

$$\Phi_m := \Phi + \Phi_\sigma = \begin{bmatrix} 0 \\ 1.763 \\ 2.47 \\ 2.827 \\ 3.193 \\ 3.58 \\ 4.022 \\ 4.579 \end{bmatrix} \times 10^{-2}, \qquad [\text{Wb}].$$

The leakage coefficient, repported to the previously adopted value (σ=1.14) is

now:

$$\sigma := \frac{\Phi_m}{\Phi} = \begin{bmatrix} 0 \\ 1.075 \\ 1.076 \\ 1.078 \\ 1.082 \\ 1.092 \\ 1.115 \\ 1.164 \end{bmatrix}.$$

The flux density calculated in the main pole is:

$$B_m := \frac{\Phi_m}{k_{Fem} l_m b_m} = \begin{bmatrix} 0 \\ 0.748 \\ 1.048 \\ 1.199 \\ 1.355 \\ 1.519 \\ 1.706 \\ 1.943 \end{bmatrix} \quad [\mathrm{T}].$$

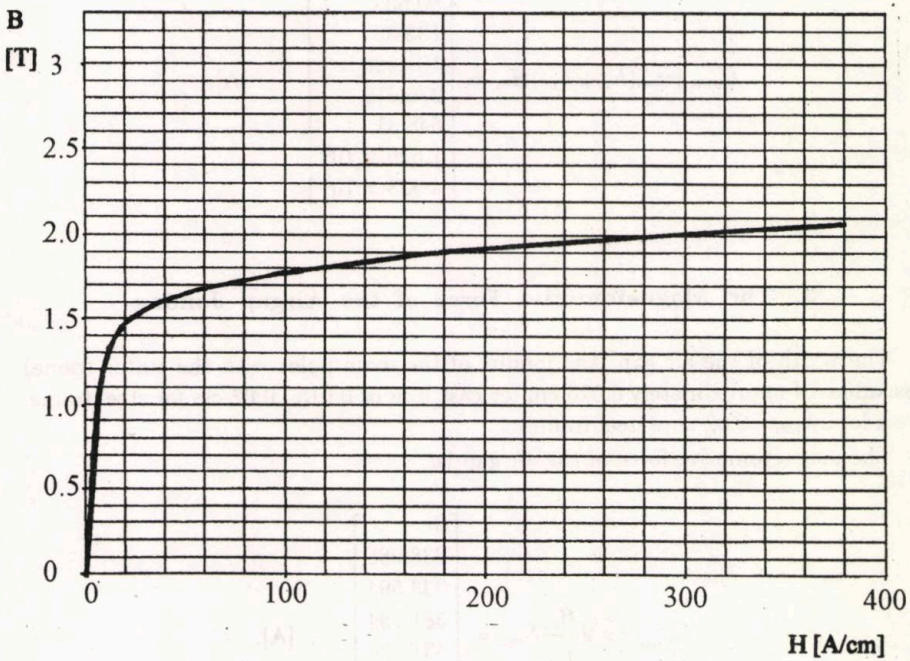

Fig. 1.– Magnetisation curve for a steel with a thickness between 1 and 2 mm for poles.

From the magnetisation curve for a steel band with a thickness between 1 and 2 mm for poles (Fig.1) the magnetising force depending on the magnetic flux density

in the pole, B_m, is obtained:

$$\text{vs} := \text{cspline}(\text{fig}^{<1>}, \text{fig}^{<0>})$$

$$H_m := \overline{\text{interp}(\text{vs}, \text{fig}^{<1>}, \text{fig}^{<0>}, B_m)} \quad [\text{A/cm}].$$

It results:

$$H_m = \begin{bmatrix} 0 \\ 3.738 \\ 6.276 \\ 8.439 \\ 12.799 \\ 25.425 \\ 73.234 \\ 228.266 \end{bmatrix} \quad [\text{A/cm}].$$

The magnetomotive force for the main pole is:

$$U_{mm} := 2(h_p + h_m)H_m = \begin{bmatrix} 0 \\ 80.605 \\ 135.35 \\ 181.996 \\ 276.019 \\ 548.31 \\ 1.579 \times 10^3 \\ 4.923 \times 10^3 \end{bmatrix} \quad [\text{A}].$$

3. The Magnetomotive Force of the Airgap Joining

The width of the air gap (the joining of the main poles with the stator frame) has values of approximately 0.025 cm for cast iron or 0.015...0.02 cm for steel frame. We adopt δ_{imb}:=0.02 cm (steel frame).

The magnetomotive force of the air gap is:

$$U_{m\delta_{\text{imb}}} := 2\frac{B_m}{\mu_0}\delta_{\text{imb}} = \begin{bmatrix} 0 \\ 238.085 \\ 333.594 \\ 381.784 \\ 431.236 \\ 483.425 \\ 543.147 \\ 618.385 \end{bmatrix} \quad [\text{A}].$$

4. The Magnetomotive Force of the Stator Frame

The average length of the magnetic line in the stator frame is:

$$L_{js} := \frac{\pi[D + 2(\delta + h_p + h_m) + h_{js}]}{2p} = 0.354 \text{ m}.$$

The exact value of the magnetic flux density in the stator frame is:

$$B_{js} := \frac{\Phi_m}{2l_c h_{js}} = \begin{bmatrix} 0 \\ 0.625 \\ 0.876 \\ 1.003 \\ 1.132 \\ 1.269 \\ 1.426 \\ 1.624 \end{bmatrix} \quad [\text{T}].$$

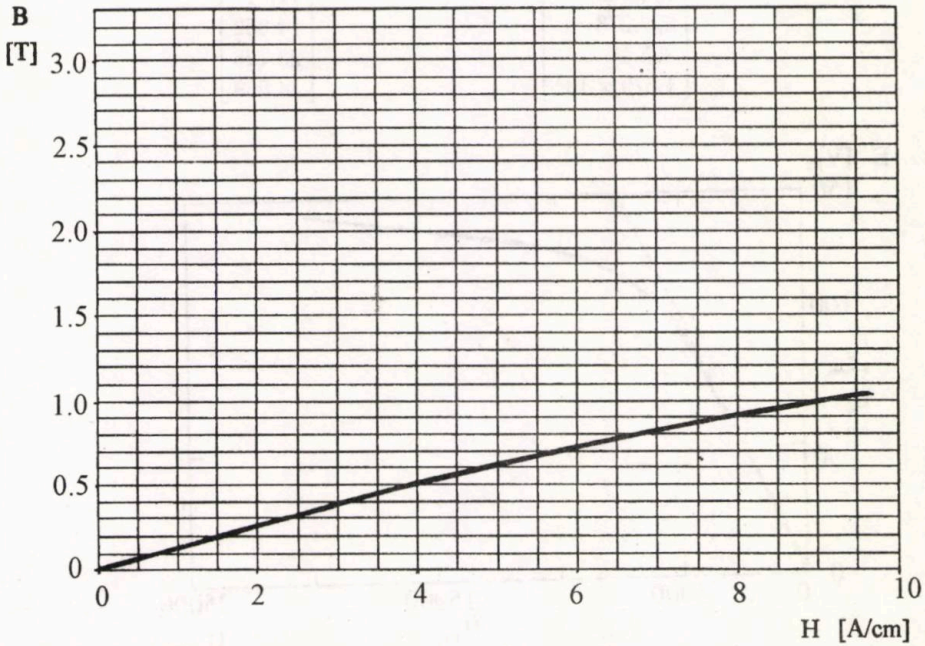

Fig. 2.– Magnetising curve for founded, forged steel, and thick laminated bands.

Depending on the value of the magnetic flux density B_{js} is determined, using the Fig.2; the value of the magnetising force in stator frame:

$$\text{vs} := \text{cspline}(\text{fig}^{<1>}, \text{fig}^{<0>})$$

$$H_{js} := \overline{\text{interp}(\text{vs}, \text{fig}^{<1>}, \text{fig}^{<0>}, B_{js})} \quad [\text{A/cm}].$$

$$B_{js} = \begin{bmatrix} 0 \\ 0.625 \\ 0.876 \\ 1.003 \\ 1.132 \\ 1.269 \\ 1.426 \\ 1.624 \end{bmatrix} \quad [\mathrm{T}].$$

The magnetomotive force of the stator frame results:

$$U_{mjs} := L_{js} H_{js} = \begin{bmatrix} 0 \\ 181.232 \\ 273.211 \\ 328.596 \\ 408.059 \\ 527.273 \\ 805.17 \\ 1.579 \times 10^3 \end{bmatrix} \quad [\mathrm{A}], \quad \text{with} \quad H_{js} = \begin{bmatrix} 0 \\ 5.115 \\ 7.711 \\ 9.275 \\ 11.517 \\ 14.882 \\ 22.726 \\ 44.569 \end{bmatrix} \quad [\mathrm{A/cm}].$$

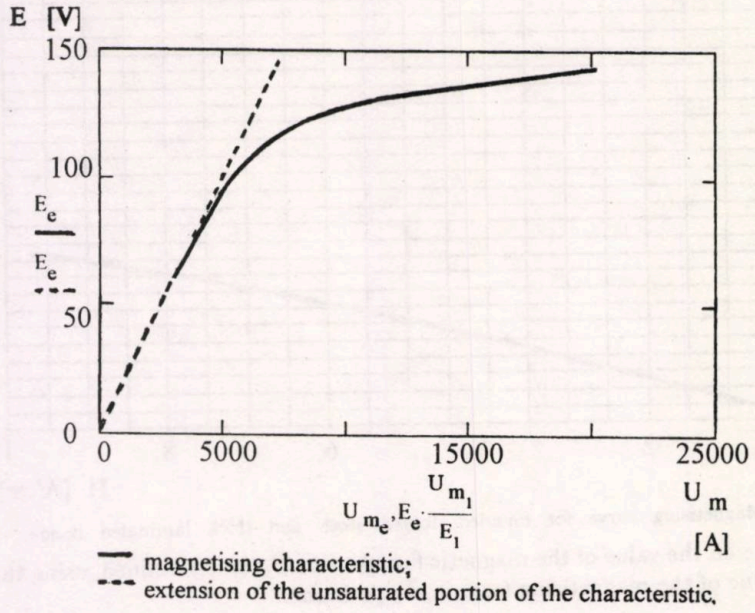

Fig. 3.– Magnetising characteristic at no load.

The magnetomotive force at no load in order to produce the nominal electromo-

tive force E_N is:

$$U_m := U_{m\delta} + U_{md} + U_{ma} + U_{mdc} + U_{mm} + U_{m\delta_{imb}} + U_{mjs} = \begin{bmatrix} 0 \\ 3.017 \times 10^3 \\ 4.307 \times 10^3 \\ 5.047 \times 10^3 \\ 6.05 \times 10^3 \\ 7.686 \times 10^3 \\ 1.138 \times 10^4 \\ 2.024 \times 10^4 \end{bmatrix} \quad [A]$$

and

$$U_{m\delta_{dac}} := U_{m\delta} + U_{md} + U_{ma} + U_{mdc} = \begin{bmatrix} 0 \\ 2.517 \times 10^3 \\ 3.565 \times 10^3 \\ 4.155 \times 10^3 \\ 4.934 \times 10^3 \\ 6.127 \times 10^3 \\ 8.454 \times 10^3 \\ 1.312 \times 10^4 \end{bmatrix} \quad [A].$$

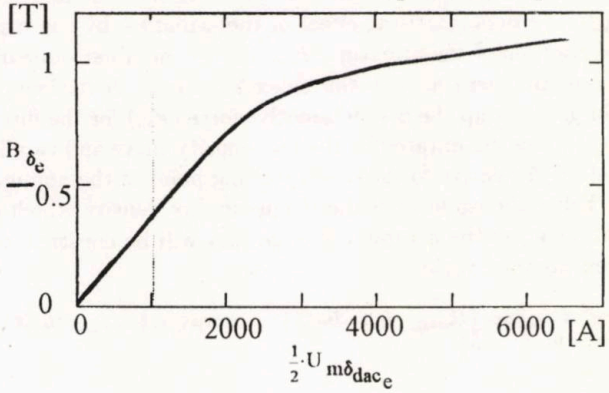

Fig. 4.– Partial magnetising characteristic of the airgap, teeth of the armature, teeth of the compensating winding and for the armature frame, for one pole.

5. The Saturation in the Machine

The magnetomotive force corresponding to the nominal magnetic flux at no load (for U_N), obtained from magnetising characteristic at no load, is U_{m0}:

$$\text{vs} := \text{cspline}(E, U_m)$$
$$U_{m0} := \text{interp}(\text{vs}, E, U_m, U_N) = 6.257 \times 10^3 \quad [A].$$

The magnetomotive force corresponding to the nominal tension U_N but considered from the extension of the linear portion of the magnetising characteristic at no

load (considering an hypothetical unsaturated state for the machine) is given by:

$$U'_{m0} := \frac{U_{m_1}}{E_1} U_N = 5.531 \times 10^3 \qquad [\text{A}].$$

The saturation coefficient is:

$$k_s := \frac{U_{m0}}{U'_{m0}} = 1.131.$$

6. Excitation Magnetomotive Force in Load

The magnetomotive force U_{mE} is determined corresponding to the flux at no load, computed for the nominal electromotive force E_N (this determination is made from the no load characteristic).

$$\text{vs} := \text{cspline}(E, U_m)$$
$$U_{mE} := \text{interp}(\text{vs}, E, U_m, E_N) = 7.686 \times 10^3 \qquad [\text{A}].$$

With the help of the partial characteristic is determined the magnetomotive force corresponding to the demagnetising effect of the armature by the magnetic field of the transversal reaction of the armature, F_{aq}. For the nominal value of the flux density in the airgap (the element with the index 5 in ours calculations) is determined the quantity for growing up the magnetomotive force (F_{aq}) for the flux per pole (calculated like the surface delimitated by the flux density curve and two lines drawed at $+0.5b_iA$ and $-0.5b_iA$ relative to the corresponding point of the nominal flux density in the airgap) being the same with the magnetic flux density which correspond to the ideal situation when the magnetic flux density will be constant across the pole and equal to her nominal value:

$$\text{vs} := \text{cspline}\left(\tfrac{1}{2}U_{m\delta_{dac}}, B_\delta\right) \quad B\delta(X) := \text{interp}\left(\text{vs}, \tfrac{1}{2}U_{m\delta_{dac}}, B_\delta, X\right)$$
$$u := 0 \qquad [\text{A}].$$

It results

$$\int_{\frac{1}{2}U_{m\delta_{dac_5}} - \frac{1}{2}b_iA + u}^{\frac{1}{2}U_{m\delta_{dac_5}} + \frac{1}{2}b_iA + u} B_\delta(X)\,\mathrm{d}X = B_{\delta_5} b_i A;$$

$$B_\delta = \begin{bmatrix} 0 \\ 0.454 \\ 0.636 \\ 0.727 \\ 0.818 \\ 0.909 \\ 1 \\ 1.091 \end{bmatrix} \qquad [\text{T}];$$

$$F_{aq} := \text{find}(u)$$

$$F_{aq} = 844.202 \qquad [\text{A}].$$

The magnetomotive force corresponding to the demagnetising effect by the longitudinal armature magnetic field reaction, per pole, is F_{ad}.

For the machines with auxiliary poles (brushes in the neutral geometrical axis) F_{ad}=0. We adopt F_{ad}:=0.

For the machines without auxiliary poles (if the brushes are decalated from the neutral axis) F_{ad}:=cA, where c=0.4($\tau - b_i$) and represents the displacement of the brushes from the neutral axis, and A – the ampere-turns.

The total magnetomotive force at nominal load, F_{eN}, corresponding to a pair of poles (equal with the excitation magnetomotive force conform to the magnetic circuit law) may be obtained:

$$F_{eN} := U_{mE} + 2(F_{aq} + F_{ad}) = 9.374 \times 10^3 \qquad [\text{A}].$$

7. Conclusions

The use of MATHCAD in electrical machines design, especially in the classroom, is a very powerful tool which increase the interest of the students.

A solution to replace the traditional computation of certain values using "graphical calculation of surfaces" with a more modern approach – a definite integral – is presented. Using this way, the magnetomotive force of the excitation winding in load is calculated.

Received, April 26, 1996

Technical University "Gh.Asachi", Jassy,
Department of General Electrotechnics
and Electrical Machines

REFERENCES

1. R a m a m o o r t y M., *Computer-aided Design of Electrical Equipment.* Ellis Horwood, Chichester, England, 1988.
2. C i o c I., N i c a C., *Proiectarea maşinilor electrice.* Ed. Did. şi Ped., Bucureşti, 199-.
3. B ă l ă C.V., *Proiectarea maşinilor electrice.* Ed. Did. şi Ped., Bucureşti, 1967.
4. D o r d e a T., B i r i e s c u M., *Proiectarea maşinilor electrice.* Vol.1-1, Universitatea Tehnică, Timişoara, 1992.

CARACTERISTICA MAGNETICĂ PARŢIALĂ ÎN PROIECTAREA MAŞINII DE CURENT CONTINUU

(Rezumat)

Se prezintă o parte a unui proiect pentru o maşină de curent continuu, realizat cu ajutorul programului MATHCAD. Această aplicaţie reprezintă un instrument de lucru modern în instruirea studenţilor în proiectarea maşinilor electrice în cadrul specializării electrotehnică. Aportul principal al lucrării constă în prezentarea unei modalităţi de a calcula şi reprezenta caracteristica magnetică

parţială a unei maşini de curent continuu utilizând facilităţile programului MATHCAD. De asemenea se prezintă o soluţie de înlocuire a calculului tradiţional al unor mărimi bazat pe „calculul grafic al unor suprafeţe" cu o abordare mai modernă, o integrală definită. Utilizând această cale se poate calcula solenaţia de excitaţie la funcţionarea în sarcină păstrând pe de o parte algoritmul tradiţional de proiectare şi pe de alta utilizând un instrument soft puternic.

BULETINUL INSTITUTULUI POLITEHNIC DIN IAŞI
Tomul XLIII (XLVII), Fasc. 3–4, 1997
Secţia III
ELECTROTEHNICĂ. ENERGETICĂ. ELECTRONICĂ

D.C. 621.395.72

ONE-BIT DIGITAL SPATIAL SWITCH USED IN LOW CAPACITY ELECTRONIC TELEPHONE EXCHANGE

BY

PETRUŢ DUMA, CLARISSA GÂTLAN and LUMINIŢA SCRIPCARIU

The hardware structure of a one-bit digital spatial switch, used in low capacity electronic telephone exchanges, which uses delta-modulation for the conversation signal is described. It can be used along with other switches for implementing connection fields in telephone exchanges.

1. Introduction

The delta-modulation represents a possibility of digital conversion of the conversation signal in a low capacity electronic telephone exchange. This modulation offers the main advantage of a transmission rate for the digitalized vocal signal of 4...32 kbits/s, insuring a high quality of the received vocal signal for a transmission rate from 16 to 32 kbits, and an acceptable quality for lower rates.

The one-bit digital spatial switch is used in the connection network of the low capacity electronic telephone exchange based on delta-modulation of the conversation signal. The switching network inputs and outputs consist of k input lines (LI) and l output lines (LE). Each line includes n one-bit conversation channels, resulted from the delta-modulation process.

The digital spatial switch performs the spatial switching of the current channel from any input line to the current channel of any output line. The network's possibilities are graphically expressed in Fig. 1, where the notations have the following meanings: LI_0, LI_1,..., LI_{k-1} – input lines; LE_0, LE_1,..., LE_{l-1} – output lines; 0, 1, 2,..., $n-1$ – one-bit digital conversation channels. It is assumed that, at a certain moment, on every input and output line is placed the same channel. The persistance duration of every channel is T_2.

The spatial switching performs, for instance, the transfer of channel 0 of LI_2 to channel 0 of LE_1, of channel 1 of LI_0 to channel 1 of LE_1, of channel 2 of LI_1 to channel 2 of LE_1, a.s.o.

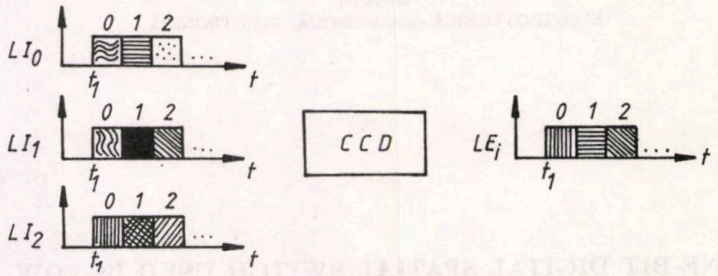

Fig. 1

2. The Hardware Structure of the Switch

The hardware structure is depicted in Fig. 2, where the notations have the following meanings: MUX_i – data digital multiplexer, REG_i – latch register, MC_i – command memory, MUX – address multiplexer, NC – channel counter, OSC – oscillator, SLC – logical combinational structure.

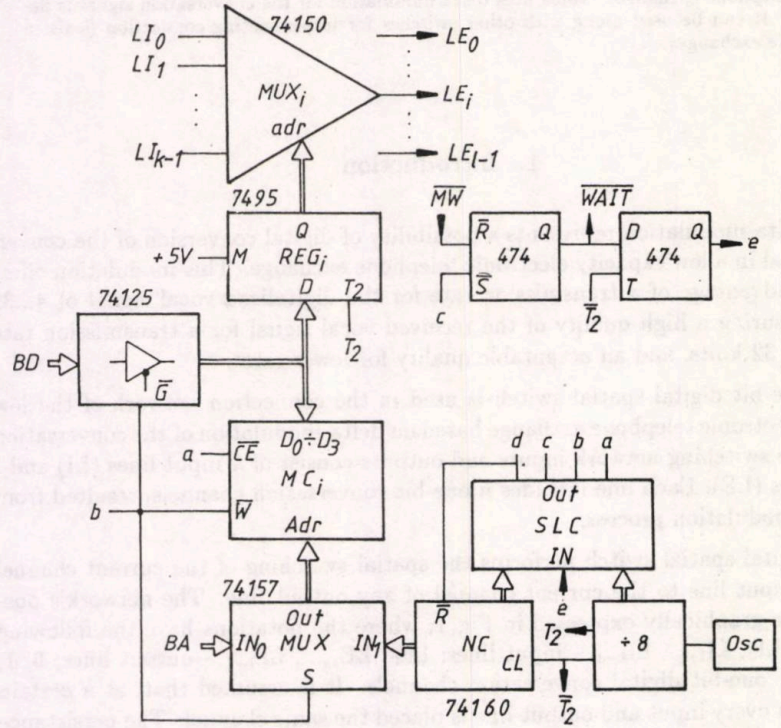

Fig. 2

The digital switch has l output lines. The figure presents the hardware structure corresponding to only one output line. The input lines are connected to all the MUX_i

digital multiplexers' inputs, where i=0,...,$l-1$. The digital multiplexer connects the input of address adr at the data output. It can be implemented by one of the logic circuits 74153, 74151, 74150 depending on the number of input lines (4, 8, 16). Through the latch register (based on 7495 circuit), the data multiplexer is driven by a command memory.

The address lines of this memory are connected to an address multiplexer (based on 74157 circuit). The data lines are connected to the inputs of the latch register on one side, in order to allow the storage of the address of the input line which is to be switched to the output line during the current channel, and to the outputs of a three-state buffer (74125) on the other side, in order to perform the writing in the command memory.

The address multiplexer is controlled by the selection signal $S = b$ allowing to connect on the memory address lines of the address delivered by the channel counter (for $S = 1$) or the address delivered by the command unit (for $S = 0$).

The current contents of the channel counter represents the number of the channel currently placed on the switch's inputs and outputs. The channel counter (implemented with 74161 circuit) is controlled by the signal generated by a quartz-driven oscillator, through a pre-scaling counter (divided by 8).

Reading the command memory is made using the signals $a = \overline{CE} = 0$ and $b = \overline{W} = 1$, when the contents of the memory location having the address defined by the channel counter is loaded on the negative transition of the signal T_2 in the latch register in order to maintain the address of the digital multiplexer during the channel. The writing signals of the command memory $a = \overline{CE} = 0$ and $b = \overline{W} = 0$ are obtained after synchronising the memory write signal ($\overline{MW}$) generated by the command unit with T_2. At the same time, the microprocessor of the command unit is set in a WAIT status.

Assume that the channel counter has the value 0 and that, in the command memory at address 0 is stored the data 0. In the second half of the channel 0 duration, the command memory is read. The data 0 is loaded at the end of the time interval corresponding to channel 0 in the latch register and, through this, is placed on the address input of the digital multiplexer. The switching of the channel 1 of LI_0 in the channel 1 of LE_i is performed in this manner. On the rising edge of T_2, the address counter is incremented (its contents becomes 01).

Afterwards, during the first half of the time interval corresponding to channel 1, the command memory is written if, during the time period corresponding to channel 0, a writing request was sent by the command unit. During the second half of time interval corresponding to channel 1, the command memory is written from address 1 where is stored the data 01. Therefore, LI_1 is switched in LE_i during the channel 2 and so on. The channel counter increment is made until the maximal value $N-1$, after which the counter is reset.

In order that the switch's operation develops as described above, it is necessary for the command unit to previously write the appropriate data in the command memory, i.e. at address 0 is stored the data 0, at address 1 – the data 1, at address 2 – the data 4, etc. The data storage operation is synchronised with two D-type

flip-flops (7474) and a logical structure.

The command signals required by the switch's operation (Fig. 3) are generated by a combinational logical structure implemented by the circuit PAL10L8NC.

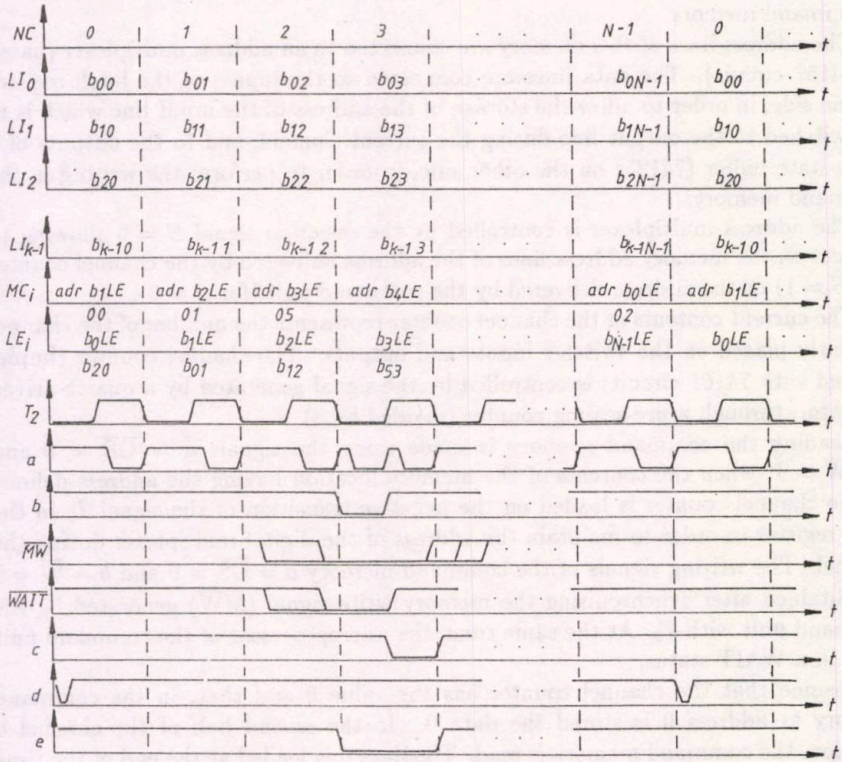

Fig. 3

The digital spatial switch presented is controlled on the output. A switch structure with input control can also be designed. In this case, instead of data digital multiplexer, data demultiplexers and a series of OR logical gates as depicted in Fig. 4 are used. This switch selects, during a channel, the number of the output line towards which is directed the input line. The input-controlled switch has a more complicated hardware structure and its command must avoid the situation of connecting two or more input lines in the same output line, during the same channel.

The maximal number of the switch channels from any input line to any output one is:

$$N_{\max} = \frac{10^5}{Q(t_{sc} + \Delta t)}$$

where: Q is the digitalized conversation signal transmission rate, [kbits/s]; t_{sc} – access time of the command memory, [ns]; Δt – delay on logical circuitry, [ns].

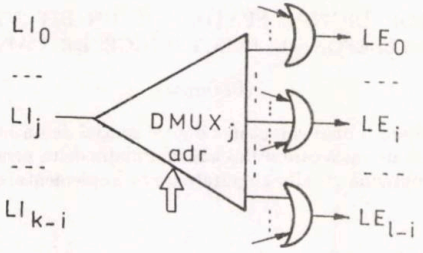

Fig. 4

3. Conclusions

The one-bit digital spatial switch described, along with other types of switches, constitutes the connection network of a low capacity electronic telephone exchange, which are used in special destination application.

For the structure presented, the maximal number of channels is 1,000 if the transmission rate of the vocal signal is of 8 kbits/s and the memory used have an access time of 100 ns.

The command for performing the switch operation is simple and is reduced to read/write requests for the command memory of the switch. The switches may be controlled by microprocessor of microcontroller-based systems, which require a very simple interfacing structure.

Received, October 1, 1996

Technical University "Gh.Asachi", Jassy,
Department of Telecommunications

REFERENCES

1. Rony P.R., Larsen D.G., Titus J.A., *Microcomputer Interfacing and Programming.* Howard W. Sams & Co. Inc., 1987.
2. Vasilescu A., *Iniţiere în telefonia digitală.* Ed. Tehnică, Bucureşti, 1988.
3. GRINSEC, *La commutation électronique.* Ed. Eyrolles, Paris, 1989.
4. Dicenet G., *Le RNIS. Techniques et atouts.* Ed. Masson, Paris, 1989.
5. Niţulescu P., *Echipamente moderne în telefonie.* Ed. Tehnică, Bucureşti, 1989.
6. Răduleşcu T., *Telecomunicaţii.* Media Publishing, Bucureşti, 1994.
7. Borcoci E., *Sisteme de comutaţie digitale.* Ed. Vega, Bucureşti, 1994.
8. Duma P., *Comutator digital temporal de un bit utilizat în centralele telefonice electronice de capacitate mică.* The XXVI-th Sci. Sess., 4, s.*10*, Transmissions, Military Technical Academy, Bucureşti, November 16-17, 1995, 47-50.
9. Duma P., *One-Level Digital Switching Network for Low Capacity Electronic Telephone Exchanges Based on Delta-Modulation for the Conversation Signal.* The 4th International Conference on Reliability of Semiconductor Devices and Systems, Chişinău, June 1996, Moldova Republic, 196-199.

COMUTATOR DIGITAL SPAŢIAL DE UN BIT UTILIZAT ÎN CENTRALELE TELEFONICE ELECTRONICE DE CAPACITATE MICĂ

(Rezumat)

Se prezintă structura hard a unui comutator digital spaţial de un bit utilizat în centralele telefonice electronice de capacitate mică care utilizează modulaţia delta pentru semnalul de convorbire. Acesta poate fi utilizat împreună cu alte comutatoare la implementarea câmpurilor de conexiune din centralele telefonice.

BULETINUL INSTITUTULUI POLITEHNIC DIN IAŞI
Tomul XLIII (XLVII), Fasc. 3–4, 1997
Secţia III
ELECTROTEHNICĂ. ENERGETICĂ. ELECTRONICĂ

D.C. 621.316.11

ABOUT THE OPTIMAL DEVELOPMENT FOR THE ELECTRIC NETWORK CONSIDERING UNCERTAIN INFORMATION

BY

EUGEN BÂRLĂDEANU and AL. POEATĂ

A model for optimizing the development of the electric network is proposed. This model takes into account uncertain information and some constraints as: framing in the environment, reliability, etc. and the objective is to minimize the costs. The objectives and the constraints are modelling using the fuzzy set theory which allows us to find easily and efficiently the optimal decisions taking into account simultaneously the elements, quantifiable or not from the economical point of view.

1. Introduction

Nowadays, in taking decisions about electric network development, we must consider new aspects concerning the reliability of the elements of the system and the impact on the environment.

Information owned by the power system operators is, generally, vague, because of the inaccuracy of the measurements or of incomplete knowledge about an event. Thus, the investment cost can be estimated with a certain error ($\pm a$) and about the reliability it can be said that is "high". Sometimes, the vague description sound like this: "the frequency of damages per year is about 5, but not less than 3 and not more than 7".

These uncertain knowledge and vague information may be represented by fuzzy numbers (FNs) whose membership functions may have different forms (Fig. 1).

The algebraic operations can be extended to FNs using the Extension Principle formulated by Z a d e h [1], [3]. In particular, given the fuzzy sets $\tilde{A} = \{x, \mu(x)\}$ and $\tilde{B} = \{y, \mu(y)\}$ the addition $\tilde{A} \dot{+} \tilde{B}$ and the product $\tilde{A} \cdot \tilde{B}$ are calculated by:

$$\begin{aligned} &\tilde{A} \dot{+} \tilde{B} = \{z, \mu_{\tilde{A} \dot{+} \tilde{B}}\}, \quad z = x \dot{+} y, \\ &\mu_{\tilde{A} \dot{+} \tilde{B}} = \text{Max} \ \{\text{Min}(\mu_{\tilde{A}}(x), \mu_{\tilde{B}}(y)\}. \end{aligned} \tag{1}$$

Likewise we can define other algebraic operations (subtraction, product with a real constant or division).

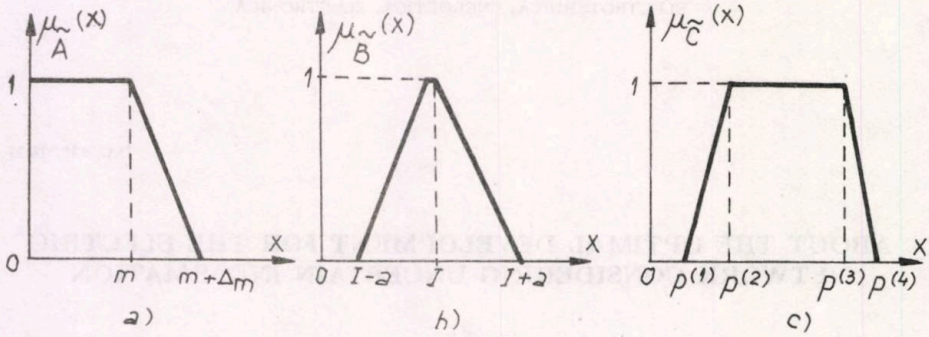

Fig. 1.– Fuzzy number.

The objective functions, which must be minimized r maximized, and the occurring constraints are, in the field of electric network, linear functions:

$$Z(X) = CX, \quad AX \leq B, \tag{2}$$

where: Z is the objective functions vector; C, A – the coefficient matrix for objective functions and constraints; X – the problem variables vector (the lengths for the electric lines, the number of the substations, etc.); B – the maximum accepted values vector.

Considering the extension of the algebraic operations to FNs and the fact that the coefficients matrix A, B and C are common or fuzzy numbers it means that finding the optimal solution is reduced to choosing the variant which satisfies the best inequalities like:

$$\check{c}x \leq \tilde{d}, \quad ax \leq \tilde{b}, \tag{3}$$

where: d, b are FNs corresponding to ideal values.

The high level of satisfaction an inequality like (3) is σ and the guarantee that the inequality is satisfy by τ which correspond to a minimum level η for membership functions (Fig. 2).

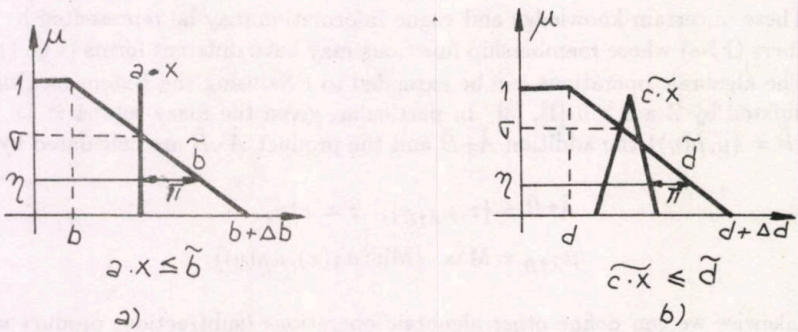

Fig. 2.– Fuzzy objectives and fuzzy constraints.

If we consider p criteria (objectives) and m constraints, the optimization problem is reduced to maximizing the high levels of satisfaction of the inequalities which correspond to the criteria in certain conditions:

$$(4) \qquad \text{Max} \sum_{i=1}^{p} \alpha_i \sigma_i, \ \alpha_i \ - \ \text{weight coefficients}; \ \pi_i \geq \theta_i = 0; \quad (i = 1, ..., p)$$

and with taking into account a certain level for constraints:

$$(5) \qquad \sigma_j \geq \tau_j, \quad \pi_j \geq \theta_j, \quad (j = 1, ..., m).$$

This approach of the problem allows us to consider many uncertainties and fuzzy information than the methods which rely on "fuzzy binary relation" [2], [5], which is important in forecasting the long-term development.

2. Fuzzy Model for the Optimization of Electric Network Development

In the optimal planning for the development of electric network, medium voltage, we must consider many criteria and respect some constraints.

The main objectives in making decisions for development are: a) the minimization of costs, b) the maximization of the reliability and c) the minimization of the impact (visual, architectural) with the environment. We can also consider other criteria related to the noxious emissions when there are local generators or social and political factors.

Uncertain information about the investment and operational costs are due to the impossibility to forecast precisely the cost of materials and the powers needed by the consumers. The vague knowledge about the investments can be represented by FN with a membership function like one in the Fig. 1 *b*, where a is the possible spread of the costs, and those who make reference to powers by FNs with membership function like in Fig. 1 *c*. If we consider only the investment costs, than the objective to minimize the costs can be written as follows:

$$(6) \qquad [\tilde{c}_1, \tilde{c}_2, \tilde{c}_3, \tilde{c}_4] \cdot \begin{bmatrix} N_s \\ l_1 \\ l_2 \\ l_3 \end{bmatrix} \leq \tilde{d}_1,$$

where: $\tilde{c}_1$ is the fuzzy cost of an electric substation; $\tilde{c}_2, \tilde{c}_3, \tilde{c}_4$ – the fuzzy costs for 1 km of overhead electric line with one circuit, two circuits and 1 km of underground electric line, respectively; N_s – the number of electric substations; l_1, l_2, l_3 – the lengths (in km) of the overhead lines, with one and two circuits, and that of the underground line; $\tilde{d}_1$ – the FN for the minimum cost for the investment who has a membership function like one in the Fig. 1 *a*, where m is the ideal value and $m + \Delta m$ – the non-ideal one.

To estimate the reliability it may be used the index named "undelivered power because of damages". On the assumption that there are considered only the damages for the electric lines, the objective of maximize the reliability is reduced now to the scope of minimization the undelivered power:

$$\sum_{i=1}^{n} \tilde{N}_i \tilde{T}_{di} \tilde{P}_i \leq \tilde{d}_2, \tag{7}$$

where $\tilde{N}_i$ is the (fuzzy) number of frequency of failures on line i (in a considered period of time); $\tilde{T}_{di}$ – the (fuzzy) time needed for reparation the line i; $\tilde{P}_i$ – the unfeeded (fuzzy) load when there is a failure on line i; n – the number of electric lines; $\tilde{d}_2$ – the FN corresponding with the undelivered power for an ideal case.

The impact of the electric network on the environment depends on many non-quantifiable elements from the economical point of view, and that is a very topical problem today. For estimating the visual impact, in generally, the experts use a series of measurable parameters (the population and transport density, the number of touristic objectives, etc.). The estimation may be a linguistic declaration (fuzzy numbers) with values in the real interval $[0, 1]$ and a triangle membership function. The inequality that corresponds to this objective (the minimization of the visual impact) is:

$$\sum_{i=1}^{n} \frac{L_i}{L} \tilde{a}_{mi} \leq \tilde{d}_3, \tag{8}$$

where: $\tilde{a}_{mi}$ is the qualificative fuzzy for the line i (zero for underground lines); L_i – the length of the line i; L – the length of all the lines.

The constraints which must be considered in the optimization model make reference at a maximum capacity for substation and electric lines and, also, at maximum voltages values. The optimal variant for the network from the network configuration and elements point of view is that which results after ordering the variants with relation (4) with respect of the inequalities (4) and (5).

3. Numerical Example

The proposed optimisation model is used to find the best variant for an electric network that feeds the consumers (Fig. 3) from nodes *1* to *4* which needed the fuzzy power (with trapezoidal membership functions) given in Table 1.

Table 1

Fuzzy Powers of Nodes

Node	$\tilde{P}$, [MW]			
	P^1	P^2	P^3	P^4
1	0.5	0.7	1	1.5
2	0.3	0.6	0.8	1.1
3	0.6	0.8	1	1.2
4	0.2	0.3	0.4	0.5

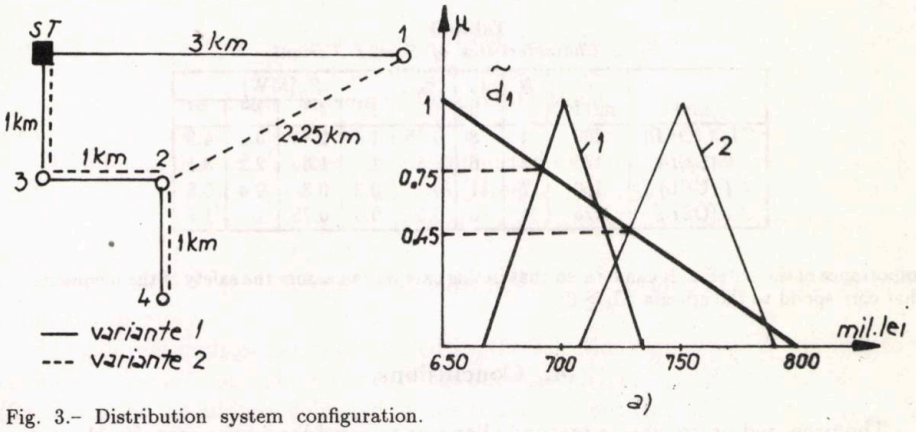

Fig. 3.– Distribution system configuration.

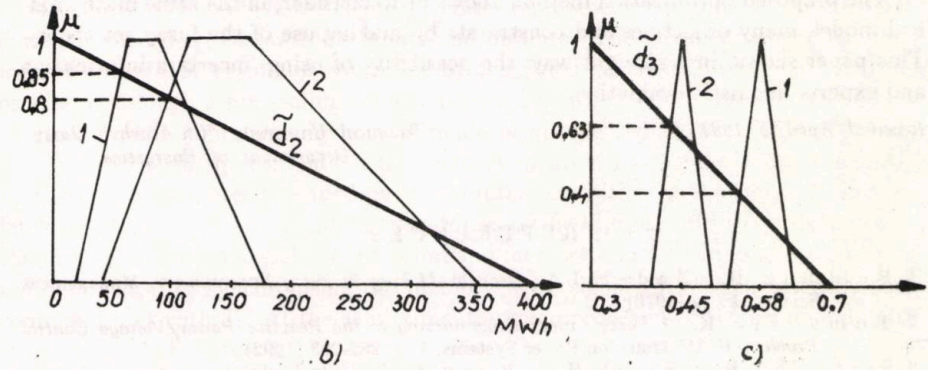

Fig. 4.– Comparison of variants.

There were considered two possible variants, made with overhead lines (OEL) and underground lines (UEL) who's fuzzy characteristics are given in Table 2 (variant *1*) and Table 3 (variant *2*) and there were discussed three criteria.

Table 2
Fuzzy Characteristics of First Variant

Line	$\tilde{c}$ mil.lei	$\tilde{N}$	$\tilde{T}_d$ h	$\tilde{a}_m$	$\tilde{P}$, [MW] P^1	P^2	P^3	P^4
ST-1 (OEL)	300	4	6	0.5	0.5	0.75	1	1.5
ST-3 (OEL)	150	3	6	0.6	1.1	1.7	2.2	2.8
3-2 (OEL)	150	2	6	0.6	0.5	0.9	1.2	1.6
2-4 (OEL)	100	2	6	0.8	0.2	0.3	0.4	0.5

The power flows on lines was calculated with relations (1). In Figs. 4 *a*, 4 *b* and 4 *c* were deduced the highest levels for satisfaction the inequalities that correspond to those three criteria (cost, visual impact and reliability). It was considered that the values spread for cost is ±5%, for visual impact is ±10% and for the reliability is ±1 for a frequency of failures ($\tilde{N}$) and ±10% for a reparation time ($\tilde{T}_d$).

If we consider the same weight coefficients for all the criteria (α_i=1) we can see that the first variant is better than the second even if from the visual point of view is worse ($0.75 + 0.88 + 0.4 > > 0.45 + 0.8 + 0.63$). By choosing the correct weight coefficients we can take into account the

Table 3
Fuzzy Characteristics of Second Variant

Line	$\tilde{c}$ mil.lei	$\tilde{N}$	$\tilde{T}_d$ h	$\tilde{a}_m$	$\tilde{P}$, [MW] P^1	P^2	P^3	P^4
ST-3 (OEL)	200	4	8	0.75	1.6	2.45	3.2	4.3
3-2 (OEL)	175	2	6	0.5	1	1.65	2.2	3.1
2-4 (UEL)	150	2	11	0	0.2	0.3	0.4	0.5
2-1 (OEL)	225	4	6	0.5	0.5	0.75	1	1.5

importance of the criteria. It can be seen that in this case we can assure the safety of the inequalities that correspond to the criteria ($\Pi_i \geq 0$).

4. Conclusions

The proposed optimization method allows us to consider, in the same mathematical model, many objectives and constraints by making use of the fuzzy set theory. This paper shows, in a straight way, the possibility of using uncertain information and experts linguistic evaluation.

Received, April 18, 1997

Technical University "Gh.Asachi", Jassy,
Department of Energetics

REFERENCES

1. Bellman R., Zadeh L.A., *Decision-Making in Fuzzy Environment.* Management Science, **17**, *4* (1970).
2. Tomsovic K., *A Fuzzy Linear Programming to the Reactive Power/Voltage Control Problem.* IEEE Trans. on Power Systems, **7**, *1*, 287-293 (1992).
3. Seitz Th., Haubrich H.J., Bovy A., *Reability Evaluation Systems with Local Generation Using Fuzzy Sets.* The 11th PSCC, Avignon, 39-45, 1993.
4. Bârlădeanu E., Poeată Al., *Aspects sur l'utilisation de la théorie des ensembles flous dans le domaine des réseaux electriques.* Bul. Inst. polit., Iaşi, **XLI (XLV)**, *5*, s.III, 577-583 (1995).
5. Bârlădeanu E., Poeată Al., *Contribuţii la modelarea matematică a unor procese manageriale din domeniul reţelelor electrice.* Energetica, B, *5*, 493-498 (1995).
6. Kagan N., Adams R.N., *Electrical Power Distribution Systems Planning Using Fuzzy Mathematical Programming.* The 11th PSCC, Avignon, 163-169, 1993.

CONTRIBUŢII LA OPTIMIZAREA DEZVOLTĂRII REŢELELOR ELECTRICE DE DISTRIBUŢIE ÎN CONDIŢIILE INFORMAŢIILOR INCERTE

(Rezumat)

Se propune un model de optimizare a dezvoltării reţelelor de distribuţie de medie tensiune care ţine seama de incertitudinea unor informaţii şi de existenţa şi a altor obiective (încadrarea în mediu, fiabilitate etc.) pe lângă obiectivul minimizării costurilor. Obiectivele şi restricţiile sunt modelate utilizând teoria mulţimilor fuzzy, ceea ce permite găsirea rapidă şi eficientă a deciziei optime considerându-se simultan factorii cuantificabili şi necuantificabili economic.

BULETINUL INSTITUTULUI POLITEHNIC DIN IAŞI
Tomul XLIII (XLVII), Fasc. 3–4, 1997
Secţia III
ELECTROTEHNICĂ. ENERGETICĂ. ELECTRONICĂ

D.C. 621.3.017; 621.316.3

AN ARTIFICIAL NEURAL NETWORK APPROACH FOR THE EVALUATION OF ACTIVE LOSSES IN POWER TRANSMISSION SYSTEMS

BY

DANIELA RĂDĂŞANU, M. GAVRILAŞ and GH. GEORGESCU

An algorithm based on training of artificial neural networks (ANN) for the evaluation of active power losses in power systems is proposed. Active and reactive power of generators and loads, as well as the voltage magnitudes of some buses are chosen as inputs to the ANN. Due to the capability of parallel information processing of the ANNs, the proposed method is fast and yet accurate. The trained ANN can be used for on-line evaluation of active power losses and for off-line simulation studies for system design and planning.

1. Introduction

The rapid and accurate evaluation of the active power losses becomes more and more important on present state, because of the necessity to take on-line decision with the view of a power transmission system operation as efficient as possible. At present, the active power losses are computed using specialized software. The accuracy of results is affected to a great extent by the representation of network components and by the mathematical model used. As a rule, all traditional methods estimate the active power losses by load flow. The main disavantage of these methods is the large amount of information which forms the input data (network topology, electric parameters, load characteristics). This difficulty and the estimation time increase as the dimension of the analysed network grows up.

Recent studies [1],...,[3] emphasize the possibility of power system state parameters evaluation by Artificial Neural Network (ANN) approaches. The literature refers frequently to ANNs like fast evaluation tools (software and hardware implementation) because they are governed by massive parallel processes. The ANNs approach for active power and energy losses evaluation in power systems may represent a valuable alternative to traditional methods.

Thus, this approach guarantees a compromise between the amount of input data, the accuracy of results and the evaluation time.

2. Feedforward Artificial Neural Networks

At present, there are a great variety of ANNs. They may be classified by different criteria . Taking into consideration the training, the literature [4] classified the neural networks into:

a) supervised networks (Hopfield, Adaline, Multilayer Perceptron, LVQ, Counterpropagation);

b) unsupervised networks (Kohonen, ART1, ART2, Herault and Jutten).

Further, we will use only the supervised learning algorithm. The neural network is trained by repeatedly presenting a representative set of input/output patterns with backward error propagation and weight adjustment to minimize the global error of the network:

$$E_p = \frac{1}{2}\sum_{j=1}^{n_0}(t_{pj} - o_{pj})^2, \tag{1}$$

where t_{pj} is the target output of neuron j and o_{pj} – the computed output of neuron j; n_0 is the number of output neurons. Subscript p refers to the input pattern p.

The successfully implementation of ANNs to solving a particular problem depends in a great extent on two previous stages:

1° Preparation of suitable training data: the input/output patterns must cover as well and as completely as possible the problem space. It is to expect that the use of data sets with a uniform and concentrate distribution inside the problem space will allow a more accurate interpolation.

2° Selection of an optimum ANN structure which guarantees the desired accuracy using the simplest structure of the neurons-sinaptic connections.

The ANN applications in approximation problems widely use the Multilayer Perceptron (MLP). This type of ANN is characterized by a relatively simple structure (one input layer, one output layer and at least one hidden layer; between these layers there are complete or partial connections) and by performant training algorithms (Backpropagation with Momentum and Adaptable Learning Rate or Resilient Propagation).

3. Evaluation of Active Power Losses Using Multilayer Perceptron

3.1. Problem Formulation

For the evaluation of active losses in power transmission systems, one must design and train an ANN-Multilayer Perceptron, in order to approximate the function:

$$\Delta P = F([x]), \tag{2}$$

where: ΔP is active losses and $[x]$ – a row matrix of the state variables:

$$[x] = [P_g\ Q_g\ P_c\ Q_c\ V] \tag{3}$$

with P_g, Q_g – row matrices of the active (MW) and reactive (MVAr) powers delivered by the sources; P_c, Q_c – row matrices of the absorbed active (MW) and reactive (MVAr) powers; V – row matrix of the bus voltage magnitude.

The matrices P_g, Q_g, P_c, Q_c and V form the inputs for the MLP. The output of the neural network is the active power losses (ΔP).

3.2. Design of the ANN

The design of the MLP includes the following steps:

a) Preparation of suitable training data: this set contains $([x], F([x]))$ pairs and is obtained using off-line traditional method (e.g., iterative load flow computation) for different $[x]$ inputs.

b) Selection of an optimal MLP structure: this step includes the selection of number of layers, the choice of the activation function and the number of neurons in each layer which determine a global error less than a fixed limit.

c) Training of the MLP: the selected network is trained using learning patterns and a conjugated gradient type algorithm. The training stage establishes the weights between the neurons of different layers. Training is stopped when the mean squared error between actual and desired outputs cease improving.

d) Evaluation of the trained network: a testing set outside the learning patterns is presented to the ANN and active power losses are evaluated.

This process applies iteratively. It is possible that the designer is not satisfied with the training and performance of the ANN. In this case the training data and/or structure of the ANN are modified and the neural network is retrained.

3.3. Application for a Test System

The proposed approach was applied to a 110 kV power transmission system, comprising eight buses (five consumer buses, two generator buses and one pilot bus). The one-line diagram of the test system is shown in Fig. 1. Table 1 presents the parameters of the lines.

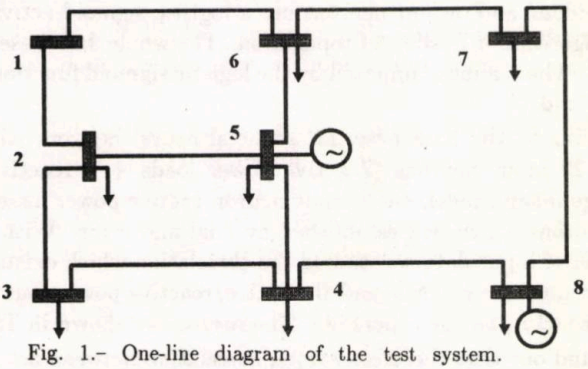

Fig. 1.– One-line diagram of the test system.

The magnitude of the pilot bus voltage is assumed between U_n and $1.1\,U_n$, where U_n is the rated voltage of the system. To generate the training set, we have assumed the lower and upper limits of the selected input variables as listed in Table 2.

Table 1
Electric Parameters for the Lines in Fig. 1

Line	R, [Ω]	X, [Ω]	$B/2$, [10^{-6} S]	$Q_c/2$, [MVAr]	Y, [10^{-3} S]
1-2	2.40	6.030	21.30	0.258	56.98–j 143.16
2-3	1.60	4.020	14.20	0.172	85.47–j 214.74
3-4	2.88	7.236	25.56	0.309	47.48–j 119.29
4-5	1.92	4.824	17.04	0.206	71.22–j 178.95
5-6	3.20	8.040	28.40	0.344	42.73–j 107.37
6-7	0.80	2.010	7.10	0.086	170.94–j 429.48
7-8	4.80	12.060	42.60	0.516	28.49–j 71.58
4-8	1.28	3.216	11.36	0.138	106.84–j 268.42
2-5	4.00	10.050	35.50	0.429	34.19–j 85.89
1-6	1.60	4.020	14.20	0.172	85.47–j 214.74

Table 2
Lower and Upper Limits for the State Variables

Bus No.	$P_{c\,\min}$ MW	$P_{c\,\max}$ MW	$P_{g\,\min}$ MW	$P_{g\,\max}$ MW	$\cos\varphi_{\min}$	$\cos\varphi_{\max}$
2	20	40	–	–	0.86	0.88
3	15	30	–	–	0.86	0.88
4	15	25	–	–	0.86	0.88
5	5	15	20	50	0.84	0.88
6	10	30	–	–	0.86	0.88
7	10	25	–	–	0.86	0.88
8	10	20	30	60	0.84	0.88

The training patterns were produced by randomly generating active and reactive powers for the loads between the lower and upper limits. 1,100 patterns were generated. From this set of patterns, 1,000 have been used for training and 100 for evaluation of the trained network.

The MLP was trained under the Stuttgart Neuronal Network Simulator (SNNS) [5]. The hidden and output neurons use a logistic sigmoid activation function. The training algorithm is Resilient Propagation. The whole data base was scaled between 0.15...0.85. The scaling is imposed by the logistic sigmoid function which takes values between 0 and 1.

According to the data base, an artificial neural network with three layers was selected: 22 input neurons (7 active power loads + 7 reactive power loads + 8 bus voltage magnitudes), one output neuron (active power losses) and a number of hidden neurons which was established by trial and error. With the view to reduce the number of input data we studied the correlation which exists between the active power losses, on the one side and the active/reactive power, bus voltage magnitudes and power factor, on the other side. The results are shown in Table 3.

We found out that there is a strong correlation between active power losses and the voltage magnitudes from buses *4* and *8*. On the other hand we obtained the weaker correlation between active power losses and active/reactive power from the same buses.

Table 3
Correlation between ΔP and $P, Q, |V|, \cos\varphi$

Correlation	Bus *1*	Bus *2*	Bus *3*	Bus *4*	Bus *5*	Bus *6*	Bus *7*	Bus *8*
$\Delta P - P$	–	−0.4633	−0.4522	−0.1129	−0.4071	−0.2861	−0.2344	−0.2799
$\Delta P - Q$	–	−0.4635	−0.4467	−0.1035	−0.4104	−0.2880	−0.2348	−0.2779
$\Delta P - \cos\varphi$	–	0.0386	−0.0177	−0.0390	−0.0309	0.0291	0.0273	−0.0242
$\Delta P - \|V\|$	−0.2450	−0.3569	−0.3837	**−0.3958**	−0.3919	−0.3291	−0.3443	**−0.3997**

Thus, we decided to form the data base from: 7 active powers, 7 reactive powers and 2 bus voltage magnitudes (for buses *4* and *8*). Therefore, the neural network will contain 16 input neurons. The ANN was trained using the learning function Rprop (Resilient Propagation) with randomly initialized weights between – 1 and 1.

The neural networks literature [6] recomands to choose the number of hidden neurons about double with respect to the input neurons number. Thus, the best results were obtained with 34 hidden neurons, as shown in Fig. 2.

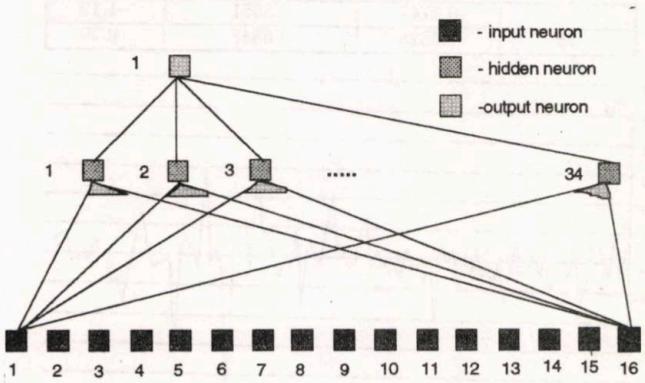

Fig. 2.– Structure of the ANN.

After 20,000 presentations of the training set to the neural network, the mean squared error/pattern was reduced to less then 4×10^{-6}, an error which was considered acceptable.

Then, the testing set with 100 patterns was presented to the trained ANN and active power losses were evaluated. The performance of the network was found to be very satisfactory. The percentage absolute mean error for the whole testing set is 0.66%. Table 4 shows the comparison of the results obtained from the ANN and load flow for the first 15 patterns of the testing set. It can be seen that the computed active power losses from the ANN are close enough to those obtained by load flow studies.

Fig. 3 shows the percentage errors for the whole testing set (100 patterns). The maximum absolute error is 4.68%, but in the most cases the percentage absolute errors are under 2%.

Table 4
Comparison of Active Power Losses as Obtained by ANN and Load Flow

Pattern No.	ΔP by ANN	ΔP by Load Flow	Error, [%]
1	0.8333	0.8376	0.51
2	0.7878	0.7829	-0.62
3	0.4715	0.4762	0.99
4	0.6184	0.6153	-0.51
5	0.5503	0.5508	0.09
6	0.9299	0.9353	0.57
7	0.4678	0.4707	0.61
8	0.5414	0.5371	-0.80
9	0.5600	0.5527	-1.32
10	1.2953	1.3024	0.54
11	0.5903	0.5878	-0.42
12	0.6506	0.6480	-0.40
13	0.5063	0.5050	-0.26
14	0.8747	0.8651	-1.12
15	0.6528	0.6547	0.29

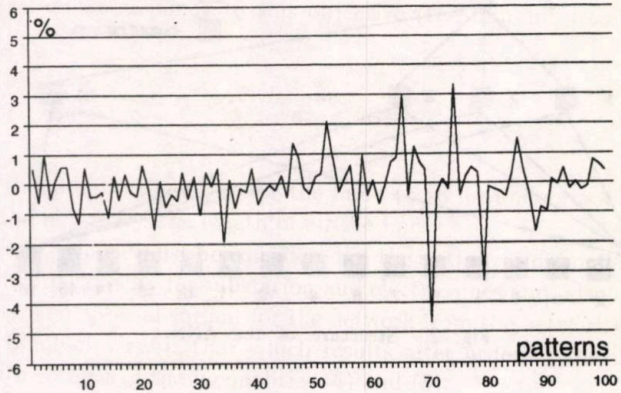

Fig. 3.– Percentage errors for testing set.

4. Conclusions

Test results have demonstrated that the trained ANN can accurately predict active power losses for power transmission systems through its generalization and adaptability capabilities. High performance has been achieved through complex mappings, modeled by ANN, between system losses and system topologies, operating conditions and load variations.

The trained ANN can be used for off-line evaluation of active power losses, as an important component of the studies for system design and planning. At the same time the trained ANN can be used for on-line computations of active power losses using metered state variables. Because of the capabilities of parallel information

processing and generalization, the artificial neural network is a fast and yet accurate approach for evaluation of capacity losses in power transmission systems.

Received, March 17, 1997

Technical University "Gh. Asachi", Jassy,
Department of Energetics

REFERENCES

1. * * * *Artificial Neural Networks for Power System. A Literature Survey.* Raport CIGRE, TF 38-06-06, Aug. 1993.
2. Sidhu T.S., Ao Z., *On-Line Evaluation of Capacity and Energy Losses in Power Transmission Systems by Using Artificial Neural Networks.* IEEE Transactions on Power Delivery, **10**, *4*, 1913-1919 (1995).
3. Cârţină Gh., Georgescu Gh., Gavrilaş M., Bonciu Cl., *Reţele neuronale şi sisteme expert în energetică.* Ed. „Gh. Asachi", Iaşi, 1994.
4. Baumann J., Germond A.J., *Application of the Kohonen Network to Short-Term Load Forecasting; Neural Networks Applications.* IEEE Technology Update Series (Ed. P.K. Simpson), IEEE Technical Activities Board, New York, 1996, 286-291.
5. * * * SNNS, *Stuttgart Neural Network Simulator.* Univ. of Stuttgart, Institute for Parallel and Distributed High Performance System, 1993.
6. Petricică D., Chirvase D., Hărsan M., *The Voltage Stability Analysis Using Network Technique.* Proc. of National Conf. on Energetics, Neptun, 1996, 209-224.

UN PROCEDEU DE UTILIZARE A REŢELELOR NEURONALE ARTIFICIALE PENTRU EVALUAREA PIERDERILOR DE PUTERE ACTIVĂ ÎN REŢELELE ELECTRICE

(Rezumat)

Se prezintă o posibilitate de utilizare a reţelelor neuronale artificiale în aplicaţii on-line pentru monitorizarea pierderilor de putere activă şi în aplicaţii off-line pentru estimarea pierderilor de putere, ca o componentă importantă în procesul de luare a deciziilor în etapele de proiectare sau planificare optimală a reţelelor electrice. Datorită capacităţii de procesare paralelă a informaţiei reţelele neuronale artificiale reprezintă mijloace de calcul rapide şi destul de exacte pentru estimarea pierderilor de putere din reţele electrice.

BULETINUL INSTITUTULUI POLITEHNIC DIN IAŞI
Tomul XLIII (XLVII), Fasc. 3–4, 1997
Secţia III
ELECTROTEHNICĂ. ENERGETICĂ. ELECTRONICĂ

D.C. 621.317.333.4

SOME CHARACTERISTICS OF THE TWO-PHASE GROUND FAULT UNDER STABILIZED CONDITIONS IN THE SUPPLY SYSTEM WITH NEURAL EARTHING

BY

JAN IGNAT and M. PROFIRE

The present study apart from the great number of characteristics values related to the under stabilized two-phase ground fault, is going to introduce another value, not presented up to now, that is the phase difference between the unbalance current, $\underline{I}_p$, and the voltage between S and T phases where the two-phase ground fault was produced.

Thus, it is possible to assure two different types protections for the two-phase ground fault.

1. Under the conditions of a two-phase ground fault in a supply system with neural earthing, the value of voltages, currents and phase differences between S and T phases depends both on the value of the resistance among R-phases (Fig. 1) and on the value of the R_D intermediate resistance acting while grounding contact.

2. Apart from the great number of characteristic values related to the two-phase ground fault under stabilized in some specific papers [1], the present study is going to introduce another one, not presented up to now, that is the phase difference between the unbalance current, $\underline{I}_p$ [1], measurable by a homopolar current filter (HT, Fig. 1) and the voltage between S and T phases where the two-phases ground fault was produced in the point where the latter was generated (k, Fig. 1).

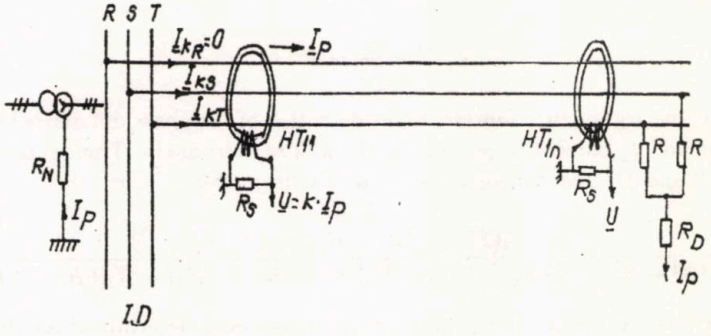

Fig. 1

So as it is known [1]:

$$(1)\quad \underline{I}_p = 3\underline{I}_0 = \frac{3(\underline{Z}_2 + R)}{\underline{Z}_2 + R + (\underline{Z}_0 + R + 3R_D)} \cdot \frac{\underline{E}_R}{\underline{Z}_1 + R + (\underline{Z}_2 + R)//(\underline{Z}_0 + R + 3R_D)}$$

or:

$$(1')\quad \underline{I} = \frac{3(\underline{Z}_0 + R)}{\underline{Z}_2 + R + (\underline{Z}_0 + R + 3R_D)}\underline{I}_{kR_1} \quad \text{and} \quad (2)\quad \underline{U}_{kST} = R(\underline{I}_{kS} - \underline{I}_{kT}).$$

By explaining the currents [3] and by marking $\underline{Z}_2 + R_2 = \underline{A}$; $\underline{Z}_0 + R + 3R_D = \underline{B}$ we set:

$$(3)\quad \underline{U}_{kST} = \left[\frac{(a^2 - a)\underline{A} + 2(a^2 - a)\underline{B}}{\underline{A} + \underline{B}}\right] \cdot \frac{\underline{E}_R}{(\underline{Z}_1 + R)(\underline{Z}_2 + R)//(\underline{Z}_0 + R + 3R_D)}R$$

or:

$$(4)\quad \underline{U}_{kST} = -\mathrm{j}\frac{\underline{A} + 2\underline{B}}{\underline{A} + \underline{B}}R\underline{I}_{kR_1} \quad \text{and} \quad (5)\quad \underline{I}_p = -\frac{3\underline{A}}{\underline{A} + \underline{B}}\underline{I}_{kR_1}.$$

Thus, from (4) and (5) it results that the phase difference between $\underline{U}_{kST}$ voltage and $\underline{I}_p$ unbalance current represents the vector argument:

$$(6)\quad \underline{Z}_k^{(1,1)} = \frac{\underline{U}_{kST}}{p\underline{I}_p} = \mathrm{j}\frac{\underline{A} + 2\underline{B}}{3\underline{A}}R.$$

Interpreting $\underline{A}$ and $\underline{B}$ and effectuating a few transformations we get:

$$(7)\quad \underline{Z}_k^{(1,1)} = \mathrm{j}\frac{R}{3}\left\{\frac{3R^2 + R_2^2 + X_2(X_2 + 2X_0) + R(4R_2 + 6R_D + 2R_0)}{X_2^2 + (R_2 + R)^2} + \right.$$
$$\left. + \frac{R_2(6R_D + 2R_0) - \mathrm{j}\,[X_2(2R + 2R_0 + 6R_D) - 2X_0(R_2 + R)]}{X_2^2 + (R_2 + R)^2}\right\}.$$

Marking:

$$(8)\quad \underline{Z}_2^{(1,1)} = \mathrm{j}\frac{R}{3}m\,e^{\mathrm{j}\varphi}$$

it results that the argument φ represents the deviation of the phase difference between $\underline{U}_{kST}$ voltage and $\underline{I}_p$ current in relation to the $\pi/2$ radiant angle. The deviation is a function of R and R_D resistances value. It results from (8):

$$(9)\quad \varphi = \operatorname{artg}\frac{-X_2(2R + 2R_0 + 6R_D) + 2X_0(R_2 + R)}{3R^2 + R_2^2 + X_2(X_2 + 2X_0) + R(4R_2 + 6R_D + 2R_0) + R_2(6R_D + 2R_0)}.$$

In Table 1 the values of the φ angular deviation were determined for different types of overhead and under ground systems and a brood range of combinations values of R and R_D resistances.

Table 1
L=1 km

R Ω	R_D Ω	LES			LEA		
		50 mm^2	95 mm^2	120 mm^2	50 mm^2	95 mm^2	120 mm^2
0	0	0	0	0	0	0	0
2	0	4.6	3.8	1.0	9.2	9.66	12.0
0	2	−0.06	−13	−30	−23	−32	−39.0
4	2	0.62	0.68	0.9	2.30	2.20	2.55
5	5	0	0	0	0	0	0
10	5	0.35	0.29	0.29	1.2	1.11	1.08
5	10	−0.48	−0.53	−0.36	−1.88	−1.86	−1.50
20	20	0	0	0	0	0	0
5	20	0.09	0.08	0.07	0.33	0.29	0.29
20	50	−0.17	−0.15	−0.135	−0.62	−0.58	−0.58
100	0	0.14	0.14	0.11	0.2	0.19	0.18
2	100	−2.75	−2.62	−2.60	−9.47	−10.11	−10.23
3	500	−1.98	−1.95	−1.81	−6.80	−7.09	−7.03
10	5,000	−0.67	−0.62	−0.56	−2.34	−2.28	−2.19
500	1,000	0	0	0	0	0	0

We notice that φ deviation of the phase difference between $\underline{U}_{kST}$ voltage and $\underline{I}_p$ current equals zero when the two resistances have the same value; they have small positive values (under $\pi/12$ radiants) when $R > R_D$ (the trend is towards a double ground rate).

If $R_D > R$ then φ deviation has small negative values (under $\pi/12$ radiants) and the fault has a tendancy to a two-phase short-circuit rate.

As, accordingly especially to the value of the R resistance, the two-phase short-circuit (small R) or of a double ground ($R \gg R_D$), and still keeping a limiting value for φ angular resistance (for instance $-\pi/12$ radiants) we get the limiting (minimum) value of R=$R_{\min} < R_D$ resistance that meets this condition.

Elucidating R_D in (9) and omiting these terms that contain $1/R_D$, we get:

$$\varphi \cong \operatorname{artg}\frac{-X_2}{R+R_2} \tag{10}$$

and for φ=$-\pi/12$ radiants we get:

$$R_{\min} = \frac{X_2}{0.268} - R_2. \tag{11}$$

As X_2 and R_2 depends on the system nature (overhead or under ground lines) and on the L distance from the fault point to the I.D. bars (Fig. 1), there had been determined the values of $R_{\min}$ resistance for different combinations of these parameters (Table 2).

So, the angular deviation φ=$-\pi/12$ radiants regardless of the value of $R_D > R_{\min}$ and $R > R_{\min}$.

Table 2

	50 mm^2	70 mm^2	95 mm^2	120 mm^2	150 mm^2	185 mm^2
R_{min}, [Ω] LES	0	0.02	0.11	0.15	0.19	0.21
R_{min}, [Ω] LEA	1.0	1.15	1.22	1.25	1.28	1.29
L=10 km						
R_{min}, [Ω] LES	0	0.1	0.55	0.75	0.95	1.05
R_{min}, [Ω] LEA	5	5.75	6.10	6.25	6.40	6.45
L=15 km						
R_{min}, [Ω] LES	0	0.2	1.1	1.5	1.9	2.1
R_{min}, [Ω] LEA	10.0	11.5	12.2	12.5	12.8	12.9

LES – underground system; LEA – overhead system.

3. In consequence, from the point of view of the phase difference between the system voltage of the phases where the two-phase ground fault was generated and the unbalance current, measured by homopolar transformers, the two-phase fault can be treated under these conditions as it follows:

a) as a two-phase short-circuit when $R < R_{min}$, detected and located by the maximum protections and by the backward current [2];

b) as a two-phase ground fault when $R \geq R_{min}$, regardless of the value of R_D resistance that can be detected and located by the control of the phase difference between the voltages and the currents in the system, as it was presented above, because this phase difference has values uniquely determined in relation to the phases between wich the fault was generated.

Conclusions

1° The two-phase ground faults generated by the resistance between the phases of big value ($R > R_{min}$) can be detected and located by a new method that is no longer based on a mechanical action of small sensitivity, but on the control of some phase differences, easily performed by the presented electronic technologies.

2° Thus, it is possible to assure two different types of protections for the two-phase ground faults whose consequences are favourable and similar to these that are characteristic to the monophase fault for the same type of system [3].

Received, February 10, 1997

Technical University "Gh.Asachi", Jassy,
Department of Building and
Industrial Installations

REFERENCES

1. U l i a n o v S.A., *Regimurile tranzitorii ale sistemelor electrice* (transl. from Russian). Ed. Tehnică. Bucureşti, 1967.

2. G o i a L.M. *et al.*, *Tratarea neutrului reţelelor de medie tensiune.* Ed. Tehnică, Bucureşti, 1985.
3. I g n a t J., G ă l ă ţ a n u C., *Observabilitatea reţelelor electrice de distribuţie de medie tensiune.* Ed. Ventura, Iaşi, 1995.

UNELE CARACTERISTICI ALE REGIMULUI STABILIZAT DE DEFECT BIFAZAT CU PUNERE LA PĂMÂNT ÎN REŢELE DE DISTRIBUŢIE CU NEUTRUL LEGAT LA PĂMÂNT

(Rezumat)

Se prezintă o mărime, neevidenţiată până acum, ce caracterizează regimul stabilizat de defect bifazat, cu punere la pământ şi anume defazajul dintre curentul de dezechilibru $\underline{I}_p$ şi tensiunile dintre fazele între care s-a produs defectul bifazat, la locul de producere al acestuia.

Caracteristicile acestui tip de defect depind şi de valoarea rezistenţei dintre faze. Ca urmare, defectul bifazat cu punere la pământ poate fi identificat cu două tipuri de protecţii.

BULETINUL INSTITUTULUI POLITEHNIC DIN IAŞI
Tomul XLIII (XLVII), Fasc. 3–4, 1997
Secţia III
ELECTROTEHNICĂ. ENERGETICĂ. ELECTRONICĂ

D.C. 621.317.333.4

DETERMINATION OF THE VARIATION RANGE OF SOME PARAMETERS SPECIFIC TO THE TWO-PHASE GROUND FAULT

BY

CĂTĂLIN-D. GĂLĂŢANU and JAN IGNAT

With the view of applying the method based on the control of phase differences between the star voltages and the unbalance currents and with the purpose of identifying and localizing the two-phase fault, the variation range of these phase differences in accordance with the parameters influencing them, is determined.

1. In the supply systems neutral earthing, the two-phase ground fault condition is determined both by the resistance value (R) between phases (Fig. 1) and the transfer resistance value when meeting the ground.

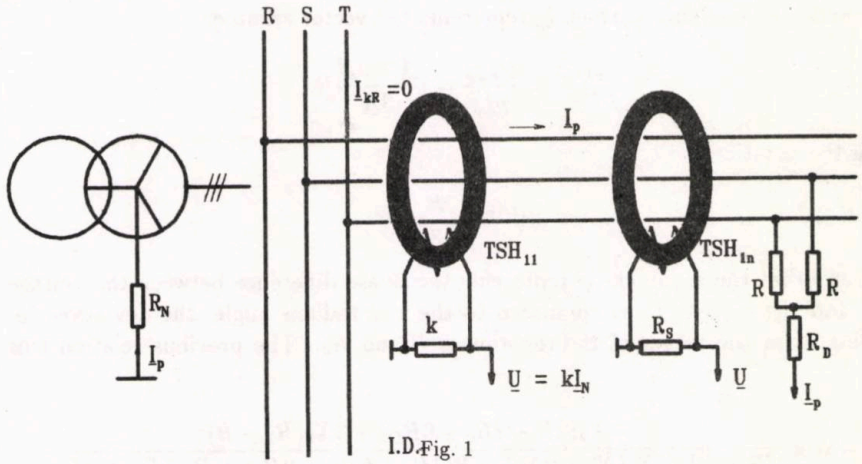

I.D.-Fig. 1

The stabilized duty of the two-phase ground fault is analysed in different papers [1]. The paper herein studies a characteristic unit not being recorded up to now, namely the phase difference between the unbalance current $\underline{I}_p$ [1], that can be measured by an invariable current filter (TSH, Fig. 1) and the voltage between the phases S and T; the two-phase ground fault is considered in the location where it occurs (K, Fig. 1).

As it is already known [1]:

$$\underline{I}_p = \frac{3(\underline{Z}_2 + R)}{\underline{Z}_2 + R + \underline{Z}_0 + R + 3R_D} \cdot \frac{\underline{E}_R}{\underline{Z}_1 + R + \frac{\underline{Z}_2 + R}{\underline{Z}_0 + R + 3R_D}}, \tag{1}$$

$$\underline{I}_p = \frac{3(\underline{Z}_2 + R)}{\underline{Z}_2 + R + \underline{Z}_0 + R + 3R_D} \underline{I}_{k_{R_1}}, \tag{2}$$

and

$$\underline{U}_{k_{ST}} = R(\underline{I}_{k_S} - \underline{I}_{k_T}). \tag{3}$$

By expliciting the currents (3) and denoting: $\underline{Z}_2 + R = \underline{A}$; $\underline{Z}_0 + R + 3R_D = \underline{B}$ it follows:

$$\underline{U}_{k_{ST}} = \frac{(a^2 - a)\underline{A} + 2(a^2 - a)\underline{B}}{\underline{A} + \underline{B}} \cdot \frac{\underline{E}_R}{\underline{Z}_1 + R + \frac{\underline{Z}_2 + R}{\underline{Z}_0 + R + 3R_D}} R, \tag{4}$$

$$\underline{U}_{k_{ST}} = -\mathrm{j}\frac{\underline{A} + 2\underline{B}}{\underline{A} + \underline{B}} R \underline{I}_{k_{R_1}}, \tag{5}$$

$$\underline{I}_p = -\frac{3\underline{A}}{\underline{A} + \underline{B}} \underline{I}_{k_{R_1}}. \tag{6}$$

Therefore, it follows from (5) and (6) that the phase difference between the voltage $\underline{U}_{k_{ST}}$ and the unbalance current $\underline{I}_p$ represents the vector argument:

$$\underline{Z}_k^{(1,1)} = \frac{\underline{U}_{k_{ST}}}{p\underline{I}_p} = \mathrm{j}\frac{\underline{A} + 2\underline{B}}{3\underline{A}} R. \tag{7}$$

Using the notation:

$$\underline{Z}_k^{(1,1)} = \mathrm{j}\frac{R}{3} m e^{\mathrm{j}\varphi} \tag{8}$$

it follows that the argument φ represents the phase difference between the voltage $\underline{U}_{k_{ST}}$ and the current $\underline{I}_p$ as compared to the $\pi/2$ radians angle, the deviation depending upon the values of the resistances R and R_0. The previous relation leds to:

(9)

$$\varphi = \operatorname{artg} \frac{-X_2(2R + 2R_0 + 6R_D) + 2X_0(R_2 + R)}{3R^2 + R_2^2 + X_2(X_2 + 2X_0) + R(4R_2 + 6R_D + 2R_0) + R_2(6R_D + 2R_0)}.$$

It is necessary to carry out the angle deviation φ of all types of overhead lines and underground cables that are usually in operation. It must cover the whole range of both variables R and R_D. It is difficult to perform an exclusively numeric (table-like) treatment of this information and such a treatment is not always conclusive.

Such being the case, one can use MATLAB facilities whose mesh function gives the space image of a defined surface represented by the a multitude of points $(\varphi(R, R_p)$,

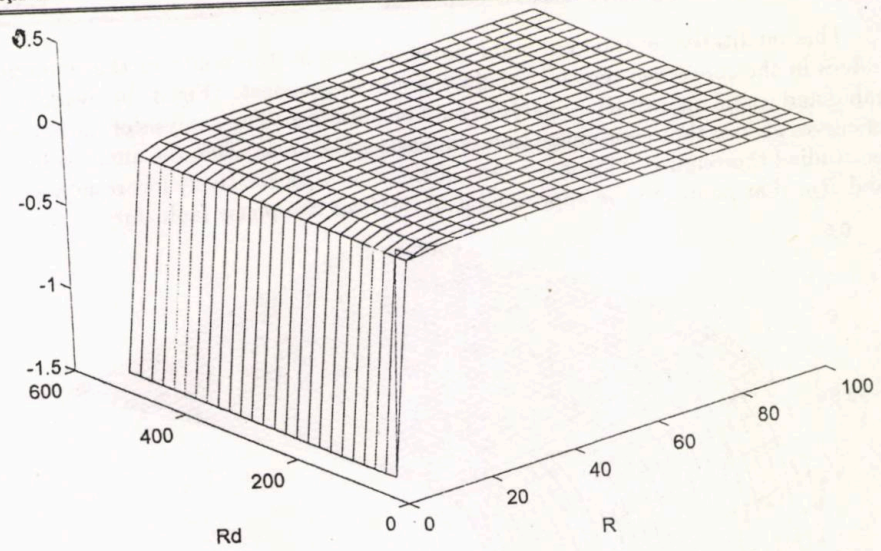

Fig. 2

R, R_D). Figs. 2 and 3 gives the score for the underground cables with 50 mm^2 section area, 1 km long, R=0...100 Ω, R_D=0...500 Ω and the phase difference expressed in sexagesimal degrees.

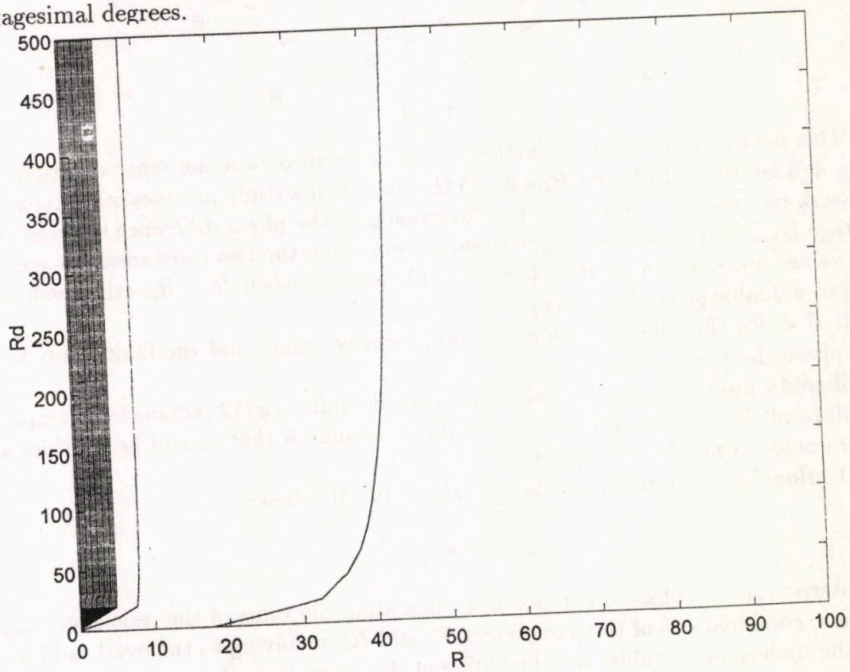

Fig. 3

This qualitative evaluation could be supported by the study of the numerical values in the concerned region. Should the curves φ=const. (Fig. 3) be available, a rapid and useful quantitative analysis could be obtained. The analysis of the two sets of curves gives a thorough image that emphasizes the areas when the analysis should be studied thoroughly. This is the case of the zone with relatively low resistances R and R_D, that points to the approaching to the firm two-phase fault duty.

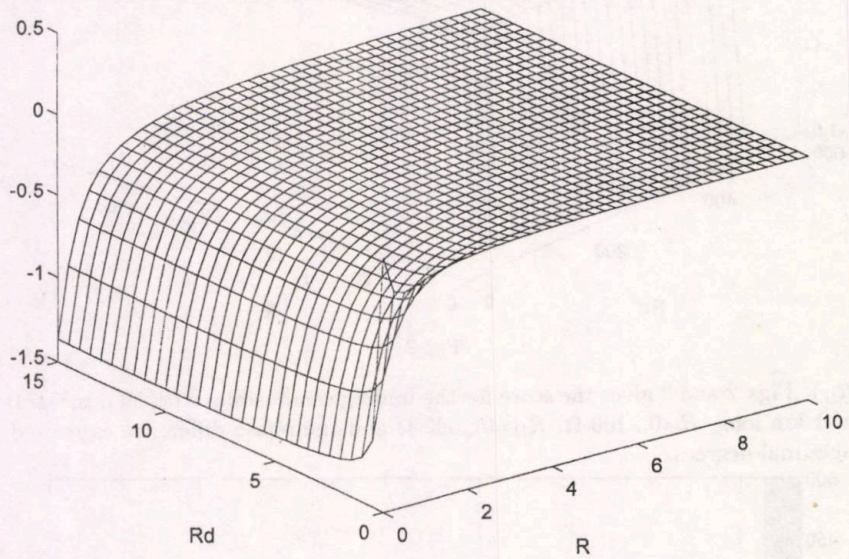

Fig. 4

This field can be extended further on, in order to obtain the representations in Figs. 4, 5 for R=0...10 Ω and R_D=0...15 Ω, when such a study involves other types of network too, one can notice that the deviation φ of the phase difference between the voltage $\underline{U}_{ksT}$ and the current $\underline{I}_p$ is equal to zero when the two resistances are equal; the values are low and positive (below $\pi/12$ radians) when $R > R_D$ (the tendency acts to a double grounding duty).

If $R < R_D$ then the deviation has low, negative values and the fault tends to a two-phase short-circuit duty.

Should a limit value be required for an angle deviation ($\pi/12$ radians for example), it will result in a minimal limit value of the resistance R that should be consider as a parameter to satisfy this condition.

Overlooking the terms containing $1/R_D$ in (9), it follows:

$$\varphi = \text{artg}\frac{-X_2}{R + R_2}. \tag{10}$$

Interpreting the phase difference and calculating the value of the resistance $R_{\min}$ for more combinations of the parameters X_2 and R_2, involving to the overhead lines and the underground cables and for different distances from the fault location and up to the bars I.D. (Fig. 1), the data from Table 1 are obtained.

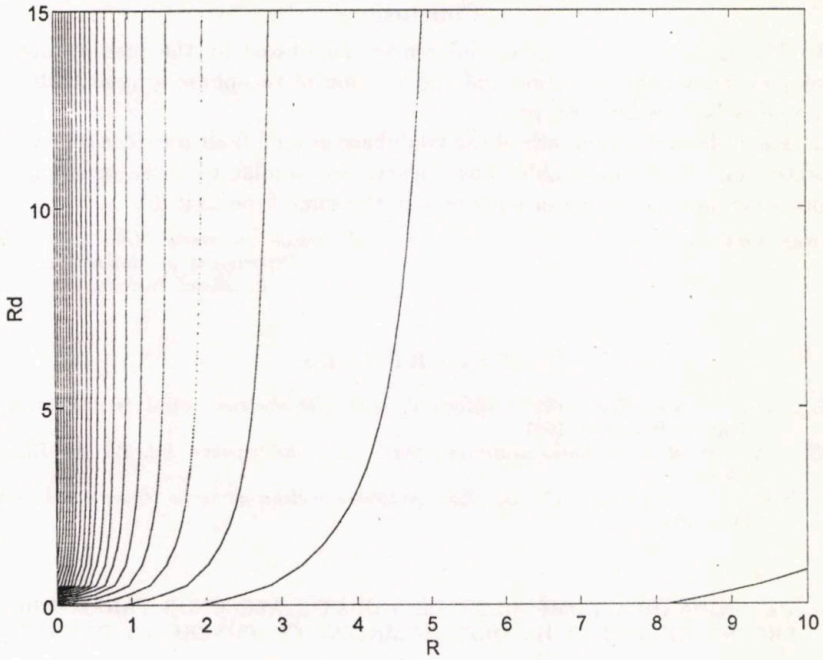

Fig. 5

Table 1

Area section, [mm^2]	50	70	95	120	150	185
$R_{\min}$ UC-1 km	0	0.02	0.11	0.15	0.19	0.21
$R_{\min}$ OL-1 km	1	1.10	1.20	1.25	1.20	1.29
$R_{\min}$ UC-5 km	0	0.01	0.55	0.75	0.94	1.05
$R_{\min}$ OL-5 km	5	5.75	6.10	6.20	6.40	6.45
$R_{\min}$ UC-10 km	0	0.12	1.10	1.50	1.90	2.10
$R_{\min}$ OL-10 km	10	11.5	12.2	12.5	12.8	12.9

It follows that the angle deviation remains lower than $\pi/12$ radians regardless the value of the resistance $R_D < R_{\min}$ and $R < R_{\min}$.

The phase difference between the system voltages of the phases where the two-phase ground fault occurs and the nonsymmetry current allows then the fault to be analyzed tinder two hypotheses:

a) as a two-phase short-circuit when $R < R_{\min}$; it is detected and located by the low-voltage protection and the inverse current filters [2];

b) as a two-phase ground fault when $R \geq R_{\min}$, regardless the value of the resistance R_D; it can be detected and located by the control of the phase difference between the system voltage and currents. As it has previously demonstrated, this phase difference has uniquely defined values depending of the phase where the fault occurred.

Conclusions

1° The control of some phase-differences, facilitated by the present electronic techniques, allows the detection and the location of two-phase ground faults given by a high resistance between phases.

2° The differential approach of the two-phase ground fault provides for two types of protection whose favourable consequences are similar to those concerning the single-phase fault occurring in a network of the same type to it [3].

Received, March 27, 1997

Technical University "Gh.Asachi", Jassy,
Department of Building and
Industrial Installations

REFERENCES

1. U l i a n o v S.A., *Regimurile tranzitorii ale sistemelor electrice* (transl. from Russian). Ed. Tehnică. Bucureşti, 1967.
2. G o i a L.M. *et al., Tratarea neutrului reţelelor de medie tensiune.* Ed. Tehnică, Bucureşti, 1985.
3. I g n a t J., G ă l ă ţ a n u C.D., *Observabilitatea reţelelor de medie tensiune.* Ed. Ventura, Iaşi, 1995.

DETERMINAREA DOMENIILOR DE VARIAŢIE ALE UNOR PARAMETRI PROPRII REGIMULUI DE DEFECT BIFAZAT CU PUNERE LA PĂMÂNT

(Rezumat)

Cu ajutorul metodei bazate pe controlul defazajelor dintre tensiunea de fază şi curentul de dezechilibru, utilizată pentru identificarea defectului bifazat, se prezintă domeniul de variaţie al acestui defazaj, în funcţie de parametrii reţelelor de distribuţie. Pentru o eficientă analiză calitativă sunt utilizate facilităţile mediului de programare MATLAB.

BULETINUL INSTITUTULUI POLITEHNIC DIN IAŞI
Tomul XLIII (XLVII), Fasc. 3–4, 1997
Secţia III
ELECTROTEHNICĂ. ENERGETICĂ. ELECTRONICĂ

RECENZII BOOK REVIEWS

CAHN R.W., HAASEN P., KRAMER E.J (Eds.), *Materials Science and Technology. A Comprehensive Treatment.* VCH, Weinheim, (vol.**16**, Processing of Semiconductors), 1996, 689 pp., ISBN 3-527-26829-4.

The 20-volume series *Materials and Technology* is the first in-depth, topic-oriented reference work devoted to this growing interdisciplinary field. A compendium of current, state-of-the-art information, it covers the most important classes of materials: metals, ceramics, glasses, polymers, semiconductors, and composites. Each volume deals with properties, processing, applications, or general phenomena associated with these materials. Edited by internationally renowned figures in materials science, this series is sure to establish itself as a seminal work.

This self-contained handbook deals with the enabling materials technology for the electronics industry. World-renowned authors have contributed to this unique treatment of the processing of semiconductors and related technologies.

Topics include: Silicon Processing; Compound Semiconductor Processing; Epitaxial Growth; Photolithography; Doping; Etching Processes in Semiconductor Manufacturing; Silicon Device Structures; Compound Semiconductor Device Structures; Silicon Device Processing; Compound Semiconductor Device Processing; Integrated Circuit Packaging; Interconnection Systems.

ELLIS H., *Electrical Interference Technology. A Guide for Designers, Manufactures, Installers and Users of Electrical and Electronic Equipment.* Butterworth-Heinemann, Oxford, 1992, 230 pp., ISBN 1-85573-080-4.

Electrical Interference Technology introduces electromagnetic interference by explaining its causes, effects and penalties. It deals with methods of minimising emissions and maximising immunity, and gives an insight into the various national and international standards and test methods.

For some time, nations have imposed legal standards to limit interference from electrical equipment sold within their boundaries, but with the implementation of the EEC Directive on EMC, compliance with both emission and susceptibility standards is mandatory. This book aims to help manufacturers comply with the requirements.

C o n t e n t s. 1. Introduction; 2. Directives, Regulations and Standards; 3. National Authorities and Standards; 4. The EMC Environment; 5. Radio Wave Propagation; 6. Susceptibility/Immunity; 7. Emission and Susceptibility Protection; 8. Conducted Interference; 9. Installation; 10. Testing; 11. Management of EMC; 12. Domestic and White Goods; 13. Information Technology; 14. Architectural Interests; 15. Transport; 16. Medical Equipment; 17. Electrical Security; 18. Illumination; Appendix I; Appendix II; Appendix III; Appendix IV; Appendix V; Appendix VI; Index.

GRAF R.F., *Modern Dictionary of Electronics.* Sixth Edition Revised and Updated, Butterworth-Heinemann, Oxford, 1997, 1162 pp., ISBN 0-7506-9870-5.

The *Modern Dictionary of Electronics*, previously published by SAMS, is a classic reference source for electronics technicians, students and hobbyists, as well as the practicing engineer. Coverage in this edition includes:

a) Definitions of approximately 25,000 electronics terms;

b) Hundreds of illustrations;

c) Special topics as: Audio electronics, Television and video, Computing, Fiber optics, Microelectronics, Communications, Industrial processes, Medical electronics;

d) Practical, concrete explanations rather than abstract or mathematical meanings;

e) Abbreviations and letter symbols;

f) Tables of SI units and schematic symbols.

Rudolf F. G r a f is a full-time technical author whose name is familiar to electronics professionals and hobbyists alike. His many books offer a practical enjoyable approach to often-complex material. Mr. G r a f is a graduate electronics engineer, and received his MBA at New York University. He is a senior member of the IEEE, a licensed amateur radio operator, and a holder of a first class radiotelephone operator's license. He currently lives in New York.

PALZ W., *Solar Electricity.* Butterworth, London, 1978, 292 pp., ISBN 0-408-70910-3.

The development of solar energy systems is one of the greatest challenges now facing our fuel-hungry and increasingly polluted world.

In this book, the non-scientific reader will find a sound introduction to the science and techniques of solar energy, written with his needs and interests in mind by a scientific specialist. Explanations are full and clear, and the mathematical treatment is kept to a minimum. Specialists and prospective users of solar devices will also be interested by the reviews of the latest research and development work, the cost projections and the technical guidelines for working systems.

All the known ways in which the sun's radiation can be converted into useful power are discussed. Attention is focused on the direct conversion of light into electricity by means of solar cells.

Comprehensive physical, technological and cost data are presented and their complex interrelations outlined.

Practical applications of the various conversion processes are described as well as the historic advances which led to the present state of the art; the potential of foreseeable future developments is analysed.

The reader will also find a review of short and long-term trends in the general energy situation which will enable him to assess the impact of solar energy in developing, as well as in industrialized countries.

C o n t e n t s. Introduction; 1. Energy Overwiew; 2. Solar Energy Conversion; 3. Solar Electricity; 4. Prospects of Solar Power for Large-scale Electricity Production; 5. Outlook.

GILLER G., *Electronics. Principles and Applications.* John Wiley & Sons Ltd., Chichester, 1991, 268 pp., ISBN 1-85058-151-7.

This is a comprehensive review of modern electronics, emphasising both the underlying fundamentals and the applications of electronic components and circuitry.

The book is equally suitable for the hobbyist and for the students of "A" levels, BTEC level 3 and first year degree courses.

Highlights of this useful book include: a) an emphasis on fundamentals; b) questions and answers for self-assessment; c) step-by-step derivations of important theorems.

Graham G i l l e r is an elementary particle physicist who is also an electronics enthusiast. He is currently at the Nuclear Physics Laboratory, Oxford University.

C o n t e n t s. 1. Basic Electricity; 2. Semiconductor Devices; 3. Operational Amplifiers; 4. Digital Electronics; 5. Audio Circuits; 6. Radio and Data Transmission; References; Mathematical Symbols in use in Electronics; The S.I. System of Units; Index.

DUTSCHKE W. (federführend), *Endmaßkalibrierung.* Expert Verlag, Renningen, Germany, 1997, 102 S., ISBN 3-8169-1431-4.

Parallelendmaße haben eine wichtige Funktion innerhalb des betriebsinternen Qualitätsmanagementsystems nach DIN/ISO 9000 ff. Sie ermöglichen die Rückführung der Längenmeßgeräte auf das Nationale Normal und sind deshalb in nahezu allen Kalibrierketten der Fertigungsmeßtechnik zu finden.

Endmaße werden sehr vielseitig eingesetzt, als Prüfmittel in der Fertigung, im Werkzeugbau und im Versuch, ferner als Gebrauchs- und Bezugsnormale innerhalb der Prüfmittelüberwachung. Endmaße verkörpern auf einfache Weise eine Länge und lassen sich zu vielen unterschiedlichen Maßen

zusammenschieben. Sie unterliegen dabei allerdings gewisser Veränderungen, können beschädigt werden, sich abnutzen oder in selteneren Fällen auch ihr Maß ändern. Von Zeit zu Zeit sollten daher sowohl die als Gebrauchsnormale als auch die als Bezugsnormale verwendeten Endmaße kalibriert werden.

Der Themenband zeigt praxisnah, wie man nach Empfehlungen des Deutschen Kalibrierdienstes (DKD) dabei vorgehen soll.

I n h a l t. Grundlagen zur Längeneinheit – Bauarten von Endmaßprüfgeräten – Rechnerunterstützte Meßwertverarbeitung – Kalibrieren von Endmaßprüfgeräten – Entwicklungstendenzen von Endmaßprüfgeräten – Anwendererfahrungen – Erfahrungen beim Kalibrieren von langen Endmaßen.

Die Interessenten: Mitarbeiter, die in Kalibrierlaboratorien, Meßräumen und im Bereich der Prüfmittelüberwachung tätig sind.

BONFIG K.W., *Sensoren und Sensorsignalverarbeitung.* Expert Verlag, Renningen, Germany, 1997, 377 S., ISBN 3-8169-1428-4.

In diesem Sammelband werden wieder wegweisende, serienreife neue Produkte und Verfahren für die Praxis vorgestellt. Damit gibt dieses Handbuch sowohl den aktuellen Stand der Sensorik auf den ausgewählten Gebieten als auch die wichtigsten Trends und Entwicklungsschwerpunkte wieder. Auch Prinzipien der Selbstüberwachung und Selbstkalibrierung und die interessanten Möglichkeiten der Oberflächenwellen-Sensorik werden vorgestellt.

Wesentliche Impulse gehen auch von der Anwendung theoretisch anspruchsvoller neuer Konzepte in der Sensorik aus. Diesem Trend tragen die Beiträge über Fuzzy Logik, Neuronale Netze, Neuro-Fuzzy und Soft-Computing Rechnung.

Es gibt auch interessante Neuentwicklungen im Gebiet der Meßelektronik und Meßsignalverarbeitung sowie bei den Feldbussen und Interfaces.

Erstmals wurde in diesem Handbuch ein Abschnitt über Meßtechnik-Software-pakete aufgenommen, der dem Leser einen Überblick über die wichtigsten, am Markt konkurrierenden Systeme und ihre speziellen Eigenschaften gibt.

Das vorliegende Buch ist nach Anwendungsgebieten gegliedert. Für die einzelnen praxisorientierten Themen wurden jeweils führende Fachkollegen als Mitautoren gewonnen, die über ihre aktuellen Fortschritte und Ergebnisse berichten.

SHULTZ G.P., *Transformers and Motors. A Single-Source Reference for Electricians.* SAMS, A Division of Prentice Hall Computer Publishing, Indiana, 320 pp., ISBN 0-672-30131-8.

The material in this book has been reviewed by the NJATC (National Joint Apprenticeship and Training Committee for the Electrical Industry) and training directors of the electrical apprenticeship committee.

The book you have in your hands is the single, in-depth source of technical information needed by all electricians who install, maintain, troubleshoot, repair, and replace transformers and motors.

Designed especially for the NJATC to train apprentice and journeyman electricians, *Transformers and Motors* provides detailed information while keeping the amount of theory and math to a minimum. In this easy-to-understand, practical sourcebook, you'll dicover: a) explanations of the fundamental concepts of transformers and motors; b) transformer connections and distribution systems; c) installation information for transformers and motors; d) preventive maintenance, troubleshooting, and repair tips and techniques; e) helpful illustrations, glossary, and appendixes; f) end-of-chapter quizzes to test your progress and understanding.

RIBBENS W.B., *Understanding Automotive Electronics.* Fourth Edition, SAMS Publishing, A Division of Prentice Hall Computer Publishing, Indianapolis, 1993, 392 pp., ISBN 0-672-27358-6.

The evolution of electronics in automobiles has been meteoric. This book provides you with a hands-on resource to this rapidly changing scene. *Understanding Automotive Electronics*, Fourth Edition, explores electronic engine control and the development of all-new automotive subsystems, so that you can understand their use and design. Step-by-step, self-paced tutorial lessons introduce you to the most vital areas of electronics within the auto environment. You learn why and how electronic circuits and devices now replace what used to be mechanical and pneumatic. Designed for

accurate and answers on determinating engine performance, fuel economy, speed control, emissions, ride control, braking, and air-bag safety through electronic or digital means. Lots of detailed, informative illustrations help ensure your electronic learning and an insightful backround deepens your understanding.

Paked with essential reference material and illustrations, this book helps you: a) understand automobile electronics fundamentals; b) define the systems approach to control and instrumentation; c) understand how sensors and actuators operate; d) discover the latest digital engine control techniques; e) understand the elements of automative instrumentation and diagnostics; f) look into the future of automative electronics systems.

C o n t e n t s. Preface; 1. Automotive Fundamentals; 2. The Systems Approach to Control and Instrumentation; 3. Electronics Fundamentals; 4. Microcomputer Instrumentation and Control; 5. Sensors and Actuators; 6. The Basics of Electronic Engine Control; 7. Digital Engine Control System; 8. Vehicle Motion Control; 9. Automotive Instrumentation; 10. Diagnostics; 11. Future Automotive Electronic; Index; Glossary; Answers to Quizzes.

SCHRÖDER K.-H. (federführend), *Werkstoffe für elektrische Kontakte und ihre Anwendungen*. Expert Verlag, Renningen, Germany, 1997, 410 S., ISBN 3-8169-1446-2

Das Buch vermittelt den Herstellern und Anwendern von Kontaktwerkstoffen, Schaltgeräten und Steckern Grundlagen zur Auswahl von Werkstoffen und Konstruktionsprinzipien sowie praxisbezogene Kenntnisse. Insbesondere werden dabei neueste Ergebnisse aus der Forschung und Entwicklung eingeschlossen, wie edelmetallsparende Technologien und der Ersatz von umweltbelastenden Legierungsbestandteilen und Beimengungen. Auch werden neue Prüf- und Meßverfahren unter Berücksichtigung elektronischer, rechnergestützter Erfassungs- und Auswertmethoden vorgestellt.

Die Anwendung von Schalt- und Steck-Kontakten in der Kraftfahrzeugtechnik, Fernmeldtechnik, Datenverarbeitung, Unterhaltungselektronik, Meß-, Steuer- und Regelungstechnik sowie bei der Energieversorgung, bei Industrieschaltgeräten und in der Hausinstallations- und Hausgerätetechnik wird unter Berücksichtigung der Entwicklung in der Elektronik erläutert. Dabei schöpft das Buch unter Beteiligung sehr namhafter Anwendungstechniker weitgehend aus praktischen Erfahrungen.

I n h a l t: Grundlagen der Werkstoffauswahl für elektrische Kontakte – Werkstoffwissenschaftliche Grundlagen – Kontaktträgerwerkstoffe auf Kupferbasis – Kontaktwerkstoffe auf Silber-Basis – Gold und Platin, Werkstoffe für niedrige und mittlere elektrische Belastungen – Löten und Schweißen elektrischer Kontakte – Prüfung von elektrischen Kontakten der Energietechnik – Anwendungsbeispiele für elektrische Kontakte in der Energietechnik – Schaltkontakte im Kraftfahrzeug – Automobilgerechte Stecksysteme – Herstellverfahren und Prüfungen für Kontaktschichten in der Nachrichtentechnik – Anwendungsbeispiele für elektrische Kontakte in der Informationstechnik – Die Zukunft elektrischer Schaltkontakte unter dem Einfluß elektronischer Bauelemente.

Data apariţiei: martie 1998, Comanda: 69
Coli tipar: 8,75, Tiraj: 275 exemplare

UNIVERSITATEA TEHNICA „GH. ASACHI" IASI
ROTAPRINT

Str. Lascăr Catargi Nr. 38

ISSN 0258-9109